

Chapter one

Introduction

Pancreas is a mixed lobulated pinkish grey colored gland lying transversely across the posterior abdominal wall extending from the concavity of duodenum to the hilum of spleen forming the stomach bed (Williams1989). Being a mixed gland, the pancreas consists of two distinct populations of cells, the exocrine cells secrete enzymes into the digestive tract, and the endocrines secrete hormones into the blood stream (McMinn1995).

pancreas is a principally important organ from the point of view of human medicine because it can be affected with two important diseases: diabetes mellitus and pancreatic cancer. Despite this medical importance, the developmental process of the pancreas has attracted only a few numbers of researchers in recent years. (Slack1995).

In the investigation of certain lesions of pancreas; the knowledge of normal dimension of the gland was found to be important. Literature indicated that different studies on the morphometry of pancreas were already done by different researchers. (Vesterhus2008)

Determination of pancreas measurements for norms by cross-sectional imaging may be necessary in the acute pancreatitis, initially, and during the course of the disease, in the long term follow-up of chronic pancreatitis, and in diabetic patients.(Balthazar 2009).Reduction of the pancreatic measurements may also affect the exocrine function of the pancreas.This also reflects the importance to know the normal size of the pancreas in order to be able to predict any changes that may occur.(Goda K 2001)

The results of previous researches had revealed that the mean length of pancreas was between 12-15cm.(Innes JT1994) All these measurements were obtained from various ethnic groups and different geographical situations, but in Sudanese context, few studies

had been done till date. Since the ethnicity, body weight, age and nutritional status also affects the size of pancreas and also considering the significance of pancreatic diseases and importance in diagnosis and treatment, it seemed justifiable to carry out a study on the pancreatic morphometry in Sudanese people.

In recent years, pancreatic imaging has improved with the introduction of Ultrasonography (US), Computerized Tomography (CT), Magnetic Resonance Imaging (MRI) and Positron Emission Tomography (PET) and may provide an advance enhancement in the morphological study of pancreas. Using the cross-sectional imaging, the pancreatic size is commonly expressed by the anterior–posterior (AP) diameters of the tail, body, and head(Balthazar2009). Thus Computer-Aided Diagnosis (CAD) systems based on image processing and artificial intelligence techniques have aroused a lot of interest, since they can provide constructive diagnosis suggestions to clinicians for decision-making. Imaging features can be derived from standard of are modalities such as contrast-enhanced computed tomography (CT), magnetic resonance imaging (MRI) and positron emission tomography (PET) without modification of the acquisition protocols making them less cost prohibitive. (Koo. et al 2017) For example, texture features from grey level co-occurrence matrices (GLCM), which generate second order statistical features have been used improved to quantify spatial texture of objects. Texture analysis techniques played a vital role in medical imaging to automatically extract parameters that are used to classify normal and abnormal tissues.(Haralick1973)

Gray Level Run Length Matrix is a statistical texture characterization method, this method consists in counting the number of pixel segments having the same intensity in a given direction, then representing the results in a matrix. A direction (0° , 45° , 90° or 135°) and a number of gray levels are decided on beforehand. The value contained in the matrix's (l,n) square is equal to the number of segments of length l and gray level n . This implies that the matrix's number of columns is dynamic, as it is determined by the

length of the longest segment. By design, this calculation is symmetrical and consequentially, it is unnecessary to consider the four complementary directions (180°, 225°, 270° or 315°, in this example 8 possible directions between a given pixel and its neighbors are taken into account).(Galloway1975)

Once the matrix obtained, 11 indexes are calculated (When using GLRLM in this study we clicks on areas represents these classes; in these areas a window of 3×3 pixel were set and the higher order statistic were calculated, which include Short Run Emphasis (SRE), Long Run Emphasis (LRE), Gray-Level Nonuniformity (GLN), Run Length Nonuniformity (RLN), Run Percentage (RP), Low Gray-Level Run Emphasis (LGLRE), High Gray-Level Run Emphasis (HGLRE), Short Run Low Gray-Level Emphasis (SRLGLE), Short Run High Gray-Level Emphasis (SRHGLE), Long Run Low Gray-Level Emphasis (LRLGLE), Long Run High Gray-Level Emphasis (LRHGLE), to determine the vector that characterizes the texture. To establish our model, the matrix for a given gray level and for four directions was calculated. Then, for each index, the average value of the four directions was taken. A systematic study found that the best model was obtained for a set of 7 indexes and 32 gray levels. The classification success rate was 84.81% by logistic regression, which is inferior to the rate obtained with the cooccurrence matrix and the Haralick features (90%).(Kurani. et, al 2004)

1.2 Problem of the study:

The diagnosis of radiological images by the radiologist mostly depend on the visual perception which is a subjective method and can be affected by the down sampling and the dynamic range. In diabetic patient mostly the intensity will look normal visually while it might not be the case when considering the texture analysis. In the same essence this change might be correlated with the duration of diabetes, and the type. Similarly the size might be affected compared to normal at the same age category and duration might take it is effects on the measurements.

1.3 Justification:

The limitations concerning the visual perception interpretation of the images necessitate development of new analysis techniques that will improve diagnostic ability. One promising technique is texture analysis, which characterizes tissues by determine internal changes or characteristics of organs at the onset of disease.

1.4 Objectives:

1.4.1 General objective of this study:

To analyse the texture of computed tomography images of pancreas in Diabetic patient .

1.4.2 Specific objectives:

- To use an algorithm and function that can extract textural feature from CT images
- To extract texture feature from pancreas in diabetic patient
- To choose the discriminant subset of texture feature for classification
- To classify the textures features of the diabetic and normal pancreas
- To measure the dimensions of the pancreas
- To classify the pancreas in diabetic patient to head, body and tail using higher order statistic.
- To calculate the sensitivity, specificity and accuracy of the classification scheme.

Chapter Two

Theoretical background and previous studies

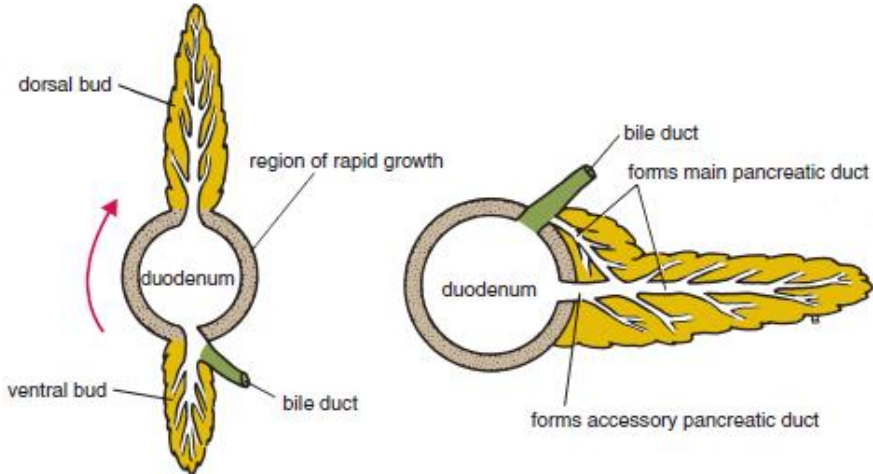
2.1 Embryonic Development of the pancreas:

The pancreas develops from a dorsal and ventral bud of entodermal cells that arise from the foregut. The dorsal bud originates a short distance above the ventral bud and grows into the dorsal mesentery. The ventral bud arises in common with the hepatic bud, close to the junction of the foregut with the midgut. A canalized duct system now develops in each bud. The rotation of the stomach and duodenum, together with the rapid growth of the left side of the duodenum, results in the ventral bud's coming into contact with the dorsal bud, and fusion occurs. (Fig2.1) Fusion also occurs between the ducts, so that the main pancreatic duct is derived from the entire ventral pancreatic duct and the distal part of the dorsal pancreatic duct. The main pancreatic duct joins the bile duct and enters the second part of the duodenum. (Richard S. Snell 2012)

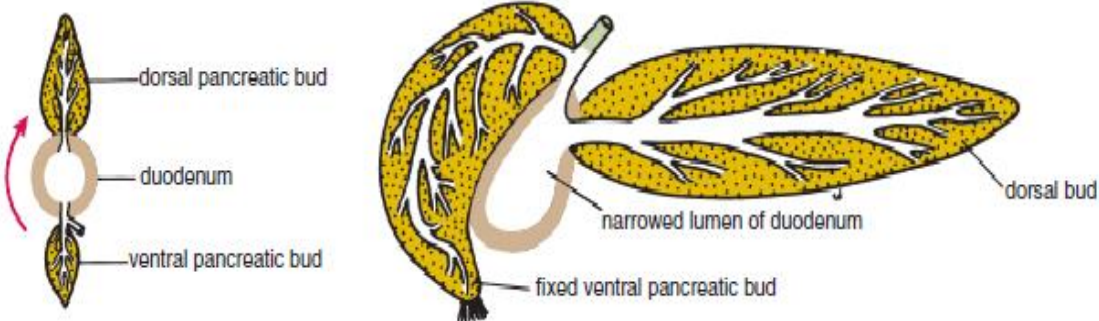
The proximal part of the dorsal pancreatic duct may persist as an accessory duct, which may or may not open into the duodenum about 0.75 in. (2 cm) above the opening of the main duct. Continued growth of the entodermal cells of the now fused ventral and dorsal pancreatic buds extends into the surrounding mesenchyme as columns of cells. These columns give off side branches, which later become canalized to form collecting ducts. Secretory acini appear at the ends of the ducts.

The pancreatic islets arise as small buds from the developing ducts. Later, these cells sever their connection with the duct system and form isolated groups of cells that start to secrete insulin and glucagon at about the 5th month. (Richard S. Snell 2012)

The inferior part of the head and the uncinete process of the pancreas are formed from the ventral pancreatic bud; the superior part of the head, the neck, the body, and the tail of the pancreas are formed from the dorsal pancreatic bud.(Fig2.1)



Fig(2.1) The rotation of the duodenum and the unequal growth of the duodenal wall lead to fusing of the ventral and dorsal pancreatic buds. (Richard S. Snell 2012)



Fig(2.2) Formation of the annular pancreas producing duodenal obstruction (Richard S. Snell 2012)

2.2 Anatomy of the Pancreas:

The pancreas lies in the upper abdomen behind the stomach. The pancreas is part of the gastrointestinal system that makes and secretes digestive enzymes into the intestine, and also an endocrine organ that makes and secretes hormones into the blood to control energy metabolism and storage throughout the body. It is worthwhile to mention a few definitions for key terms as used in the context of the pancreas: Exocrine pancreas, the portion of the pancreas that makes and secretes digestive enzymes into the duodenum. This includes acinar and duct cells with associated connective tissue, vessels, and nerves. The exocrine components comprise more than 95% of the pancreatic mass. And endocrine pancreas, the portions of the pancreas (the islets) that make and secrete insulin, glucagon, somatostatin and pancreatic polypeptide into the blood. Islets comprise 1-2% of pancreatic mass. Since we are dealing with a three dimensional solid structure, the aphorism that “a picture is worth a thousand words” seems to pertain accordingly. (Daniel S, et al, 2014).

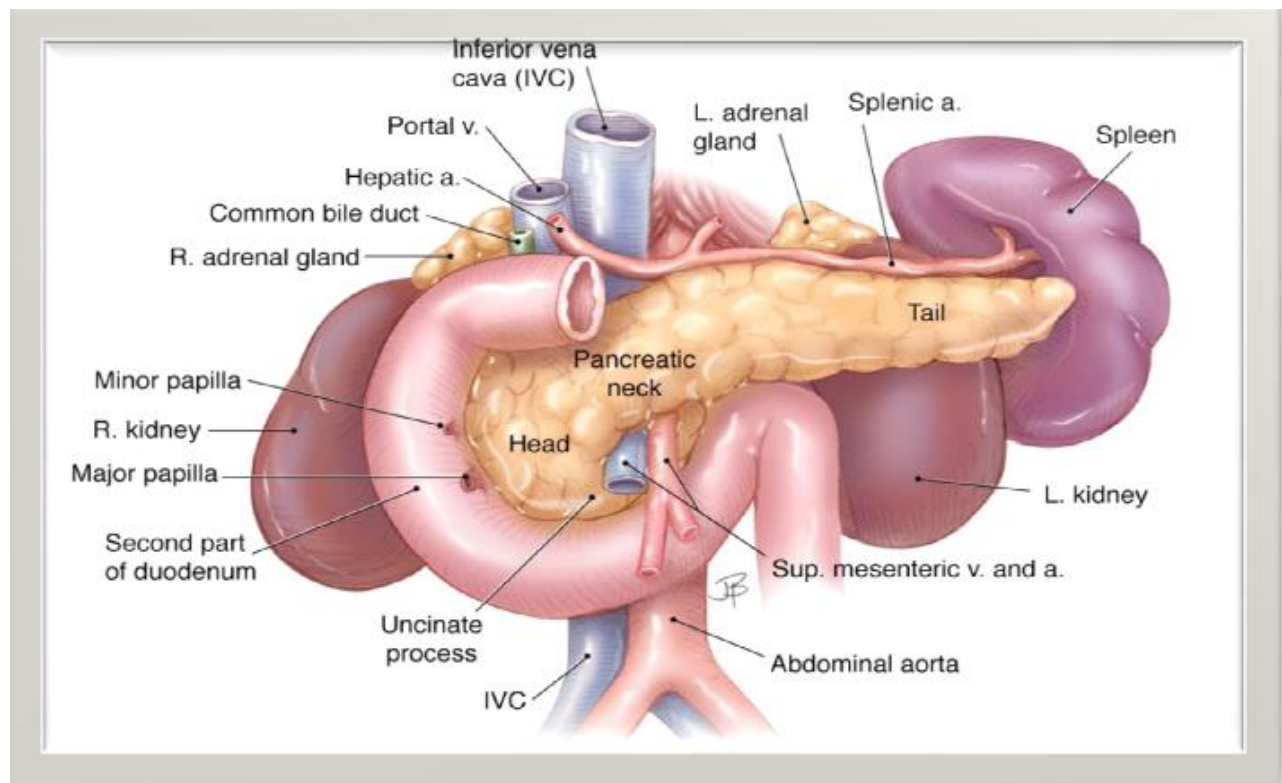


Figure.2.3 Anatomic relationships of the pancreas with surrounding organs and structures (Daniel S, et al, 2014).

2.2.1 Head of the pancreas

is the expanded part of the gland that is embraced by the C-shaped curve of the duodenum to the right of the superior mesenteric vessels just inferior to the trans pyloric plane. It firmly attaches to the medial aspect of the descending and horizontal parts of the duodenum. The uncinate process, a projection from the inferior part of the pancreatic head, extends medially to the left, posterior to the superior mesenteric artery. The pancreatic head rests posteriorly on the inferior vena cava, right renal artery and vein, and left renal vein. On its way to opening into the descending part of the duodenum, the bile duct lies in a groove on the posterosuperior surface of the head.(Moore, et al 2014)

2.2.2 Neck of the pancreas

Is short (1.5–2 cm) and overlies the superior mesenteric vessels, which form a groove in its posterior aspect. The anterior surface of the neck, covered with peritoneum, is adjacent to the pylorus of the stomach. The SMV joins the splenic vein posterior to the neck to form the hepatic portal vein. (Moore, et al 2014)

2.2.3 Body of the pancreas

Continues from the neck and lies to the left of the superior mesenteric vessels, passing over the aorta and L2 vertebra, continuing just above the trans pyloric plane posterior to the omental bursa. The anterior surface of the body of the pancreas is covered with peritoneum and lies in the floor of the omental bursa and forms part of the stomach bed. The posterior surface of the body is devoid of peritoneum and is in contact with the aorta, SMA, left suprarenal gland, left kidney, and renal vessels. (Moore, et al 2014)

2.2.4 Tail of the pancreas

Lies anterior to the left kidney, It is closely related to the splenic hilum and the left colic flexure. The tail is relatively mobile and passes between the layers of the splenorenal ligament with the splenic vessels. (Moore, et al 2014)

2.2.5 Main pancreatic duct

Begins in the tail of the pancreas and runs through the parenchyma of the gland to the pancreatic head, it turns inferiorly and is closely related to the bile duct. The main pancreatic duct and bile duct usually unite to form the short, dilated hepatopancreatic ampulla (of Vater), which opens into the descending part of the duodenum at the summit of the major duodenal papilla. At least 25% of the time, the ducts open into the duodenum separately. The sphincter of the pancreatic duct (around the terminal part of the pancreatic duct), the sphincter of the bile duct (around the termination of the bile duct), and the hepatopancreatic sphincter (of Oddi) are smooth muscle sphincters that control the flow of bile and pancreatic juice

into the ampulla and prevent reflux of duodenal content into the ampulla. (Moore, et al 2014)

2.2.6 Accessory pancreatic duct

Opens into the duodenum at the summit of the minor duodenal papilla. The accessory duct communicates with the main pancreatic duct. In some cases, the main pancreatic duct is smaller than the accessory pancreatic duct and the two may not be connected. In such cases, the accessory duct carries most of the pancreatic juice. (Moore, et al 2014)

2.2.7 Arterial supply of the pancreas

Is derived mainly from the branches of the markedly tortuous splenic artery. Multiple pancreatic arteries form several arcades with pancreatic branches of the gastroduodenal and superior mesenteric arteries. As many as 10 branches may pass from the splenic artery to the body and tail of the pancreas. The anterior and posterior superior pancreaticoduodenal arteries, branches of the gastroduodenal artery, and the anterior and posterior inferior pancreaticoduodenal arteries, branches of the SMA, form anteriorly and posteriorly placed arcades that supply the head of the pancreas. (Moore, et al 2014)

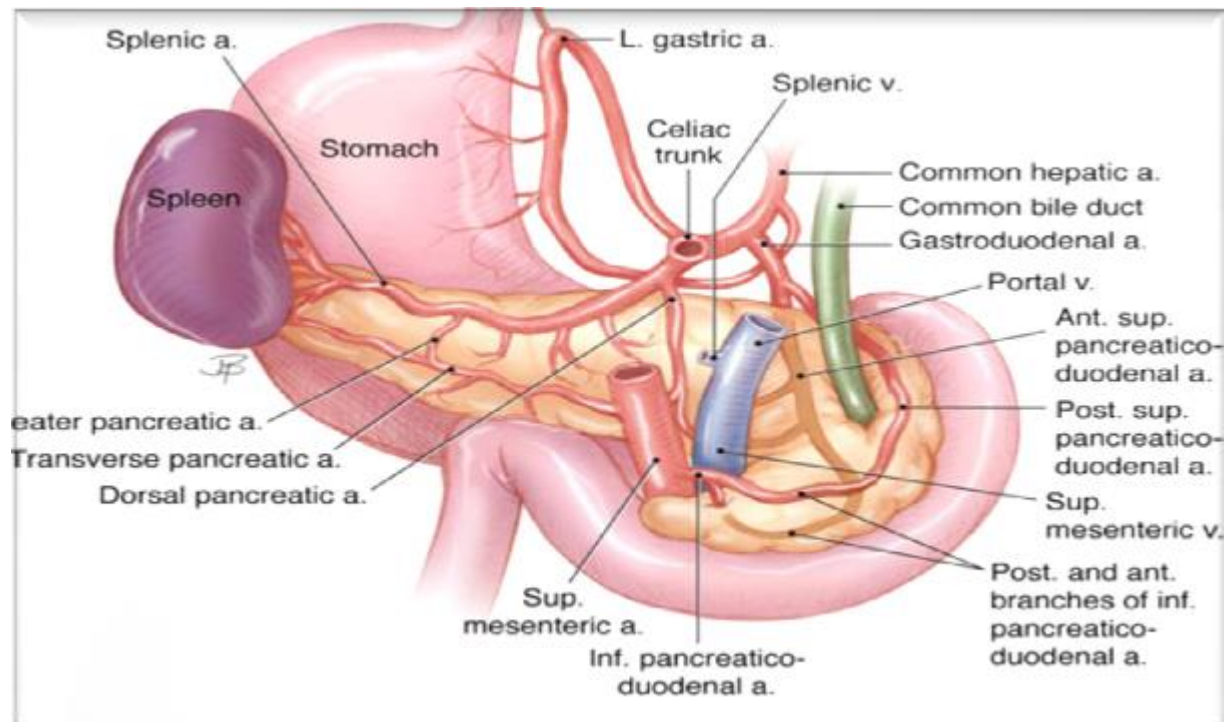


Figure 2.4. The arterial blood supply of the pancreas. (Doniel S, et al, 2014).

2.2.8 Venous drainage from the pancreas

occurs via corresponding pancreatic veins, tributaries of the splenic and superior mesenteric parts of the hepatic portal vein; most empty into the splenic vein. (Moore, et al 2014)

2.2.9 pancreatic lymphatic vessels

Most vessels end in the pancreaticosplenic lymph nodes, which lie along the splenic artery. Some vessels end in the pyloric lymph nodes. Efferent vessels from these nodes drain to the superior mesenteric lymph nodes or to the celiac lymph nodes via the hepatic lymph nodes. (Moore, et al 2014)

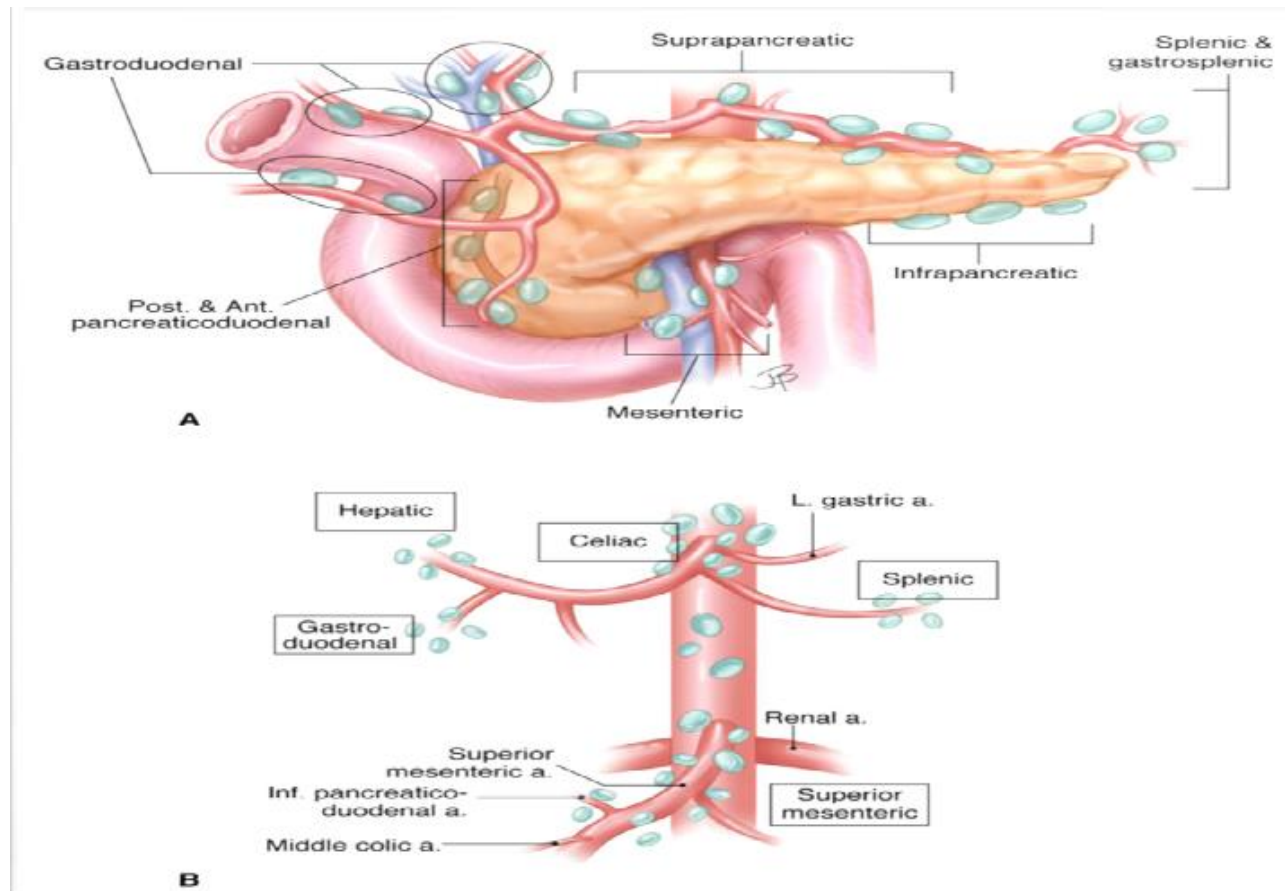


Figure 2.5. Lymph nodes draining the pancreas (Daniel S, et al 2014)

2.2.10 Nerves of the pancreas

Are derived from the vagus and abdominopelvic splanchnic nerves passing through the diaphragm. The parasympathetic and sympathetic fibers reach the pancreas by passing along the arteries from the celiac plexus and superior mesenteric plexus. In addition to sympathetic fibers that pass to blood vessels, sympathetic and parasympathetic fibers are distributed to pancreatic acinar cells and islets. The parasympathetic fibers are secretomotor, but pancreatic secretion is primarily mediated by secretin and cholecystokinin, hormones formed by the epithelial cells of the duodenum and proximal intestinal mucosa under the stimulus of acid contents from the stomach. (Moore, et al 2014)

2.3 Physiology of the pancreas:

The pancreas is a complex lobulated organ with distinct endocrine and exocrine elements. The endocrine portion constitutes only 1% to 2% of the pancreas and is composed of about 1 million cell clusters, the islets of Langerhans; these cells secrete insulin, glucagon, and somatostatin. (Eric. et al .2008)

The exocrine pancreas is composed of acinar cells that produce the digestive enzymes, and the ductules and ducts that convey them to the duodenum. The acinar cells produce mostly proenzyme forms of digestive enzymes and store them in membrane-bound zymogen granules. When acinar cells are stimulated to secrete, the granules fuse with the apical plasma membrane and release their contents into the central acinar lumen. (Eric. et al .2008)

These secretions are transported to the duodenum through a series of anastomosing ducts. The epithelial cells lining the ducts are also active participants in pancreatic secretion: cuboidal epithelial cells lining the smaller ductules secrete bicarbonate-rich fluid, while the columnar epithelial cells lining the larger ducts produce mucin, the exocrine products of the pancreas are secreted as enzymatically inert proenzymes (e.g. trypsinogen); amylase and lipase are exceptions and are secreted in an active form.(Eric. et al .2008)

The strategy of producing most pancreatic enzymes in an inactive zymogen form is largely to prevent self-digestion; it also focuses the eventual work of the activated enzymes to the duodenal lumen. The proenzymes remain largely inactive until they reach the duodenum; there, enteropeptidase (a brush-border enzyme) cleaves trypsinogen into active trypsin. Activated trypsin then functions to catalyze the cleavage of the other proenzymes. (Eric. et al .2008)

The majority of pancreatic enzymes are synthesized as inactive proenzymes. The proenzymes are sequestered in membrane-bound zymogen granules.Activation of proenzymes requires conversion of trypsinogen to trypsin by duodenal enteropeptidase (enterokinase).Trypsin inhibitors (e.g., serine protease inhibitor Kazal type I or SPINK1)

are also secreted by acinar and ductal cells. Trypsin contains a critical self-recognition cleavage site that allows trypsin to inactivate itself in situations wherein there is a high local concentration of activated enzyme.

Most of the secreted enzymes have acidic pH optima and are relatively inactive in the bicarbonate-rich pancreatic fluid. Enzymes within lysosomes can degrade zymogen granules if normal acinar secretion is blocked. Acinar cells are remarkably resistant to the action of activated enzymes such as trypsin, chymotrypsin, and phospholipase A₂. (Eric. et al .2008)

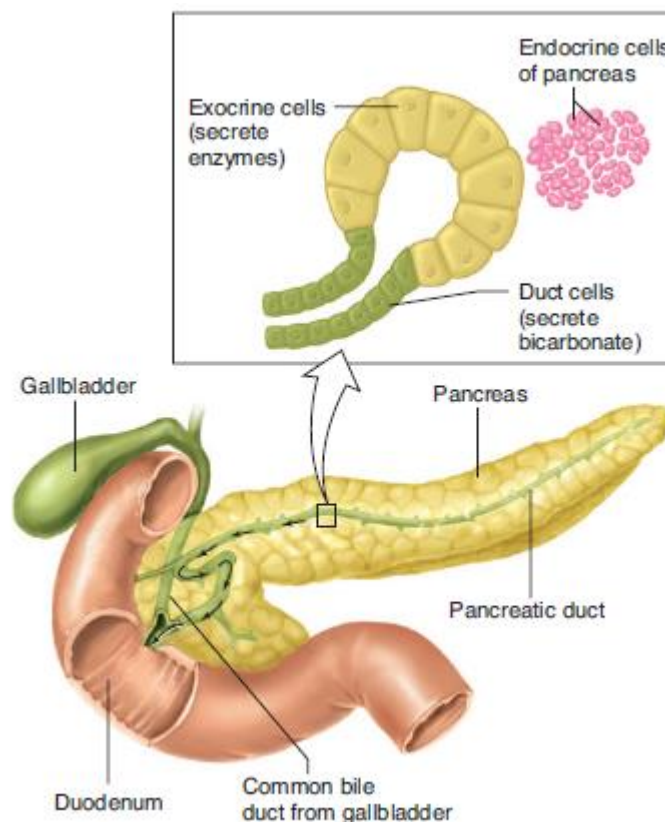


Fig 2.6 Structure of the pancreas (Eric. et al .2008)

2.3.1 Pancreatic Secretions

The exocrine portion of the pancreas secretes bicarbonate ions and a number of digestive enzymes into ducts that converge into the pancreatic duct, which joins the common bile duct from the liver just before it enters the duodenum. The enzymes are secreted by gland cells at the pancreatic end of the duct system, whereas bicarbonate ions are secreted by the epithelial cells lining the ducts. (Eric. et al .2008)

The mechanism of bicarbonate secretion is analogous to that of hydrochloric acid secretion by the stomach, except that the directions of hydrogen ion and bicarbonate ion movement are reversed. Hydrogen ions, derived from a carbonic anhydrase-catalyzed reaction between carbon dioxide and water, are actively transported out of the duct cells by an H⁺/K⁺-ATPase pump and released into the blood, while the bicarbonate ions are secreted into the duct lumen. (Eric. et al .2008)

The enzymes secreted by the pancreas digest fat, polysaccharides, proteins, and nucleic acids to fatty acids, sugars, amino acids, and nucleotides, respectively. The proteolytic enzymes are secreted in inactive forms (zymogens), as described for pepsinogen in the stomach, and then activated in the duodenum by other enzymes. Like pepsinogen, the secretion of zymogens protects pancreatic cells from autodigestion. A key step in this activation is mediated by enterokinase, which is embedded in the luminal plasma membranes of the intestinal epithelial cells. It is a proteolytic enzyme that splits off a peptide from pancreatic trypsinogen, forming the active enzyme trypsin. Trypsin is also a proteolytic enzyme, and once activated, it activates the other pancreatic zymogens by splitting off peptide fragments. This function is in addition to the role of trypsin in digesting ingested protein. The nonproteolytic enzymes secreted by the pancreas (for example, amylase and lipase) are released in fully active form. Pancreatic secretion increases during a meal, mainly as a result of stimulation by the hormones secretin and CCK. Secretin is the primary stimulant for bicarbonate secretion, whereas CCK mainly stimulates enzyme secretion. (Eric. et al .2008)

Since the function of pancreatic bicarbonate is to neutralize acid entering the duodenum from the stomach, it is appropriate that the major stimulus for secretin release is increased acidity in the duodenum. In analogous fashion, since CCK stimulates the secretion of digestive enzymes, including those for fat and protein digestion, it is appropriate that the stimuli for its release are fatty acids and amino acids in the duodenum. Luminal acid and fatty acids also act on afferent nerve endings in the intestinal wall, initiating reflexes that act on the pancreas to increase both enzyme and bicarbonate secretion. Thus, the organic nutrients in the small intestine initiate, via hormonal and neural reflexes, the secretions involved in their own digestion. Although most of the pancreatic exocrine secretions are controlled by stimuli arising from the intestinal phase of digestion, cephalic and gastric stimuli, by way of the parasympathetic nerves to the pancreas, also play a role. Thus, the taste of food or the distension of the stomach by food will lead to increased pancreatic secretion. (Eric. et al .2008)

2.3.2 Insulin

Insulin is the most important controller of organic metabolism. Its secretion, and thus plasma concentration, are increased during the absorptive state and decreased during the post absorptive state. The metabolic effects of insulin are exerted mainly on muscle cells (both cardiac and skeletal), adipose tissue cells, and liver cells. The effects of a reduction in plasma insulin are the same as the events of the post absorptive pattern. The reason for these correspondences is that an increased plasma concentration of insulin is the major cause of the absorptive-state events, and a decreased plasma concentration of insulin is the major cause of the post absorptive events. Like all peptide hormones, insulin induces its effects by binding to specific receptors on the plasma membrane of its target cells. This binding triggers signal transduction pathways that influence the plasma membrane transport proteins and intracellular enzymes of the target cell. For example, in muscle cells and adipose tissue cells an increased insulin concentration stimulates cytoplasmic vesicles that contain a particular type of glucose

transporter (GLUT-4) in their membrane to fuse with the plasma membrane. The increased number of plasma membrane glucose transporters resulting from this fusion then causes a greater rate of glucose movement from the extracellular fluid into the cells by facilitated diffusion. (Eric. et al .2008)

There are multiple subtypes of glucose transporters that mediate this process, and the subtype GLUT-4, which is regulated by insulin, is found mainly in muscle and adipose tissue cells. The insulin brings about its ultimate responses by multiple actions. Let us take its effects on muscle cells as an example. In these cells, insulin favors glycogen formation and storage by increasing glucose transport into the cell, stimulating the key enzyme (glycogen synthase) that catalyzes the rate-limiting step in glycogen synthesis, and inhibiting the key enzyme (glycogen phosphorylase) that catalyzes glycogen catabolism. Thus, insulin favors glucose transformation to and storage as glycogen in muscle through three pathways. Similarly, for protein synthesis in muscle cells, insulin increases the number of active plasma membrane transporters for amino acids, thereby increasing amino acid transportation to the cells, stimulates the ribosomal enzymes that mediate the synthesis of protein from these amino acids, and inhibits the enzymes that mediate protein catabolism. (Eric. et al .2008)

2.3.2.1 Control of Insulin Secretion

The major controlling factor for insulin secretion is the plasma glucose concentration. An increase in plasma glucose concentration, as occurs after a meal, acts on the B cells of the islets of Langerhans to stimulate insulin secretion, whereas a decrease inhibits secretion. Following a meal, the increase in plasma glucose concentration stimulates insulin secretion. The insulin stimulates the entry of glucose into muscle and adipose tissue, as well as net uptake, rather than net output, of glucose by the liver. These effects eventually reduce the blood concentration of glucose to its pre-meal level, thereby removing the stimulus for insulin secretion, which returns to its previous level.

In addition to plasma glucose concentration, there are many other insulin-secretion controls. For example, elevated amino acid concentrations stimulate insulin secretion. This is another negative feedback control: Amino acid concentrations increase after ingestion of a protein-containing meal, and the increased plasma insulin stimulates the uptake of these amino acids by muscle (and other cells as well). There are also important hormonal controls over insulin secretion. For example, a hormone-glucose dependent Insulinotropic peptide (GIP) secreted by endocrine cells in the gastrointestinal tract in response to eating stimulates the release of insulin. This response provides a feed forward component to glucose regulation during the ingestion of a meal. (Eric. et al .2008)

This mechanism minimizes the likelihood of large “spikes” in plasma glucose after a meal, the autonomic neurons to the islets of Langerhans also influence insulin secretion. Activation of the parasympathetic neurons, which occurs during the ingestion of a meal, stimulates the secretion of insulin and constitutes a second type of feed forward regulation. In contrast, activation of the sympathetic neurons to the islets or an increase in the plasma concentration of epinephrine (the hormone secreted by the adrenal medulla) inhibits insulin secretion. The significance of this relationship for the body’s response to low plasma glucose (hypoglycemia), stress, and exercise all situations in which sympathetic activity is increased. (Eric. et al .2008)

The insulin plays the primary role in controlling the metabolic adjustments required for feasting or fasting. Other hormonal and neural factors, also play significant roles. They all oppose the action of insulin in one way or another and are known as glucose counter regulatory controls. These hormonal and neural factors are glucagon, epinephrine, sympathetic nerve fibers, cortisol, and growth hormone. (Eric. et al .2008)

2.4 Pathology of the pancreas:

2.4.1 Congenital Anomalies

2.4.1.1 Agenesis

Very rarely, the pancreas may be totally absent, a condition usually (but not invariably) associated with additional severe malformations that are incompatible with life. Pancreatic duodenal homeobox 1 is a homeodomain transcription factor critical for normal pancreatic development, and mutations of the PDX1 gene, located on chromosomal locus 13q12.1, have been associated with pancreatic agenesis. (Vinay Kumar, et al 2013)

2.4.1.2 Anular Pancreas

In anular pancreas, the ventral pancreatic bud becomes fixed so that, when the stomach and duodenum rotate, the ventral bud is pulled around the right side of the duodenum to fuse with the dorsal bud of the pancreas, thus encircling the duodenum. This may cause obstruction of the duodenum, and vomiting may start a few hours after birth. Early surgical relief of the obstruction is necessary. (Kumar, et al 2013)

2.4.1.3 Ectopic Pancreas

Ectopic pancreatic tissue may be found in the submucosa of the stomach, duodenum, small intestine (including Meckel's diverticulum), and gallbladder, and in the spleen. It is important in that it may protrude into the lumen of the gut and be responsible for causing intussusception. (Kumar, et al 2013)

2.4.1.4 Congenital Fibrocystic Disease

Congenital fibrocystic disease in the pancreas is caused by an abnormality in the secretion of mucus. The mucus produced is excessively viscid and obstructs the pancreatic duct, which leads to pancreatitis with subsequent fibrosis. The condition also involves the lungs, kidneys, and liver. (Kumar, et al 2013)

2.4.1.5 Pancreas divisum

Is the most common clinically significant congenital pancreatic anomaly, with an incidence of 3% to 10% in autopsy series. It occurs when the duct systems of the fetal pancreatic primordia fail to fuse. As a result, the main pancreatic duct drains only a small portion of the head of the gland, while the bulk of the pancreas (from the dorsal pancreatic primordium) drains through the minor sphincter, which has a narrow opening. As a result of this defect in drainage, persons with pancreas divisum have elevated intraductal pressures throughout most of the pancreas and are at increased risk for chronic pancreatitis.(Kumar, et al 2013)

2.4.2 Trauma of the Pancreas

The pancreas is deeply placed within the abdomen and is well protected by the costal margin and the anterior abdominal wall. Blunt trauma, such as in a sports injury when a sudden blow to the abdomen occurs, can compress and tear the pancreas against the vertebral column. The pancreas is most commonly damaged by gunshot or stab wounds. Damaged pancreatic tissue releases activated pancreatic enzymes that produce the signs and symptoms of acute peritonitis.(Kumar, et al 2013)

2.4.3Pancreatitis

Inflammatory disorders of the pancreas range in severity from mild, self-limited disease to life-threatening, widely destructive process, and are accordingly associated with deficits that may be trivial and transient or serious and permanent. In acute pancreatitis, function can return to normal if the underlying cause of inflammation is removed. By contrast, chronic pancreatitis is defined by irreversible destruction of exocrine pancreatic parenchyma.(Kumar, et al 2013)

2.4.3.1 Acute Pancreatitis

Acute pancreatitis is a reversible inflammatory disorder that varies in severity, ranging from focal edema and fat necrosis to widespread hemorrhagic parenchymal necrosis.

Acute pancreatitis is relatively common, with an annual incidence of 10 to 20 per 100,000 people in the Western world. Approximately 80% of cases are attributable to either biliary tract disease or alcoholism. Roughly 5% of patients with gallstones develop acute pancreatitis, and gallstones are implicated in 35% to 60% of cases overall. (Kumar, et al 2013)

2.4.3.2 Chronic Pancreatitis

Chronic pancreatitis is characterized by long-standing inflammation, fibrosis, and destruction of the exocrine pancreas; in its late stages, the endocrine parenchyma also is lost. Although chronic pancreatitis can result from recurrent bouts of acute pancreatitis, the chief distinction between acute and chronic pancreatitis is the irreversible impairment in pancreatic function in the latter. The prevalence of chronic pancreatitis is difficult to determine but probably ranges between 0.04% and 5% of the U.S. population. By far the most common cause of chronic pancreatitis is long-term alcohol abuse; middle-aged men constitute the bulk of patients in this etiologic group. (Kumar, et al 2013)

As many as 40% of persons with chronic pancreatitis have no recognizable predisposing factors. As with acute pancreatitis, a growing number of these “idiopathic” cases are associated with inherited mutations in genes important for normal pancreatic exocrine function. For example, genetic testing reveals that 25% to 30% of patients with “idiopathic” pancreatitis harbor germ line mutations in the *CFTR* gene, albeit distinct from the ones that lead to classic multisystem cystic fibrosis. (Kumar, et al 2013)

2.4.4 Pancreatic duct obstruction

Impaction of a gallstone or biliary sludge, or extrinsic compression of the ductal system by a mass blocks ductal flow, increases intraductal pressure, and allows accumulation of an enzyme-rich interstitial fluid. Since lipase is secreted in an active

form, local fat necrosis may result. Injured tissues, periacinar myofibroblasts, and leukocytes then release proinflammatory cytokines that promote local inflammation and interstitial edema through a leaky microvasculature. Edema further compromises local blood flow, causing vascular insufficiency and ischemic injury to acinar cells. (Vinay Kumar, et al 2013)

2.4.5 Defective intracellular transport of proenzymes within acinar cells

In normal acinar cells, digestive enzymes intended for zymogen granules (and eventually extracellular release) and hydrolytic enzymes destined for lysosomes are transported in discrete pathways after synthesis in the endoplasmic reticulum, at least in some animal models of metabolic injury, pancreatic proenzymes and lysosomal hydrolases become packaged together. This results in proenzyme activation, lysosomal rupture (action of phospholipases), and local release of activated enzymes. The role of this mechanism in human acute pancreatitis is not clear. (Vinay Kumar, et al 2013)

2.4.6 Pancreatic Pseudocysts

A common sequela of acute pancreatitis (and in particular, alcoholic pancreatitis) is a pancreatic pseudocyst. Liquefied areas of necrotic pancreatic tissue become walled off by fibrous tissue to form a cystic space, lacking an epithelial lining (hence the designation pseudo). The cyst contents are rich in pancreatic enzymes, and a laboratory assessment of the cyst aspirate can be diagnostic. Pseudocysts account for approximately 75% of all pancreatic cysts. While many pseudocysts spontaneously resolve, they can become secondarily infected, and larger pseudocysts can compress or even perforate into adjacent structures. (Vinay Kumar, et al 2013)

2.4.7 Cystic Neoplasms

Only 5% to 15% of all pancreatic cysts are neoplastic; these constitute less than 5% of all pancreatic neoplasms. Some of these are entirely benign (e.g., serous cystadenoma); others, such as mucinous cystic neoplasms, can be benign or malignant. (Vinay Kumar, et al 2013)

2.4.8 Serous Cystadenomas

Serous cystadenomas account for approximately 25% of all pancreatic cystic neoplasms; they are composed of glycogen-rich cuboidal cells surrounding small cysts containing clear, straw-colored fluid. The tumors typically manifest in the seventh decade of life with nonspecific symptoms such as abdominal pain; the female-to-male ratio is 2 : 1. These tumors are almost uniformly benign, and surgical resection is curative in the vast majority of patients. Most serous cystadenomas carry somatic mutations of the von Hippel-Lindau (VHL) tumor suppressor gene, the product of which binds to hypoxia-inducible factor 1 alpha (HIF1alpha) and results in its degradation. (Vinay Kumar, et al 2013)

2.4.9 Mucinous Cystic Neoplasms

Close to 95% of mucinous cystic neoplasms arise in women, usually in the body or tail of the pancreas, and manifest as painless, slow-growing masses. The cystic spaces are filled with thick, tenacious mucin, and the cysts are lined by a columnar mucinous epithelium with an associated densely cellular stroma resembling that of the ovary.

Based on the degree of cytologic and architectural atypia in the lining epithelium, noninvasive mucinous cystic neoplasms are classified as harboring *low-grade*, moderate, or severe dysplasia. Up to one third of these cysts can be associated with an invasive adenocarcinoma. Distal pancreatectomy for noninvasive cysts typically is curative, even in the setting of severe dysplasia. (Vinay Kumar, et al 2013)

2.4.10 Pancreatic Carcinoma

Infiltrating ductal adenocarcinoma of the pancreas (more commonly referred to as “pancreatic cancer”) is the fourth leading cause of cancer death in the United States, preceded only by lung, colon, and breast cancers. Although it is substantially less common than the other three malignancies, pancreatic carcinoma is near the top of the list of killers because it carries one of the highest mortality rates. Over 44,000 Americans were diagnosed with pancreatic cancer in 2010, and virtually all will die of it; the 5-year survival rate is dismal—less than 5%. Sadly, Ralph Steinman, one of the 2011 Nobel

Laureates in physiology or medicine died of pancreatic cancer, three days before the announcement of his award. (Vinay Kumar, et al 2013)

2.4.10.1 Clinical Features

Carcinomas of the pancreas typically remain silent until their extension impinges on some other structure. Pain usually is the first symptom, but by that point these cancers are often beyond cure. Obstructive jaundice can be associated with carcinoma in the head of the pancreas, but it rarely draws attention to the cancer soon enough for timely intervention. Weight loss, anorexia, and generalized malaise and weakness are manifestations of advanced disease. Migratory thrombophlebitis (Trousseau syndrome) occurs in about 10% of patients and is attributable to the elaboration of platelet aggregating factors and pro-coagulants from the tumor or its necrotic products. (Vinay Kumar, et al 2013)

The clinical course of pancreatic carcinoma is rapidly progressive and distressingly brief. Less than 20% of pancreatic cancers are resectable at the time of diagnosis. It has long been recognized that there is a profound need for biomarkers capable of detecting early, potentially curable, pancreatic cancers. Although serum levels of many enzymes and antigens (e.g., carcinoembryonic and CA19-9 antigens) are elevated, these markers are neither specific nor sensitive enough to be useful for screening. Several imaging techniques, such as endoscopic ultrasonography and high-resolution CT scans, are helpful for investigation in cases of suspected cancer but are not useful as screening tests. (Vinay Kumar, et al 2013)

2.4.11 Overview: Diabetes mellitus (DM)

Is a common disease in which the blood sugar (glucose) is abnormally elevated. Normally, the body obtains glucose from food The produces insulin, which enables glucose to enter cells and serve as fuel for the body. In patients with diabetes, glucose accumulates in the blood instead of being properly transported into cells. Excess blood sugar is a serious problem that may damage the blood vessels, and other organs (Carla,

2011). Diabetes can be due to a deficiency of insulin, or to a decreased responsiveness to insulin. Thus, diabetes is not one but several diseases with different causes. Classification of these diseases rests on how much insulin a person's pancreas is secreting. In type 1 diabetes mellitus (T1DM; formerly called insulin-dependent diabetes mellitus), insulin is completely or almost completely absent from the islets of Langerhans and the plasma. (Eric. et al .2008)

In type 2 diabetes mellitus (T2DM, formerly called non-insulin dependent diabetes mellitus), insulin is usually present in plasma at nearly normal or even above-normal levels, and therapy does not normally require insulin administration (although in roughly one-third of T2DM patients, insulin therapy is beneficial). T1DM is less common, affecting approximately 10 percent of diabetic patients in the United States. T1DM is due to the total or near-total destruction of the pancreatic beta cells by the body's own white blood cells. The triggering events for this autoimmune response are not yet fully established. (Eric. et al .2008)

Treatment of T1DM always involves the administration of insulin (by injection, since oral administration of insulin would not be effective due to the actions of gastrointestinal enzymes). It is very likely that future therapies for T1DM will make use of alternative routes of insulin administration, such as inhalers and nasal sprays. It is also possible that transplantation of normal islet cells into a person with T1DM will someday prove to be an effective therapy. Administration of insulin by any route, however, is not a cure for T1DM. Ultimately, the cure for T1DM will involve prevention of the autoimmune response. (Eric. et al .2008)

Because of insulin deficiency, untreated patients with T1DM always have elevated glucose concentrations in their blood. The increase in glucose occurs because glucose fails to enter insulin's target cells normally, and the liver continuously makes glucose by glycogenolysis and gluconeogenesis, and secretes the glucose into the blood. Recall

also that insulin normally suppresses lipolysis and ketone formation. Thus, another result of the insulin deficiency is pronounced lipolysis with subsequent elevation of plasma glycerol and fatty acids. Many of the fatty acids are then converted by the liver into ketones. (Eric. et al .2008)

If extreme, these metabolic changes culminate in the acute life-threatening emergency called diabetic ketoacidosis. Some of the problems are due to the effects that extremely elevated plasma glucose concentration produces on renal function. The elevated plasma glucose of diabetes increases the filtered load of glucose beyond the maximum tubular re absorptive capacity, and therefore large amounts of glucose are excreted. For the same reasons, large amounts of ketones may also appear in the urine. These urinary losses deplete the body of nutrients and lead to weight loss. The fact that of these un reabsorbed solutes cause an osmotic diuresis increased urinary excretion of sodium and water, which can lead to hypotension, brain damage, and death. The other serious abnormality in diabetic ketoacidosis is the increased plasma hydrogen ion concentration caused by the accumulation of ketones. Two ketones, known as hydroxybutyric acid and acetoacetic acid, are acidic at the pH of blood. This increased hydrogen ion concentration causes brain dysfunction that can contribute to the development of coma and death. (Eric.P et al .2008)

Diabetic ketoacidosis is seen primarily in patients with untreated T1DM. About 90 percent of diabetics are in the T2DM category and rarely develop metabolic derangements severe enough to go into diabetic ketoacidosis. T2DM is a disease mainly of overweight adults, typically starting in middle life. Given the earlier mention of progressive weight loss in T1DM as a symptom of diabetes. One major problem is target cell hypo responsiveness to insulin, termed insulin resistance. Obesity accounts for much of the insulin resistance in T2DM. Is that the excess adipose tissue overproduces a messenger that causes down regulation of insulin-responsive glucose transporters or in some other way blocks insulin's actions. One

putative messenger, or hormone, has been named resistin, but its physiological actions are still under investigation. In addition, components (possibly genetic) of insulin resistance, not related to obesity and not yet understood, may also occur with T2DM. (Eric. et al .2008)

Most people with T2DM not only have insulin resistance but also have a defect in the ability of their beta cells to secrete insulin in response to a rise in plasma glucose concentration. Insulin resistance is the primary factor inducing hyperglycemia in T2DM, an as-yet-unidentified defect in beta cell function prevents these cells from responding maximally to the hyperglycemia. (Eric. et al .2008)

The most effective therapy for obese persons with T2DM is weight reduction, since obesity is a major cause of insulin resistance. An exercise program is also very important, because insulin responsiveness is increased by frequent endurance-type exercise, independent of changes in body weight. If plasma glucose concentration is not adequately controlled by a program of weight reduction, exercise, and dietary modification (specifically low-fat diets), then the person may be given orally active drugs that lower plasma glucose concentration by a variety of mechanisms. The sulfonylureas lower plasma glucose by acting on the beta cells to stimulate insulin secretion. Other drugs increase insulin sensitivity or decrease hepatic gluconeogenesis. A people with either form of diabetes mellitus tend to develop a variety of chronic abnormalities, including atherosclerosis, kidney failure, small-vessel and nerve disease, susceptibility to infection, and blindness. Elevated plasma glucose contributes to most of these abnormalities either by causing the intracellular accumulation of certain glucose metabolites that exert harmful effects on cells when present in high concentrations, or by linking glucose to proteins, thereby altering their function. The reason for this is that insulin normally inhibits glucagon secretion, and the low insulin of T1DM releases glucagon secretion from this inhibition. Finally, as we have seen, all the systems that increase plasma glucose concentration are activated during stress,

which explains why stress worsens the symptoms of diabetes. Since diabetic ketoacidosis itself constitutes a severe stress, a positive feedback cycle is triggered in which a lack of insulin induces ketoacidosis, which elicits activation of the glucose-counter regulatory systems, which worsens the ketoacidosis. (Eric.P et al .2008)

Long-term complications of diabetes include retinopathy with potential loss of vision; nephropathy leading to renal failure; peripheral neuropathy with risk of foot ulcers, amputations, and Charcot joints; and autonomic neuropathy causing gastrointestinal, genitourinary, and cardiovascular symptoms and sexual dysfunction. Patients with diabetes have an increased incidence of atherosclerotic cardiovascular, peripheral arterial, and cerebrovascular disease. Hypertension and abnormalities of lipoprotein metabolism are often found in people with diabetes. (American Diabetes Association, 2014).

2.5 Computerized Tomography Scanning(Over View)

Computed tomography uses a computer to process information collected from the passage of x-ray beams through an area of anatomy. The images created are cross-sectional. To visualize CT, the often-used loaf of bread analogy is useful. If the patient's body is imagined to be a loaf of bread, each CT slice correlates to a slice of the bread. The crust of the bread is analogous to the skin of the patient's body; the white portion of the bread, the patient's internal organs.(Lois.2011)

The individual CT slice shows only the parts of the anatomy imaged at a particular level. For example, a scan taken at the level of the sternum would show portions of lung, mediastinum, and ribs, but would not show portions of the kidneys and bladder. Computed tomography requires a firm knowledge of anatomy, in particular the understanding of the location of each organ relative to others. (Lois.2011)

Each CT slice represents a specific plane in the patient's body. The thickness of the plane is referred to as the Z axis. The Z axis determines the thickness of the slices.

The operator selects the thickness of the slice from the choices available on the specific scanner. Selecting a slice thickness limits the x-ray beam so that it passes only through this volume; hence, scatter radiation and superimposition of other structures are greatly diminished. Limiting the x-ray beam in this manner is accomplished by mechanical hardware that resembles small shutters, called collimators, which adjust the opening based on the operator's selection.

The data that form the CT slice are further sectioned into elements: width is indicated by X , while height is indicated by Y . Each one of these two-dimensional squares is a pixel (picture element). A composite of thousands of pixels creates the CT image that displays on the CT monitor. If the Z axis is taken into account, the result is a cube, rather than a square. This cube is referred to as a voxel (volume element). (Lois.2011)

A matrix is the grid formed from the rows and columns of pixels. In CT, the most common matrix size is 512. This size translates to 512 rows of pixels down and 512 columns of pixels across. The total number of pixels in a matrix is the product of the number of rows and the number of columns, in this case 512×512 (262,144). Because the outside perimeter of the square is held constant, a larger matrix size (i.e., 1,024 as opposed to 512) will contain smaller individual pixels. Each pixel contains information that the system obtains from scanning. Is completely absorbed by an object cannot be detected; the place on the image is white. An object that has the ability to absorb much of the x-ray beam is often referred to as having high attenuation. Areas of intermediate attenuations are represented by various shades of gray. (Lois.2011)

The number of the photons that interact depends on the thickness, density, and atomic number of the object. Density can be defined as the mass of a substance per unit volume. More simply, density is the degree to which matter is crowded together, or concentrated. For example, a tightly packed snowball has a higher density than a loosely packed one. Dense elements, those with a high atomic number,

have many circulating electrons and heavy nuclei and, therefore, provide more opportunities for photon interaction than elements of less density.

To better understand how these physical properties of an object affect the degree of beam attenuation, envision a single x-ray photon passing through an object. The more atoms in its path (the greater the object's thickness and density), the more likely that an atom in the object will interact with the photon. Similarly, the more electrons, neutrons, and protons in each atom, the higher the likelihood of photon interaction. Therefore, the number of photons that interact increases with the density, thickness, and atomic number of the object. (Lois.2011)

2.5.1 Helical Scanning

in the late 1980s, helical CT has revolutionized clinical imaging. Also called spiral (or continuous acquisition) scanning, helical scanning brought dramatic improvement in scanning speed by eliminating the inter scan delay. There are three basic ingredients that define a helical scan process: a continually rotating x-ray tube, constant x-ray output, and uninterrupted table movement. Increasing the scan speed results in improved image resolution owing to the ability to obtain images with improved iodinated contrast concentration, decreased respiratory and cardiac motion artifact, and superior multiplanar and three dimensional reformation capabilities. In addition to improved diagnostic accuracy, the speed associated with helical scanning is also beneficial in regards to patient comfort and department productivity.(Lois.2011)

Helical scanners were constructed with a single row of detectors. Since then, multi detectors computed tomography systems with as many as 64 detector rows have been introduced. By further improving scan speed, these systems have made clinical applications, such as computed tomography angiography and virtual bronchoscopy, feasible. This section briefly reviews the technology of helical scanning from its inception to current day. In much the same way that a student must first learn

arithmetic before studying algebra, we first review the evolution of single-detector helical systems before moving to the more complicated MDCT systems.(Lois .2011)

2.5.1.1 Historical Perspective

Many of the long-standing problems with standard axial CT were overcome with the introduction of helical scanning. Helical scanning offers many advantages, including the ability to optimize iodinated contrast agent administration, the reduction of respiratory mis registration, and the reduction of motion artifacts from organs such as the heart. Helical scanning is often referred to as volumetric scanning. This refers to the fact that the end result of such a scanning method is a block of data, not separate slices, as occurs in traditional axial scanning. Acquiring information in a volume allows data manipulation possibilities not previously available with the older axial methods. However, it is important to remember that although the end result is a block of data, in the majority of cases the information is acquired in ribbons and not a block at a time, thus placing certain limitations on data manipulation.

To take helical scanning from theory to practice, many obstacles associated with traditional axial CT had to be overcome. The major improvements leading to its development were 1) x-ray gantries with a slip ring design, 2) more-efficient tube cooling, 3) higher x-ray output (i.e., increased mA capability), 4) smoother table movement, 5) software that adjusts for table motion, 6) improved raw data management, and 7) more-efficient detectors. (Lois .2011)

2.5.2 Slip Rings

Before helical scanning systems, CT gantries moved first in one direction, then stopped as the table moved to the next position. The gantry then reversed direction for the next acquisition. Each 360° rotation produced one image. On these older systems, when the x-ray tube stops to move in the opposite direction, all the momentum is lost, considerably slowing the scan process. In contrast, within newer systems slip rings allow the tube to move continually in the same direction. Slip ring

technology eliminates cumbersome electrical cables and makes possible a data-gathering system using a continuous rotation of the x-ray source. The x-ray source can reach much higher speeds, thereby decreasing the time necessary for each data acquisition. Before slip ring technology scanners took from 2 to 5 seconds to complete a single rotation, whereas a slip ring scanner can rotate in 1 second or less. Also important is the role slip ring technology plays in eliminating the inter scan delay. In conventional scanning, this is the time required between each acquisition when the table moves to the next scan position and the scanner readies itself for the next acquisition. On older CT systems, this inter scan delay could range from 3 to 15 seconds per slice. (Lois .2011)

2.5.3Pitch

During a helical scan acquisition, the x-ray tube is continually on while the table moves through the gantry. Pitch is a parameter that is commonly used to describe the CT table movement. It is most commonly defined as the travel distance of the CT scan table per 360° rotation of the x-ray tube, divided by the x-ray beam collimation width. When the table feed and beam collimations are identical, pitch is 1. When the table feed is less than the beam collimation, pitch is less than 1 and scan overlap occurs. (Lois .2011)

2.5.3.1Pitch in MDCT Systems

The simultaneous data acquisition from parallel rows of detectors requires rapid table advancement during scanning. MDCT stretches our earlier concept of pitch. Pitch is still defined as the relationship between slice thickness and table travel per rotation. But we must remember that the terms collimation and slice thickness are no longer synonymous (Fig. 5-15). This detail has given rise to more than one definition of pitch as it relates to MDCT systems. The most common definition is referred to as beam pitch, and relates more closely. Increasing the pitch will result in a scan covering more anatomy lengthwise for a given total acquisition time. It will also

reduce the radiation dose to the patient. A decrease in pitch slows down the table speed. A pitch of less than 1 will result in overlapping slices. Therefore, decreasing the pitch will decrease the amount of anatomy to the definition established in SDCT. Beam pitch can be defined as table movement per rotation divided by beam width. The beam width can be determined by multiplying the number of slices by slice thickness. (Lois .2011)

2.5.4MDCT:

MDCT, known as multislice, multidetector CT .Systems offer opportunities for retrospectively changing slice thickness that are not available on SDCT systems. The choices available for the reconstructed slice thickness are not unlimited, even with the MDCT scanners. It is important to keep in mind that the thinnest images that can be reconstructed for a data set are predetermined by the slice thickness used for the data acquisition. The degree that the acquired slice thickness limits the reconstructed slice thickness varies according to manufacturer and specific model of scanner (information is included in the product literature). On all systems images acquired at a thin slice thickness, 0.5 mm for example, can be added together to create a thicker slice for viewing. Hence, four slices of 0.5 mm each could be combined to create a 2-mm slice for viewing. However, on many systems the reverse is not true. That is, if the data are acquired with a slice thickness of 2 mm, the data cannot retrospectively be divided to produce four 0.5-mm slices. In addition, even on scanners that allow the wider slice to be divided retrospectively, scan parameters (mAs and kvp) that are adequate for the wider slice may be insufficient for good image quality in a narrower slice produced from the same data. It is important to remember with MDCT that there is a fundamental difference in how the images are acquired and how they are viewed. This difference has resulted in the necessity to differentiate between slice thickness (how the data were acquired) and image thickness (how the data are reconstructed). To restate, the image thickness may be greater than the slice

thickness, but the image thickness should not be less than the slice thickness.(Lois.2011)

2.6 Texture Analysis

Texture is one of the important characteristics used in identifying objects or regions of interest in an image, whether the image be a photomicrograph, an aerial photograph, or a satellite image. In recent years, medical CT Images have been applied in clinical diagnosis widely. That can assist physicians to detect and locate Pathological changes with more accuracy. Computed Tomography images can be distinguished for different tissues according to their different gray levels. The images, if processed appropriately can offer a wealth of information which is significant to assist doctors in medical diagnosis. A lot of research efforts have been directed towards the field of medical image analysis with the aim to assist in diagnosis and clinical studies.(Duncan. 2000)

It also helps the radiologist in analyzing the digital images to bring out the possible outcomes of the diseases. The medical images are obtained from different imaging systems such as MRI scan, CT scan and Ultra sound B scan. The computerized tomography has been found to be the most reliable method for early detection of tumors because this modality is the mostly used in radio therapy planning for two main reasons. The first reason is that scanner images contain anatomical information which offers the possibility to plan the direction and the entry points of radio therapy rays which have to target only the tumor region and to avoid other organs. (Duncan. 2000)

The second reason is that CT scan images are obtained using rays, which is same principle as radio therapy. This is very important because the intensity of radio therapy rays have been computed from the scanned image. Image texture, defined as a function of the spatial variation in pixel intensities (gray values), is useful in a

variety of applications and has been a subject of intense study by many researchers. One immediate application of image texture is the recognition of image regions using texture properties. Texture is the most important visual cue in identifying these types of homogeneous regions. This is called texture classification. Image analysis techniques have played an important role in several medical applications. In general, the applications involve the automatic extraction of features from the image which is then used for a variety of classification tasks, such as distinguishing normal tissue from abnormal tissue. Depending upon the particular classification task, the extracted features capture morphological properties, color properties, or certain textural properties of the image.(Tourassi,1999)

Texture is a combination of repeated patterns with a regular frequency. In visual interpretation texture has several types, for example, smooth, fine, coarse etc., which are often used in the classification of forest types. Texture analysis is defined as the classification or segmentation of textural features with respect to the shape of a small element, density and direction of regularity. In the case of digital image, it is difficult to 24 treat the texture mathematically because texture cannot be standardized quantitatively and the data volume is so huge. (Tourassi,1999)

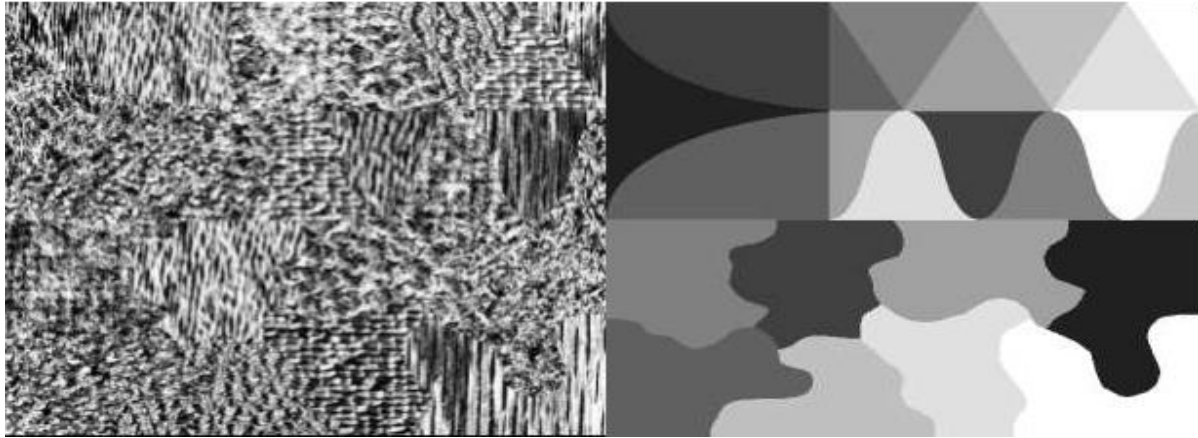


Fig. 2.7 Example of image segmentation using texture analysis to determine the boundary between distinct regions of texture. Left, mosaic image of eight Brodatz textures represented in approximately equal proportions. Right, grey-level texture map showing the ideal segmentation of the textures (Weber, 2004).

2.6.1 Texture Analysis Types

Approaches to texture analysis are usually categorized into: Structural, Statistical, Model-based and Transform.

2.6.1.1 Statistical Approaches for Texture Analysis

To examine an image using texture analysis the image is treated as a 3D textured surface. In first-order statistical texture analysis, information on texture is extracted from the histogram of image intensity. This approach measures the frequency of a particular grey-level at a random image position and does not take into account correlations, or co-occurrences, between pixels. In second-order statistical texture analysis, information on texture is based on the probability of finding a pair of grey-levels at random distances and orientations over an entire image. Extension to higher-order statistics involves increasing the number of variables studied. Many conventional approaches used to study texture have concentrated on using 2D techniques to compute features relating to image texture. This traditional approach has been used extensively to describe different image

textures by unique features and has found application in many disparate fields such as: discrimination of terrain from aerial photographs (Connors & Harlow, 1980); in vitro classification of tissue from intravascular ultrasound (Nailon, 1997); identification of prion protein distribution in cases of Creutzfeldt-Jakob disease (CJD) (Nailon & Ironside, 2000); classification of pulmonary emphysema from lung on high-resolution CT images (Uppaluri et al., 1997; Xu et al., 2004; Xu et al., 2006); and identifying normal and cancerous pathology (Karahaliou et al., 2008, Zhou et al., 2007; Yu et al., 2009). Higher-order approaches have been used to localise thrombotic tissue in the aorta (Podda, 2005) and to determine if functional vascular information found in dynamic MR sequences exists on anatomical MR sequences (Winzenrieth, 2006).

Extension of these approaches to 3D is continuing to develop within the machine vision community. Several authors have reported the application of 2D texture analysis methods on a slice-by-slice basis through volumetric data, however, it has been reported that with this approach information may be lost (Kovalev et al., 2001; Kurani et al., 2004). Findings reported by Xu et al., on the use of 3D textural features for discriminating between smoking related lung pathology, demonstrate the power of this approach for this particular application (Xu et al., 2006). Kovalev et al., showed that an extended 3D co-occurrence matrix approach can be used for the classification and segmentation of diffuse brain lesions on MR image data (Kovalev et al., 2001).

Texture analysis has also been used to identify unique pathology on multi-modality images of cancer patients. Using the local binary operator to analyze the weak underlying textures found in transrectal ultrasound images of the prostate, Kachouie and Fieguth demonstrated that the approach was suitable for segmentation of the prostate (Kachouie & Fieguth, 2007).

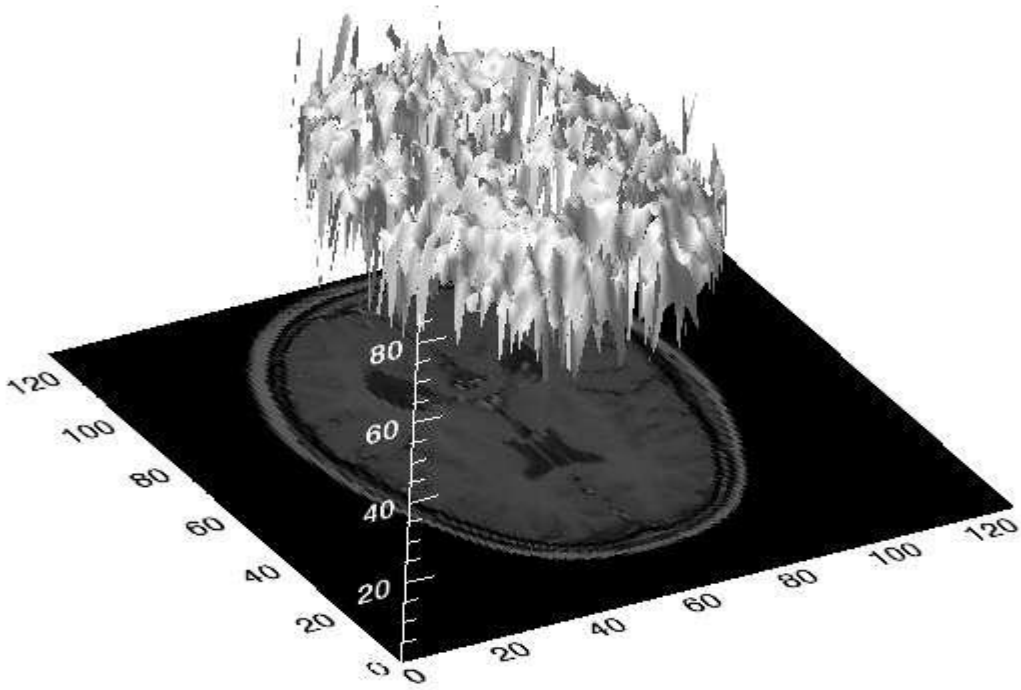


Fig. 2.8. Three-dimensional textured intensity surface representation of a medical image. A: Two- dimensional magnetic resonance image of the brain. B: Pixel values of the magnetic resonance image plotted on the vertical axis to produce a 3D texture surfa

With the proliferation of 3D medical image data of near isotropic quality there is an increasing demand for artificial intelligence methods capable of deriving quantitative measures relating to distinct pathology.

2.6.2 Gray-Level Co-Occurrence Matrices

The gray-level co-occurrence matrix (GLCM), a frequency matrix, is a useful method for enhancing details and is frequently used as an aid for interpretation of an image. The GLCM is a tabulation of how often different combinations of pixel brightness values (grey levels) occur in an image. The GLCM indicates the frequency of a pair of pixels that are at “exactly the same distance and direction of the displacement vector”. From this principal, it uses to computes the relationships of pixel intensity to the intensity of its neighboring pixels which are based on hypothesis that the same gray level configuration is repeated in a texture and pixels that are close together tend to be more related than pixels that are far away from each other.

GLCM was introduced by Haralick in 1979 and some authors, Carstensen (2002); Cooper (2004); Basset (2000); Barber et al., 1993 and Lefebvre et al., 2000. They had suggested that the GLCM could describe the probability of finding pixels of gray level value i and j at a given displacement h .

The GLCM, c , is defined with respect to given (row, column) displacement h . And element (i, j) , denoted c_{ij} , is the number of times a point having gray level j occurs in position h relative to a point having gray level i . Let N_h be the total number of pairs, then $C_{ij} = c_{ij} / N_h$ is the elements of the normalized GLCM, C . Gray co matrix creates the GLCM by calculating how often a pixel with gray-level (gray scale intensity) value i occurs horizontally adjacent to a pixel with the value j . Each element (i,j) in glcm specifies the number of times that the pixel with value I occurred horizontally adjacent to a pixel with value j .

The co-occurrence probabilities provide a second-order method for generating texture features. These probabilities represent the conditional joint probabilities of all pair wise combinations of grey levels in the spatial window of interest given two parameters: inter pixel distance (δ) and orientation (θ). The probability measure can be defined as:

$$\Pr(x) = \{C_{ij} | (\delta, \theta)\}$$

Where C_{ij} (the co-occurrence probability between grey levels i and j) is defined

$$C_{ij} = \frac{P_{ij}}{\sum_{i,j=1}^G P_{ij}}$$

Where P_{ij} represents the number of occurrences of grey levels i and j within the given window, given a certain (δ, θ) pair; G is the quantized number of grey levels.

The sum in the denominator thus represents the total number of grey level pairs (i, j) within the window.

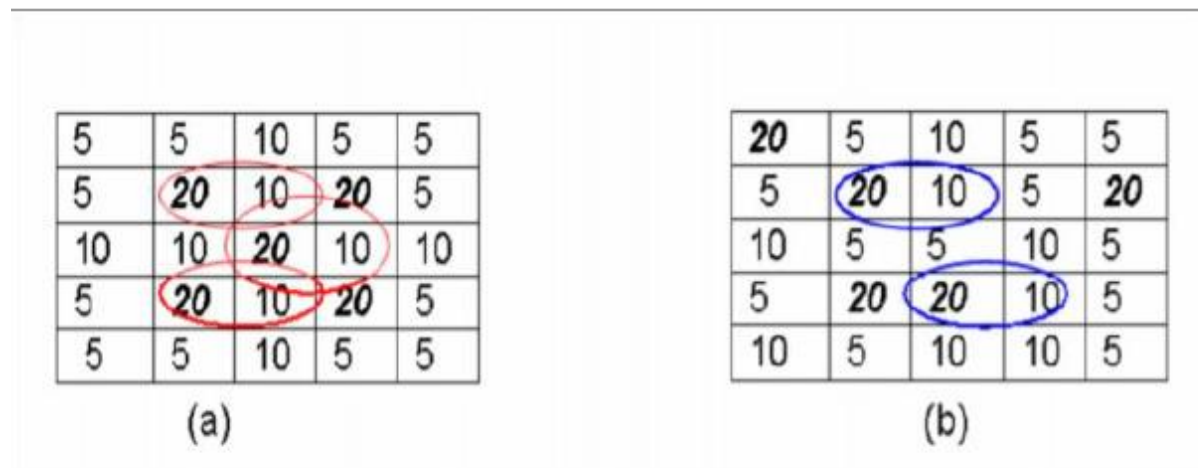


Fig 2.9 Example of matrix for GLCM

If $h = (0, 1)$, i.e., one step in the horizontal direction, then c (GLCM) will be

i/j	5	10	20
5	4	2	2
10	2	2	3
20	2	3	0

(a)

i/j	5	10	20
5	2	3	3
10	7	1	0
20	1	2	1

(b)

Fig 2.10 GLCM of the matrix

The position of each element in the matrix indicates which pixel values are being compared (Figure 2.9). The value at row i and column j gives the number of times that a pixel with the value j was to the immediate right of a pixel with the value i . Hence, the value 3 in the 2nd column, 3rd row of Figure 3.2 indicates that a pixel value of 10 was to the right of a pixel with the value 20 counted 3 times. Meanwhile, the value 2 in the same position of GLCM from Figure 3.2 means a pixel value of 10 was to the right of a pixel with the value 20 counted 2 times.

GLCM texture considers the relation between two pixels at a time, called the reference and the neighbor pixel. In the illustration, the neighbor pixel is chosen to be the one to the east (right) of each reference pixel. This can also be expressed as a $(1,0)$ relation: 1 pixel in the x direction, 0 pixels in the y direction.

Each pixel within the window becomes the reference pixel in turn, starting in the upper left corner and proceeding to the lower right. Pixels along the right edge have no right hand neighbor, so they are not used for this count.

2.6.2.1 Forming the matrix framework

The top left cell is filled with the number of times the combination 0,0 occurs, i.e. how many times within the image area a pixel with grey level 0 (neighbor pixel) falls to the right of another pixel with grey level 0 (reference pixel).

2.6.2.2 Creating a texture image

The result of a texture calculation is a single number representing the entire window. This number is put in the place of the centre pixel of the window, then the window is moved one pixel and the process is repeated of calculating a new GLCM and a new texture measure. In this way an entire image is built up of texture values.

2.6.3 Calculating texture measures from the GLCM

Haralick defined a large number of features based on co-occurrence matrices, such as contrast, homogeneity, correlation, energy and entropy. (Haralick, 1973)

These features are briefly discussed in this section.

2.6.3.1 Contrast

Contrast is also called "sum of squares variance. Spatial frequency is the difference between the highest and the lowest values of a contiguous set of pixels. This definition holds for the GLCM contrast expression as well, in particular when the module of the displacement vector is equal to one. This implies that a low contrast image is not necessarily characterized by a narrow gray level distribution, i.e., it does not necessarily present a low variance value, but the low contrast image certainly features low spatial frequencies. The conclusion is that the GLCM contrast tends to be highly correlated with spatial frequencies while the module of the displacement vector tends to one. With regard to the GLCM variance and contrast pair, the only condition that relates these two parameters to each other is the following: a sufficient, but not necessary, condition to keep contrast low is to maintain variance low (while the vice versa is not true). A low contrast image presents a GLCM concentration term around the principal diagonal and,

consequently, a low value of the GLCM contrast. This result means that high contrast values imply high contrast texture, first-order statistics contrast and GLCM contrast are strongly related. GLCM contrast and variance were also found to be highly correlated with the first order statistic standard deviation, but this condition,

according to the Theoretical discussion presented above, must be considered as a particular case for the contrast parameter. (Haralick, 1973) Mathematically, contrast can be represented as:

$$\sum_{i,j} |i - j|^2 P(i, j)$$

When i and j are equal, the cell is on the diagonal and $(i-j) = 0$. These values represent pixels entirely similar to their neighbor, so they are given a weight of 0.

If i and j differ by 1, there is a small contrast, and the weight is 1. If i and j differ by 2, contrast is increasing and the weight is 4. The weights continue to increase exponentially as $(i-j)$ increases.

2.6.3.2 Homogeneity

Homogeneity is also called the "Inverse Difference Moment". Mathematically, it can be written as:

$$\sum_{i,j} \frac{P(i, j)}{1 + |i - j|}$$

This parameter is also called Uniformity.

2.6.3.3 Correlation

GLCM correlation is expressed by the correlation coefficient between two random variables i and j , where i represents the possible outcomes in gray tone measurement for the first element of the displacement vector, while similarly j is associated with gray tones of the second element of the displacement vector.

Its mathematical formula is given below:

$$\sum_{i,j} \frac{(i - \mu_i)(j - \mu_j)P(i, j)}{\sigma_i \sigma_j}$$

Correlation is a measure of gray tone linear-dependencies in the image; in particular, the direction under investigation is the same as vector displacement. High correlation values (close to 1) imply a linear relationship between the gray levels of pixel pairs. Thus, GLCM correlation is uncorrelated with GLCM energy and entropy, i.e., to pixel pairs repetitions. Correlation reaches its maximum regardless of pixel pair occurrence, as high correlation can be measured either in low or in high energy situations. GLCM correlation is also uncorrelated to GLCM contrast, as high predictability of the gray level of one pixel from the second one in a pixel pair is completely independent from contrast. As a limiting case of linear-dependency a completely homogeneous area may be considered, for which correlation is equal to 1. (Haralick, 1973)

2.6.3.4 Energy

The mathematical formula for energy is given as:

$$\sum_{i,j} P(i, j)^2$$

Energy measures textural uniformity, i.e., pixel pairs repetitions; when the image patch under consideration is homogeneous (only similar gray level pixels are present) or when it is texturally uniform (the vector displacement always falls on the same (i, j) gray level pair). A few (possibly only one) elements of GLCM will be greater than

0 and close to 1, while many elements will be close to 0. In this case, energy reaches values close to its maximum, equal to 1. Thus, high energy values occur when the gray level distribution over the window has either a constant or a periodic form. This result means that energy is strongly uncorrelated to first order statistical variables such as contrast and variance. Indeed, energy may reach its maximum with either maximum or no variance and contrast values. Energy is the opposite of entropy. Energy can be used to do useful work. In that sense, it represents orderliness. This is why "Energy" is used for the texture that measures order in the image. (Haralick, 1973)

2.6.3.5 Entropy

Entropy is a notoriously difficult term to understand; the concept comes from thermodynamics. It refers to the quantity of energy that is permanently lost to heat ("chaos") every time a reaction or a physical transformation occurs. Entropy cannot be recovered to do useful work. Because of this, the term is used in non-technical speech to mean irremediable chaos or disorder. The equation used to calculate physical entropy is very similar to the one used for the texture measure. Its mathematical formula is given below:

$$-\sum_{i,j} P(i,j) \log(P(i,j))$$

However by definition the sum of $P_{ij} = 1$. With this constraint, the overall maximum of the sum (i.e. of ENT) is 0.5. This maximum is reached when all probabilities are equal. This parameter measures the disorder of an image. When the image is not texturally uniform, many GLCM elements have very small values, which imply that entropy is very large. As an example, consider a window with completely random values of gray level pixel values (white noise). The histogram for such a window is a

constant function, all $g(i, j)$ are the same, and the entropy parameter reaches its maximum. From a conceptual point of view, entropy is strongly, but inversely, correlated to GLCM energy. Theoretically, similar results are expected for energy and entropy clustering. (Haralick, 1973)

2.7 Previous Study

Alzaid et al. (2006) evaluated pancreas in diabetic by ultrasound, This study was in USA and the method was tested on 57 diabetic patients: 14 with Type 1 (insulin-dependent) diabetes, 10 insulin-treated and 33 tablet-treated patients with Type 2 (non-insulin-dependent) diabetes, and 19 nondiabetic subjects. In this study measure the head (area medially to SMA) and body (area anterior to SV) of pancreas. The result of their study, The pancreas of patients with Type 1 diabetes was markedly smaller ($p < 0.0001$) than the pancreas in non-diabetic subjects. The pancreas of patients with Type 2 diabetes was more moderate in size: larger ($p < 0.001$) than that of Type 1 diabetic patients but smaller ($p < 0.5$) than the pancreas of the control group. Pancreatic size of patients with Type 2 diabetes was also related to basal insulin secretion with insulin deficient patients (low or undetectable C-peptide) having smaller ($p < 0.05$) pancreases than those with normal insulin secretion. There was no difference in the size of the pancreas in the different treatment groups of Type 2 diabetic patients. Pancreatic size did not correlate with age, body mass index or the duration of diabetes. We conclude that the pancreas is a smaller organ in patients with diabetes mellitus and that the decrement in size is maximal in insulin-dependent/insulin deficient subjects. Ultrasonography, therefore, can potentially serve to discriminate between the different types of diabetes.

Afraa et al. (2014) characterized pancreas in Sudanese Population Using Computerized Tomography ,A total number of 241 Sudanese subjects were included in the study, 161 (66.8%) were males and 80 (33.2%) were females, their mean ages were 40.6 ± 16.1 ; all were examined Using cross-sectional computerized tomography (CT) imaging for abdomen. The subject's ages and gender were recorded and the body characteristics including height, weight, BMI, abdomen circumference (AC), were evaluated and correlated with pancreas size and CT number. This study revealed that the head of pancreas size was 27.9 ± 4.5 mm, the body was 23.1 ± 3.7 mm, and tail was 19.0 ± 3.1 mm, while the CT number (Hounsfield unit) was 59.1 ± 14 , 57.3 ± 12.6 and 55.2 ± 13.1 respectively. Also the study showed a significant relation between the pancreas size, pancreas CT number, age, and AC at ($p < 0.05$). they study The measurements were taken from the operator council of the CT machine; the axial images were obtained through the middle of the pancreatic portion (head, body and tail) .Anterior-posterior diameters (AP) were measured at right angles to the longitudinal axis of the organ. The largest diameter of the pancreas lying to the left of the middle of the Vertebral body was considered the head .The body of the pancreas was measured on the left margin of the vertebral body and the tail opposite to the medial margin of the left kidney. The transverse diameter of the adjacent vertebral body was measured and used as a reference and marker of body character as applied by Andreas . The CT numbers for the pancreas head, body and tail were measured(Hounsfield). The CT number of the lumber Vertebra was also been evaluated. They founded the concluded that axial CT scan is considered a an appreciable radiological method for measuring the pancreas size and characterizing its structure using CT number (Hounsfield). The study also revealed that the Sudanese pancreas is different from what was mentioned in the literature and other previous studies, and also pancreas size and CT number had significant relations with age and other body habitus. Sudanese pancreas size and CT number were best

described by the established formulae for age, weight, height, AC, VBTD, VDCT. Local references for Sudanese pancreas measurements and CT number were established.

Reza (2007) studied the Ultrasonographic alterations of pancreas in diabetic patients. Pancreas as the insulin-producing gland is subjected to destruction and change in the diabetes-producing process. Real time sonography can assess the gland in 95% of cases and its accuracy in diagnosis of pancreatic disease matches that of CT-scan. The purpose of this study was to evaluate pancreatic diameter and echogenicity by sonography and to examine the correlation of these two factors with duration of disease in diabetes types I and II in comparison with controls. In two groups of 60 diabetic patients and healthy controls, diameter and echogenicity of pancreas was determined. They described that diameter of pancreas was significantly different in diabetic patients and correlated with duration of disease. In type I diabetes, decrease in the size of pancreas was more prevalent than in type II diabetes and these changes become more prominent over time.

Kreel et al. (1977) demonstrated the normal anatomy of the pancreas by using computed tomography (CT) (EMI) in 50 patients with no known pancreatic disease and in 15 comparable postmortem studies. The size of the normal pancreas was found to be up to 3.0 cm for the head, 2.5 cm for the neck and body, and 2.0 cm for the tail. In assessing these values, it is important to be sure that adjacent structures such as the portal vein, splenic vein, and duodenum are not included in the measurement, that the measurements are taken on scans of maximum resolution with no movements, and that the measurements are strictly related to the anteroposterior diameter. It is considered that gantry tilt will also distort these figures.

The density, contour and thickness of the pancreas in diabetics were measured in CT images, the findings in 57 patients, which studied by Gilbeau et al, (1992). group of diabetics were examined; 20 insulin dependent pt, 25 type 2 {not treated}, 12 treated with but not depended on it. 57 control subjects with similar in age to those of diabetics patient. CT shows reduction in size and increase in lobulations, especially on insulin treated pts, but no change in density of them. size did not correlate with age, body mass index or the duration of diabetes. They conclude that the pancreas is a smaller organ in patients with diabetes insulin-dependent/insulin-deficient subjects.

According to Ravi et al, 2001 reports, the findings were that the total area of the pancreas was significantly smaller in patients with type 1 diabetes mellitus when compared with healthy controls and with increasing duration of diabetes there was a reduction of the dimensions of the head, body, tail and total area of pancreas which are more evident if diabetes is of more than 10 years duration.

Saisho et al (2007) studied Pancreas Volumes in Humans from Birth to Age One Hundred Taking Into Account Sex, Obesity, and Presence of Type-2 Diabetes, A total number of 135 (male 77, female 58) subjects aged 20 years and under were evaluated We measured pancreas volume in 135 children and 1,886 adults (1,721 non diabetic and 165 with type-2 diabetes) with no history of pancreas disease who had undergone abdominal CT scan between 2003 and 2006. Pancreas volume was computed from the contour of the pancreas on each CT image. In addition to total pancreas volume, parenchymal volume, fat volume, and fat/parenchyma ratio (F/P ratio) were determined by CT density. We also quantified pancreatic fat in autopsy tissue of 47 adults (24 non diabetic and 23 with type-2 diabetes). During childhood and adolescence, the volumes of total pancreas, pancreatic parenchyma, and fat increase linearly with age. From age 20–60 years, pancreas volume reaches a plateau (72.4 ± 25.8 cm³ total; 44.5 ± 16.5 cm³ parenchyma) and then declines thereafter. In

adults, total (*32%), parenchymal (*13%), and fat (*68%) volumes increase with obesity. Pancreatic fat content also increases with aging but is not further increased in type-2 diabetes. We provide lifelong population data for total pancreatic, parenchymal, and fat volumes in humans. Although pancreatic fat increases with aging and obesity, it is not increased in type-2 diabetes.

Stefanovic et al (2012) CT volumetry of normal pancreas: correlation with the pancreatic diameters measurable by the cross-sectional imaging, and relationship with the gender, age, and body constitution. 220 CT examinations were analyzed retrospectively (102 females, 118 males; age 16–82, average 56). Following diameters were measured: cranial–caudal— CC pancreas, CC body & tail, CC body, CC head; anterior–posterior— AP tail, AP body, AP head; lengths—LL head, L body & tail; and maximal transversal diameter of the L1 vertebral body (LLL1) and thickness of the abdominal subcutaneous fat (APASF), as markers of body constitution. The average volume of the pancreas was $79.2 \pm 24.1 \text{ cm}^3$ (ranging from 37.4 to 168.2 cm^3). Pancreatic volume strongly correlated with all measured diameters of the pancreas ($P < 0.0001$). Pancreatic volume significantly correlated with gender (M:F = 86.1:72.8 cm^3 , $P = 0.002$) and the LLL1 ($r = 0.185$, $P = 0.008$), and did not correlate with the age ($r = -0.110$, $P = 0.151$) and the APASF ($r = -0.115$, $P = 0.104$). Correlation of vertebral body– pancreas volume ratio of each subject and the age was strongly negative ($r = -0.202$, $P = 0.006$). Conclusions Marked individual variations in normal pancreas volume were observed. Pancreatic volume could be computed using the diameters measurable by the cross sectional imaging employing the formula: $V = (\text{AP tail} + \text{AP body})/2 * \text{L body \& tail} * \text{CC body} + (\text{AP head}/2)^2 * 3.14 * \text{CC head}$.

In 1987 Heuck et al. Age-related morphology of the normal pancreas on computed tomography. Abdominal computed tomographic scans were performed on a group of 360 patients between the ages of 20 and 80 years. The anteroposterior diameter of the pancreatic head, body, and tail, the age-related ratio of vertebral body-pancreas diameter, and the external and internal contours of the organ were analyzed. The age-related changes in the pancreas were compared with known anatomical findings. In 20_30 years old an average diameters of $28.6 \pm 3.8\text{mm}$ was registered in pancreas head area. This had recorded to $24.0 \pm 3.6\text{mm}$ in 6th decade and diminished to $21.2 \pm 4.3\text{mm}$ in 70_80years old. The largest defriend between neighboring groups were visible between 3rd and 4th and between 7th and 8th decades. The antroposterior (AP) pancreas diameter was related to the transversal vertebral body diameter from same scan. The vertebral body = 100% and from this corresponding pancreatic diameter were calculated. This relative pancreatic size shows the involving of the organ most distinctly.

Jayaprakash et al. (2012) studied the development of pancreatic CT Scan image dataset and retrieval process for diagnosis. A database consisting of 50 pancreas image was composed, clinical diagnosis was also ascertained by pathologist. Feature properties of all 50 image were calculated for different angle orientation. Statistical mean values for each case of feature characteristic were worked out. Difference between various structural features of query in constructed database were compared.

In 1973, Haralick et. al. proposed general procedure for extracting textural properties of blocks of image data. These features were calculated in the spatial domain, and the statistical nature of texture was taken into account in the procedure, which was based on the assumption that the texture information in an image I was contained in the overall or "average" spatial relationship which the gray tones in the image have to

one another. They computed a set of gray tone spatial-dependence probability-distribution matrices for a given image block and suggested a set of 14 textural features, which can be extracted from each of these matrices. These features contained information about such image textural characteristics as homogeneity, gray-tone linear dependencies (linear structure), contrast, number and nature of boundaries present, and the complexity of the image. It was important to note that the number of operations required computing any one of these features was proportional to the number of resolution cells in the image block. It was for this reason that these features were called quickly computable.

In 1988, John et. al. proposed a method for choosing the direction of the displacement vector that was based on the most dominant edge obtained from gradient analysis. In addition, the anatomy of the liver was used to suggest the most important inter sample spacing in constructing co-occurrence matrices for the evaluation of diffuse liver disease. For an inter sample spacing of 3 pixels, the most dominant edge was found to be 45° for the three normal cases and 135° for the case with fatty infiltration. Based on these preliminary results it was concluded that the gradient direction is more uniformly distributed in the fatty infiltration case than it was in the three normal cases.

In 2000, Qiang et. al. described a texture image analysis technique for characterizing and recognizing typical, diagnostically most important, vascular patterns relating to cervical lesions. A generalized texture analysis technique was proposed based on combining the conventional statistical and structural approaches using a statistical description of geometric textural primitives. Preliminary experimental study demonstrated the feasibility of the proposed technique in discriminating between cervical texture patterns indicative of different stages of cervical lesions.

In 2001, Sharma et. al. used five different texture feature extraction methods that were most popularly used in image understanding studies. One of the features of this study was the use of a publicly available benchmark that further studies can use. Their results show that there was considerable performance variability between the various texture methods. Their finding, that co-occurrence matrices and Law's method perform better than other techniques, was supported by previous comparative studies in this area. It was however difficult to generalize this for all cases. The difference in results between the linear analysis and nearest neighbor method was also noteworthy. The best overall result using nearest neighbor methods was obtained with co-occurrence matrices, whereas using linear analysis the best result was obtained using combined set of features. It appears that since different texture methods capture different aspects of the image texture, and combining features from them has certainly much utility.

In 2001, Vassili et. al. proposed a method for three-dimensional (3-D) texture analysis of magnetic resonance imaging brain datasets. The method was based on extended, multi sort co-occurrence matrices that combine intensity, gradient and anisotropy image features in a systematic and consistent way. They suggested co-occurrence descriptors are natively 3-D, reflection and translation invariant and, to some extent, rotation-insensitive. Normalization of co-occurrence descriptors provided a basis for inter subject analysis and comparisons of brain regions with different size. They showed that the extended co-occurrence descriptors could be used as an efficient tool in various MRI brain image analysis tasks such as classification of brain datasets and segmentation of diffuse brain lesions.

In 2007, Sheppard and Shih studied to double the accuracy of ultrasound diagnosis and biopsy guidance, an efficient, integrated platform for image textural analysis and clustering of trans rectal prostate ultrasound images into clusters potentially representing cancerous or normal tissue areas. Preliminary image texture analysis showed the potential for doubling diagnosis accuracy from 38-42% for prostate cancer with current clinical methods, to 88-92%. In addition, image texture analysis made prostate cancer tumor locating possible for more precise, less invasive biopsy/treatment, instead of 6-way random biopsy. An efficient Image Texture Analysis tool platform on Window PC was constructed via innovative sparse co-occurrence matrix techniques with linked lists to speed up the processing from 8 days to about 5 seconds per image on a PC. The approach was based on Haralick's textural features and the Mean Squared Error (MSE) clustering algorithm. Ultrasound diagnosis was proven less invasive, even portable, at lower screening cost than most other medical imaging. However, being less visual than most, ultrasound image diagnosis was difficult even for trained professionals, and thus could benefit greatly from computer enhancement.

Chapter Three Materials and Methods

3.1 Material: Equipment (CT machine)

Toshiba sensation 64 with Kvp/120, mAS 350 in Royal care international Hospital.

Toshiba sensation 64 with Kvp/140,mAs 500 in Azzytona specialize Hospital.

3.2 Study Design :

This was descriptive analytical study case-control study (which include diabetic and normal).

3.3 Duration and place of study:

It was achieved at radiology department - Royal Care international Hospital and ALzaytona Specialist Hospital (Toshiba 64 slice) during the period from 2015 to 2017.

3.4 study population and sample size

The population of this study consisted of diabetic patients as well as normal non diabetic patient; all patient with other pathology affected the pancreas were excluded.

A total of 213 non diabetic patients were included in this study. Patients were in both genders, 142 were Males constituting 66.7% and 71 were females and constituting 33.3%. Patients' ages were <2 >97 years old. All were selected for CTKUB. Patients' ages, pancreases CT number, pancreas head size, pancreas body size, pancreas tail size, vertebral body width were all been evaluated.

A total of 100 diabetic patients were included in this study. All were selected for CTKUB to classify the pancreas parts to head, body and tail the features of the

classified regions of the whole images (as raw data) were classified further using linear discriminant analysis.

3.5 Exclusion criteria:

Patients having pathological changes such as; ascites, retro peritoneal mass, Ca head of pancreas, pancreatitis or any pathology affecting the measurement of the pancreas were excluded.

3.6 Technique and protocol:

3.6.1 CT KUB protocol

A CT scans were performed including protocol of axial images from the xiphoid process covers all abdominal area and pelvic down to pubic bone with patient in supine position, head first. The images were obtained at 100/120 kv and 60/80 mAs, with 5 mm slice thickness. Reconstruction used 3mm to obtain coronal views of KUB. Light diets and fasting for 6 hours was preparation for patient who's undergone CT KUB.

5.6.2 Texture analysis

analyzing the images with Interactive Data Language IDL software to measure the grey level distribution of images, to classify the pancreas parts to head, body and tail the features of the classified regions of the whole images (as raw data) were classified further using linear discriminant analysis.

3.7 Method of Pancreas Measurement

The measurements were taken from the operator console of the CT machine; the axial images were obtained through the middle of the pancreatic portion (head, body and tail) .Anterior-posterior diameters (AP) were measured at right angles to the longitudinal axis of the organ. The largest diameter of the pancreas lying to the left of

the middle of the vertebral body was considered the head .The body of the pancreas was measured on the left margin of the vertebral body and the tail opposite to the medial margin of the left kidney. The transverse diameter of the adjacent vertebral body was measured and used as a reference and marker of body character. The CT numbers for the pancreas head, body and tail were measured in (Hounsfield).

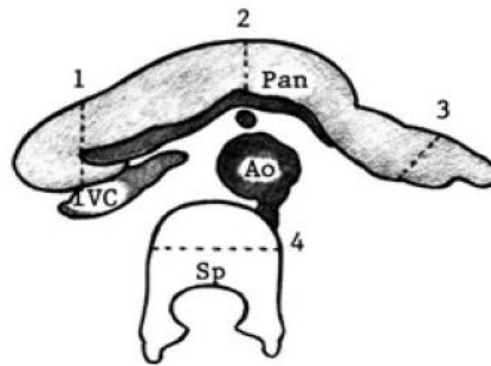


Fig 3.1 shows the method of pancreas measurements

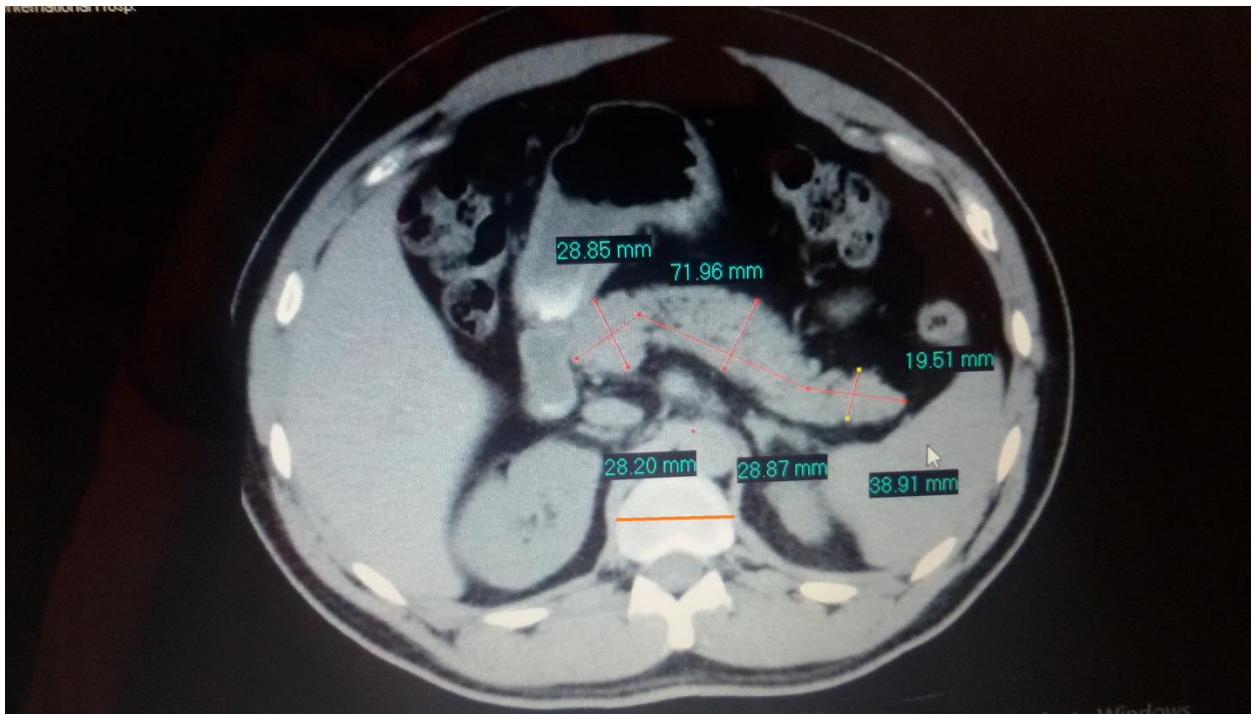


Figure 3.2 Axial CT for abdomen shows the vertebral width as reference plane

3.8 Data Analysis:

Data obtained were entered into a Microsoft Excel spreadsheet and analyzed using Interactive data language (IDL) and Statistical Package for Social Sciences (SPSS) version 16 (SPSS Inc., Chicago, IL, USA). Data statistical test of significance was done with t-test , $P \leq 0.05$ was considered statistically significant. Ethical clearance for this study was obtained from the Ethics and Research Committee of Sudan University of Science and technology./00388

3.9 Ethical approval

- There was official written permission to Khartoum state diagnostic centers to take the data.
- No patient data will be disclose also the data was kept in personal computer with personal password.

Chapter Four

Result

Computerized Tomography Scanning was performed in the Radiology Unit of the Azzytona Specialized Hospital and Royal Care International Hospital in Khartoum-Sudan. The data was collected from 213 normal subjects and 100 patients had preexisting diabetes. Patients age, pancreases CT number, spleen CT number, pancreas head AP& length , pancreas body AP& length, pancreas tail AP& length, vertebral body width, for normal group were recorded and Measurement were made. Data were presented as mean and standard deviation (SD) for all of the variables. Detailed results are shown in the tables and figures below. This study was using image processing techniques by IDL, Interactive Data language program.

Table No (4.1) Distribution of study sample according to Participant's Gender for non-diabetic

Gender	Frequency	Percent (%)
Male	142	66.7
Female	71	33.3
Total	213	100.0 (%)

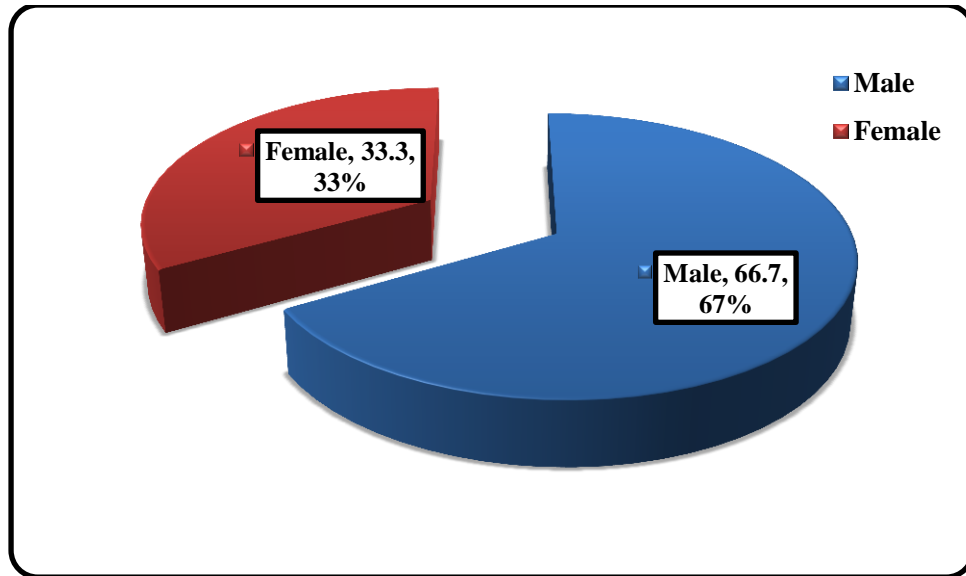


Figure No (4.1) Distribution of study sample according to Participant's Gender for non-diabetic

Table No (4.2) Distribution of study sample according to Participant's age for non-diabetic

<i>Age</i>	<i>Frequency</i>	<i>Percent (%)</i>
<10	6	2.8
11-20	19	8.9
21-30	27	12.7
31-40	46	21.6
51-60	37	17.4
50-60	46	21.6
61+	32	15.0
Total	32	100.0 (%)

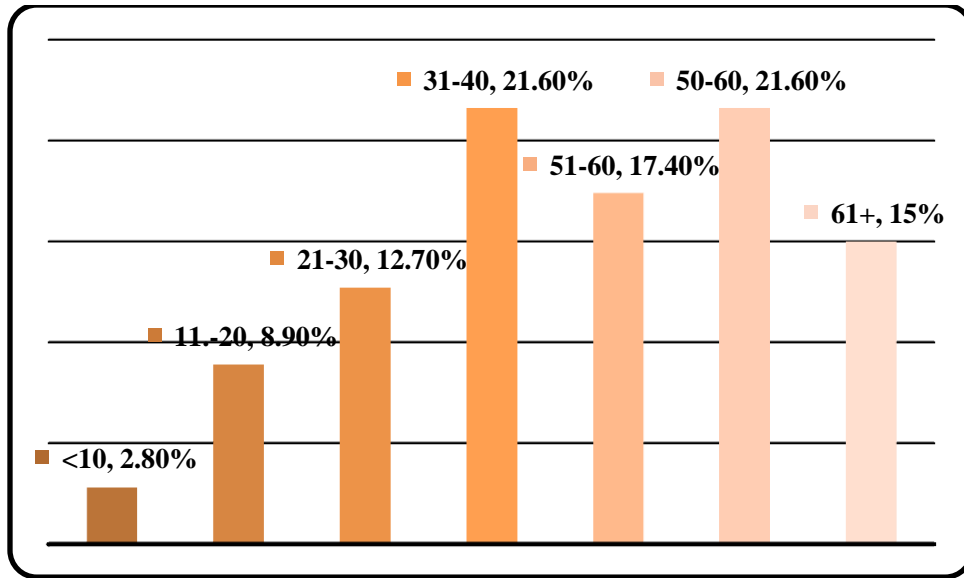


Figure No (4.2) Distribution of study sample according to Participant's age for non-diabetic

Table 4.3 Shows descriptive statistics of Sudanese pancreas measurements for non-diabetic

<i>Descriptive Statistics</i>					
	<i>N</i>	<i>Minimum</i>	<i>Maximum</i>	<i>Mean</i>	<i>Std. Deviation</i>
Age	213	2.00	97.00	43.5681	17.90808
pancreas CT No	213	23.00	69.00	49.1174	8.81039
Spleen CT No	213	21.00	70.00	49.4695	8.03326
vertebra diameter	213	21.22	52.30	37.6182	5.65851
head length	213	16.50	53.50	29.9492	6.36454
Head AP	213	12.50	40.60	25.079	5.62876
Body length	213	25.00	98.90	61.431	15.36927
Body AP	213	9.29	51.20	22.741	6.08338
Tail length	213	11.98	86.93	33.945	9.11623
Tail AP	213	7.00	42.70	19.836	6.43507

Table 4.4 Shows descriptive statistics of Sudanese pancreas measurements between male & female for non-diabetic

<i>Group Statistics</i>					
	Gender	N	Mean	Std. Deviation	P-value
pancreas CT No	Male	142	49.5423	8.80975	.321
	Female	71	48.2676	8.81226	
Spleen CT No	Male	142	49.6338	8.12009	.674
	Female	71	49.1408	7.90352	
vertebra dimeter	Male	142	38.0418	6.07808	.123
	Female	71	36.7708	4.63304	
head length	Male	142	29.8199	6.07680	.676
	Female	71	30.2079	6.94227	
Head Ap	Male	142	25.4178	5.89229	.216
	Female	71	24.4028	5.03223	
Body length	Male	142	62.4833	16.6885	.158
	Female	71	59.3266	12.1515	
Body AP	Male	142	22.9865	6.11815	.408
	Female	71	22.2525	6.02641	
Tail length	Male	142	33.7411	8.94080	.644
	Female	71	34.3555	9.50885	
Tail AP	Male	142	20.1192	6.22258	.366
	Female	71	19.2710	6.85078	

Table 4.5 Shows descriptive statistics of Sudanese pancreas measurements using T-test for non-diabetic

		<i>Descriptives</i>					P-value
		N	Mean	Std. Deviation	Minimum	Maximum	
pancreas CT No	<10	6	50.1667	6.17792	44.00	61.00	.000
	11-20	19	54.7895	7.84983	43.00	65.00	
	21-30	27	54.1481	6.72369	42.00	68.00	
	31-40	46	51.1304	8.33096	32.00	68.00	
	51-60	37	46.0811	8.33126	32.00	69.00	
	50-60	46	47.9130	8.68159	29.00	65.00	
	61+	32	43.6563	8.26422	23.00	59.00	
	Total	213	49.1174	8.81039	23.00	69.00	
Spleen CT No	<10	6	48.5000	4.32435	45.00	57.00	.000
	11-20	19	53.2632	7.83753	38.00	64.00	
	21-30	27	55.2593	6.60764	38.00	70.00	
	31-40	46	50.3478	6.41948	35.00	62.00	
	51-60	37	48.5946	7.91784	31.00	64.00	
	50-60	46	47.4348	7.23157	28.00	60.00	
	61+	32	45.1875	9.59986	21.00	63.00	
	Total	213	49.4695	8.03326	21.00	70.00	
vertebra diameter	<10	6	24.4767	4.08350	21.22	29.74	.000
	11-20	19	34.6205	3.68275	28.20	39.80	
	21-30	27	35.2141	4.26177	30.42	46.40	
	31-40	46	36.2789	3.90006	30.20	46.32	
	51-60	37	37.9505	5.00856	29.03	49.90	
	50-60	46	40.0530	4.95335	31.00	49.77	
	61+	32	41.9313	5.61973	34.20	52.30	
	Total	213	37.6182	5.65851	21.22	52.30	

head length	<10	6	19.4167	1.74652	17.10	21.10	.000
	11-20	19	27.4437	5.86711	19.70	44.50	
	21-30	27	30.3285	5.83769	20.90	39.20	
	31-40	46	31.1365	5.09477	20.57	41.70	
	51-60	37	27.8841	5.61635	20.90	43.30	
	50-60	46	31.5739	6.59221	16.50	53.50	
	61+	32	31.4375	7.19262	20.20	46.30	
	Total	213	29.9492	6.36454	16.50	53.50	
Head Ap	<10	6	16.2217	1.06802	15.40	18.24	.000
	11-20	19	21.0574	5.65670	12.50	29.60	
	21-30	27	26.0267	4.15951	19.00	36.30	
	31-40	46	26.1128	5.56687	14.40	38.80	
	51-60	37	24.3076	5.28384	13.24	37.50	
	50-60	46	26.4765	5.62395	15.00	40.60	
	61+	32	25.7281	5.34482	17.40	33.60	
	Total	213	25.0795	5.62876	12.50	40.60	
Body length	<10	6	45.4550	7.03250	35.89	53.63	.004
	11-20	19	53.8037	11.29662	31.90	72.40	
	21-30	27	61.3878	14.35136	37.80	95.60	
	31-40	46	60.1517	17.05878	31.30	98.90	
	51-60	37	67.6992	13.64539	37.30	97.25	
	50-60	46	63.6663	15.63775	25.00	91.60	
	61+	32	60.3703	14.96669	32.00	88.15	
	Total	213	61.4311	15.36927	25.00	98.90	
Body AP	<10	6	13.9450	1.75317	11.33	15.90	.001
	11-20	19	20.7611	5.54650	12.90	32.60	
	21-30	27	22.5341	5.27315	13.60	30.90	
	31-40	46	24.6007	6.92913	11.09	41.60	
	51-60	37	22.5100	5.06003	9.29	34.50	
	50-60	46	23.8939	6.52195	13.30	51.20	

	61+	32	21.6825	4.94873	13.20	33.60	
	Total	213	22.7418	6.08338	9.29	51.20	
Tail length	<10	6	22.0817	12.97231	11.98	38.58	.030
	11-20	19	32.1437	5.21662	24.80	41.70	
	21-30	27	33.1011	7.52071	20.46	46.30	
	31-40	46	33.6811	7.71023	20.49	56.60	
	51-60	37	34.6008	11.63444	20.40	86.93	
	50-60	46	34.9396	8.69385	15.60	60.00	
	61+	32	36.1484	9.37037	20.10	54.60	
	Total	213	33.9459	9.11623	11.98	86.93	
Tail AP	<10	6	9.8517	1.61784	8.04	11.68	.000
	11-20	19	18.2579	6.74123	7.00	31.80	
	21-30	27	19.2804	6.16857	12.10	34.40	
	31-40	46	21.9037	6.60462	10.29	40.50	
	51-60	37	20.4673	4.95471	11.25	32.00	
	50-60	46	20.7772	6.61259	9.50	37.60	
	61+	32	18.0616	6.05737	9.90	42.70	
	Total	213	19.8364	6.43507	7.00	42.70	

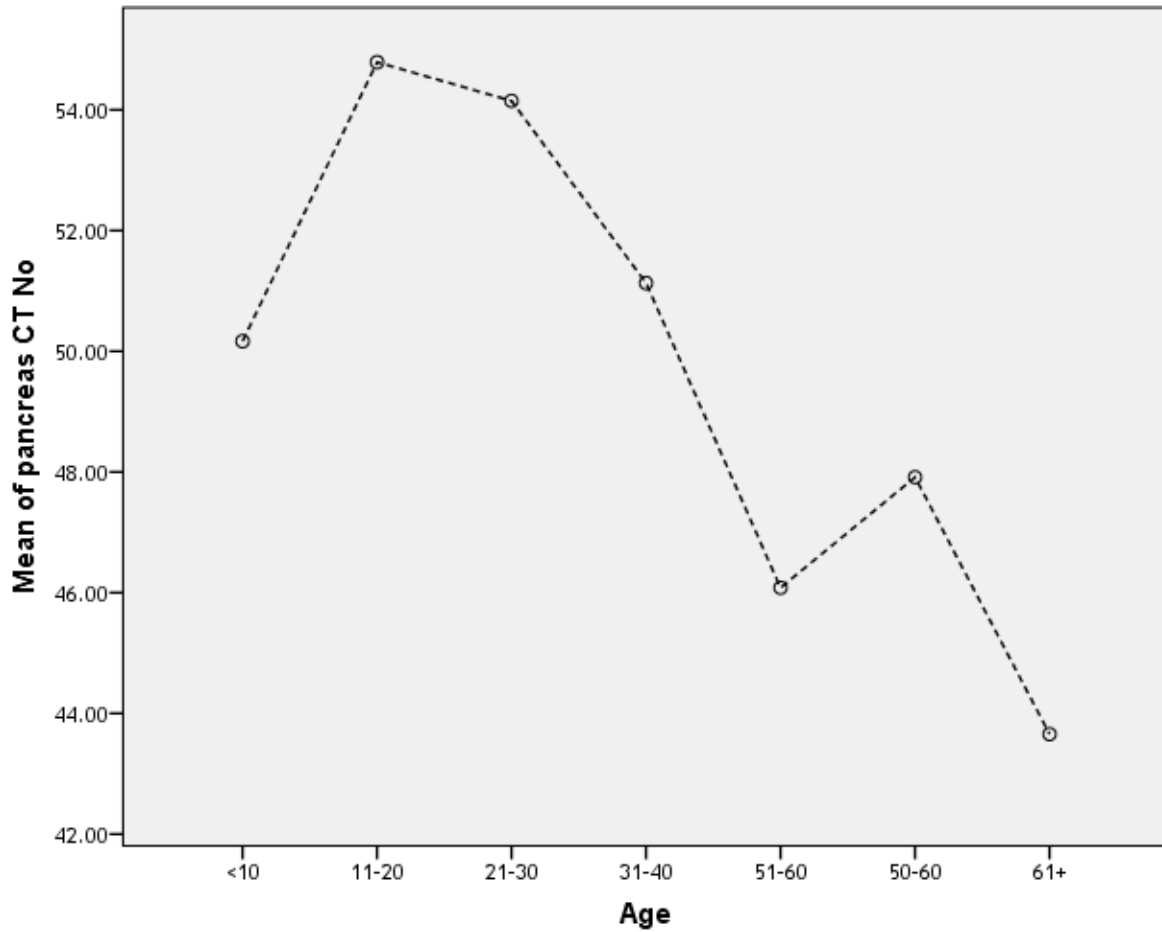


Figure 4.3 show relation between the subjects ages and pancreas CT No(HU) for non-diabetic

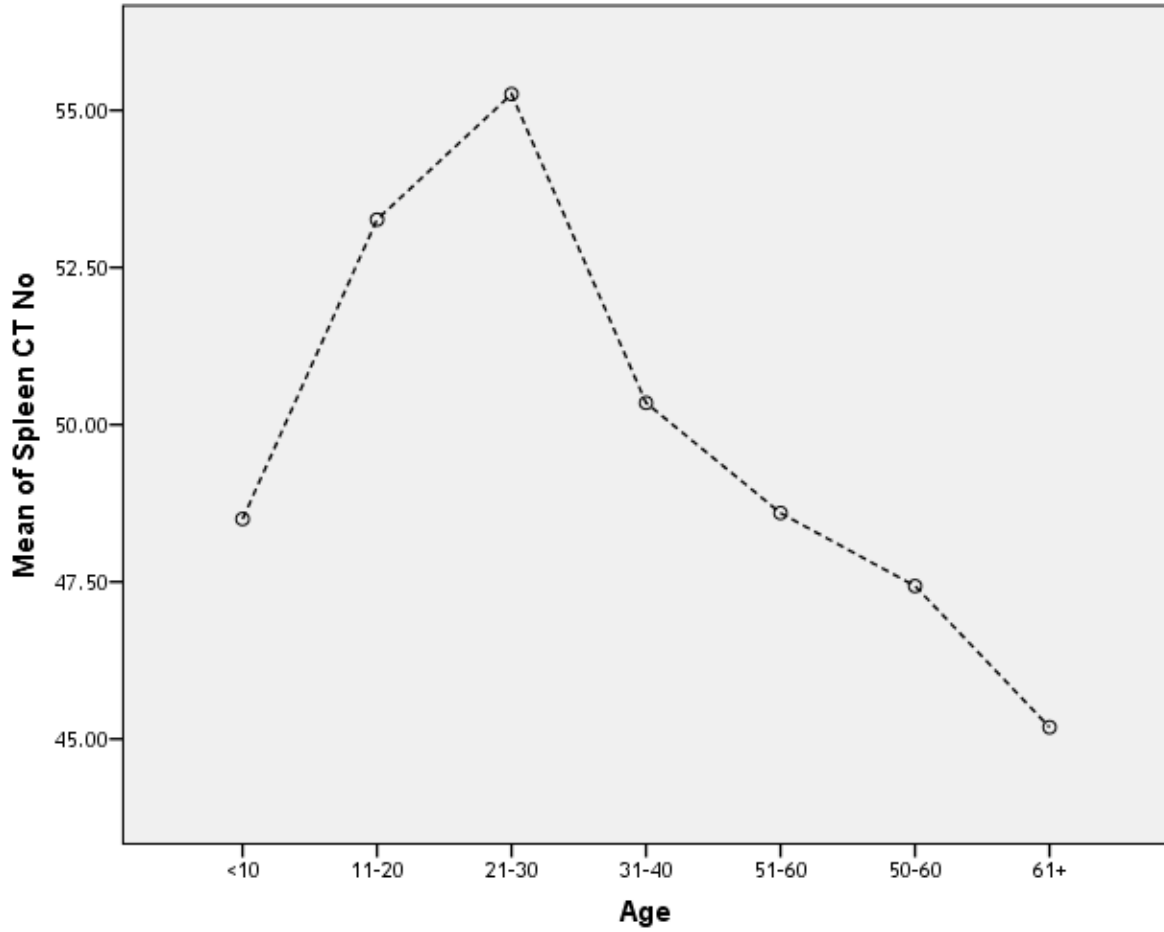


Figure 4.4 show relation between the subjects ages and spleen CT(HU) for non-diabetic

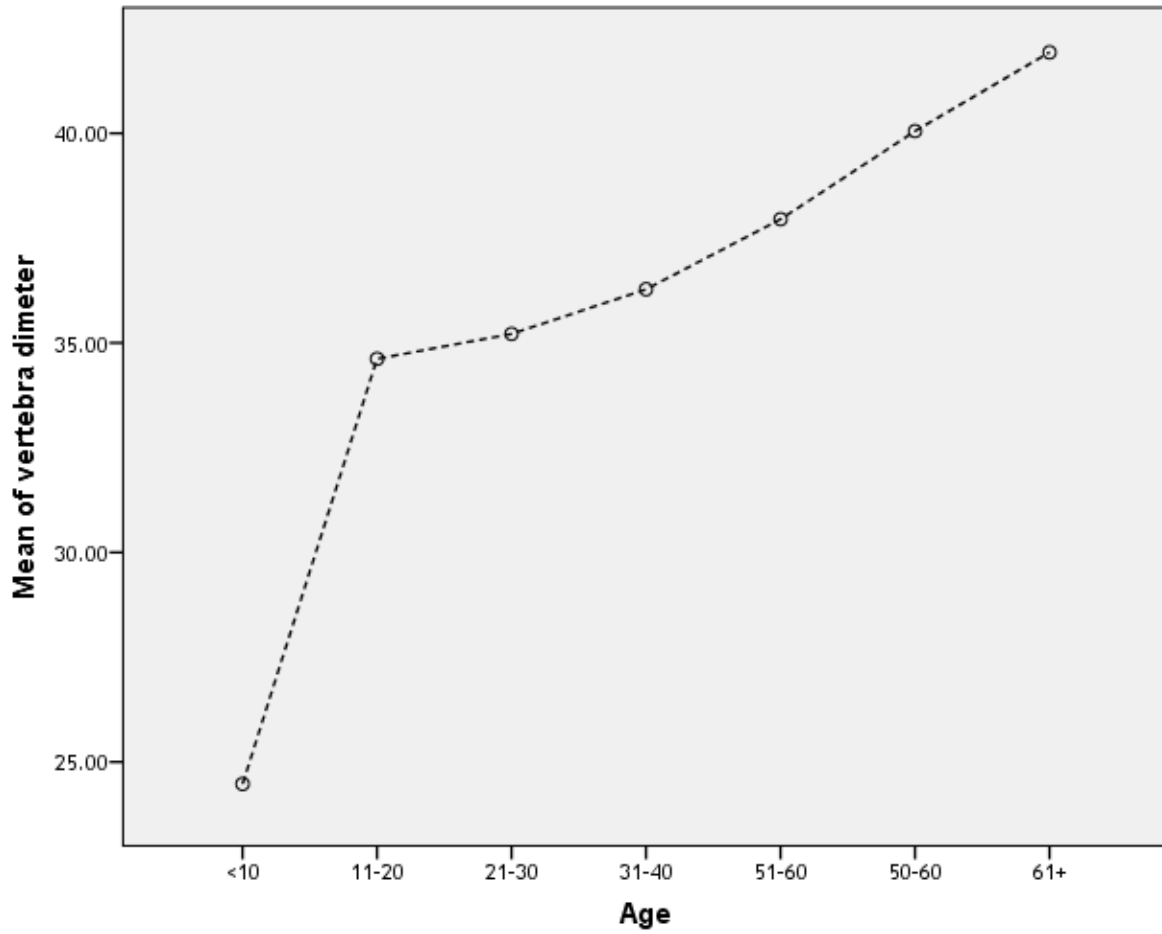


Figure 4.5 show relation between the subjects ages and vertebral diameter for non-diabetic

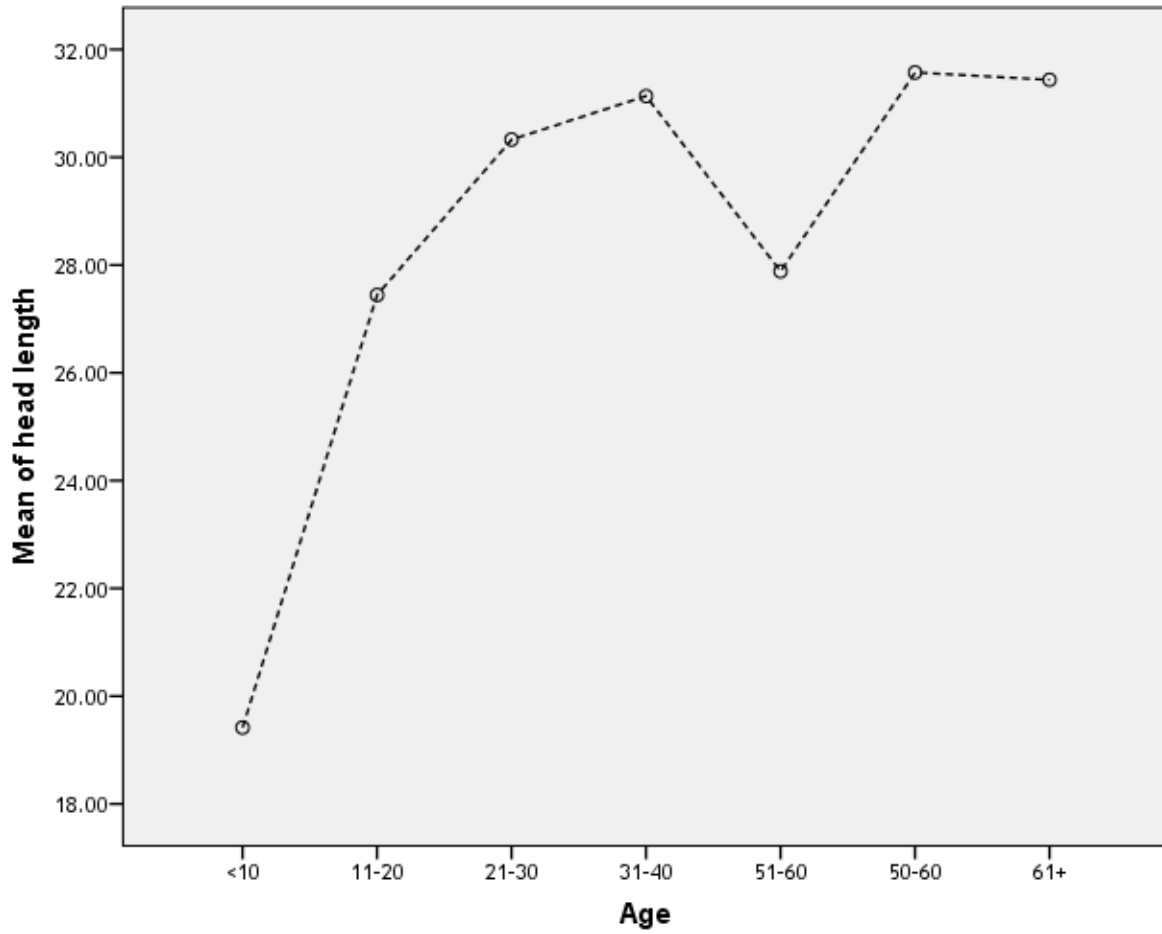


Figure 4.6 show the relation between the subjects ages classified in to age classes and pancreas head length for non-diabetic

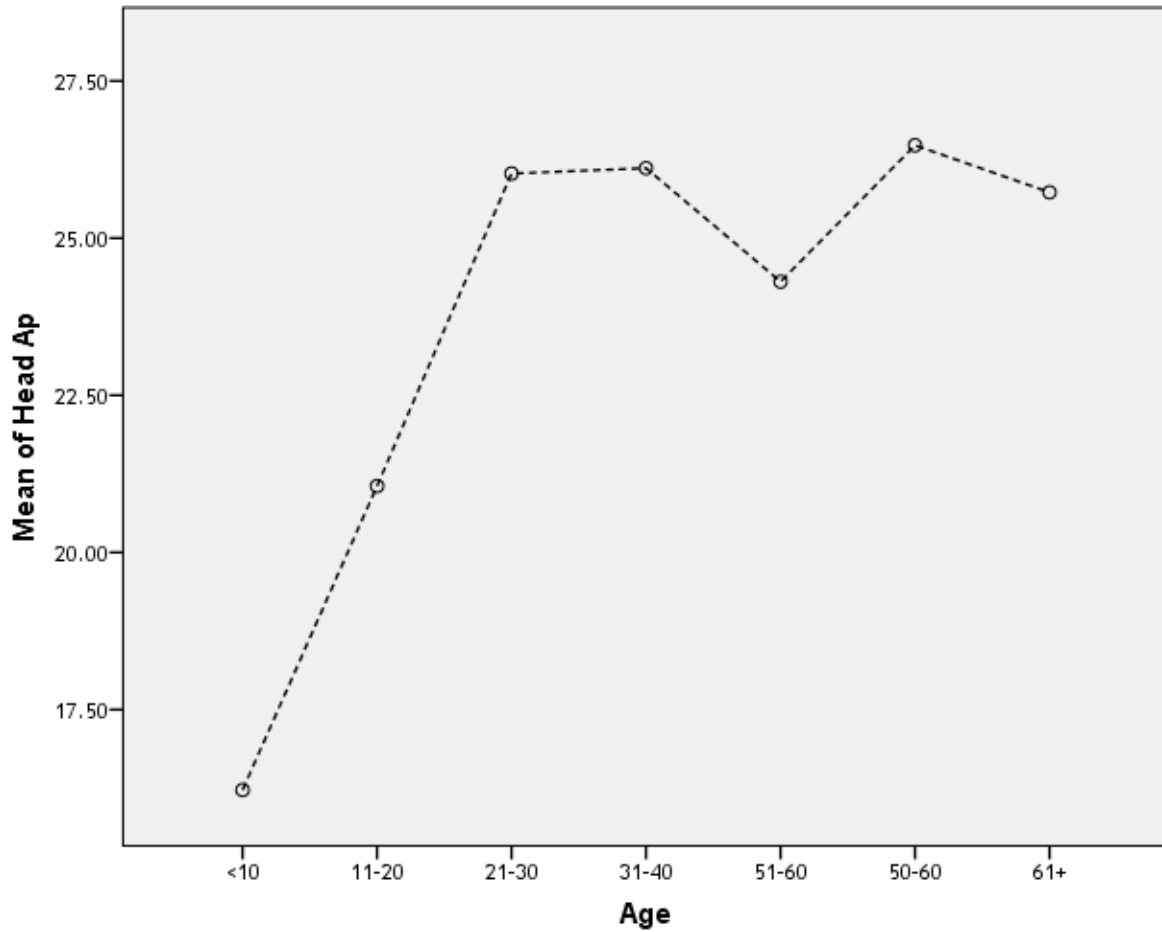


Figure 4.7 show the relation between the subjects ages classified in to age classes and pancreas head AP diameter for non-diabetic

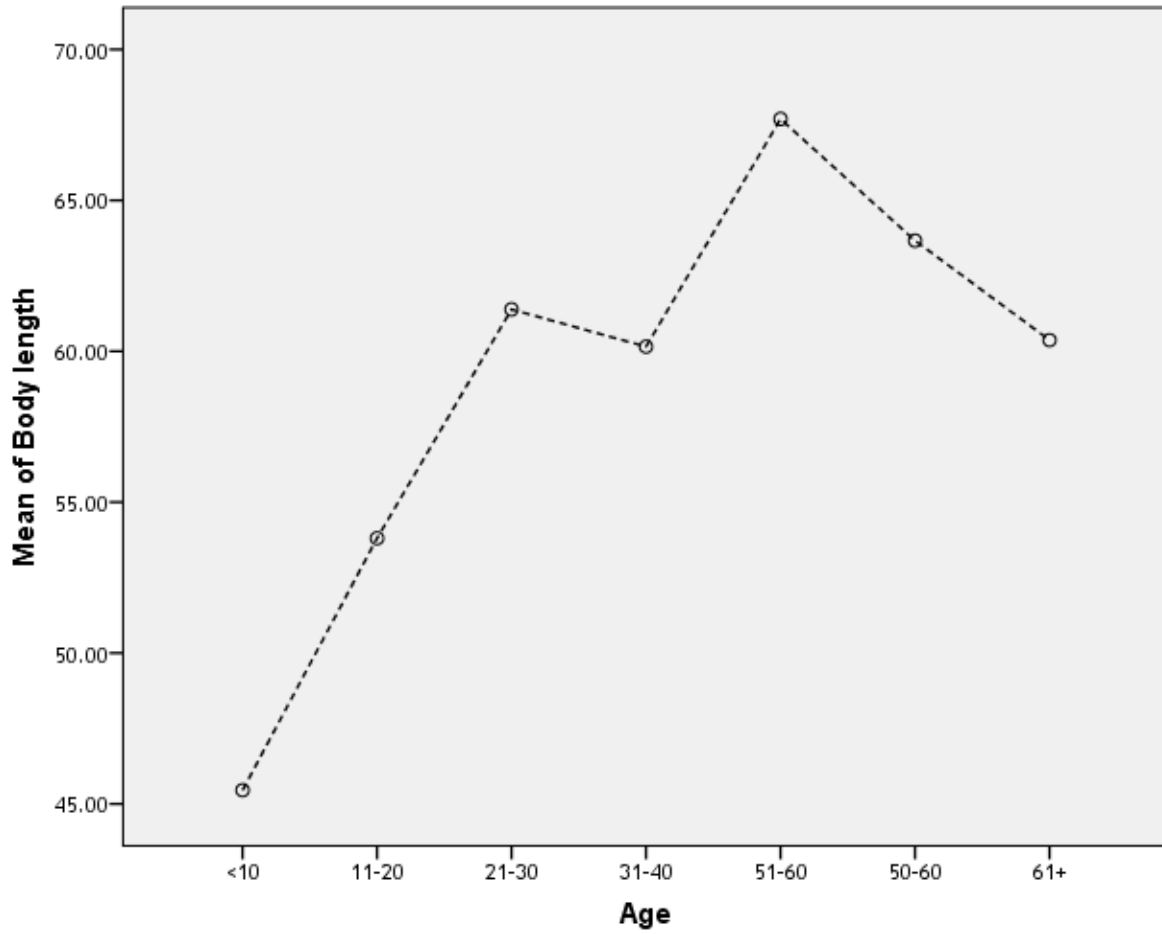


Figure 4.8 show the relation between the subjects ages classified in to age classes and pancreas body length for non-diabetic

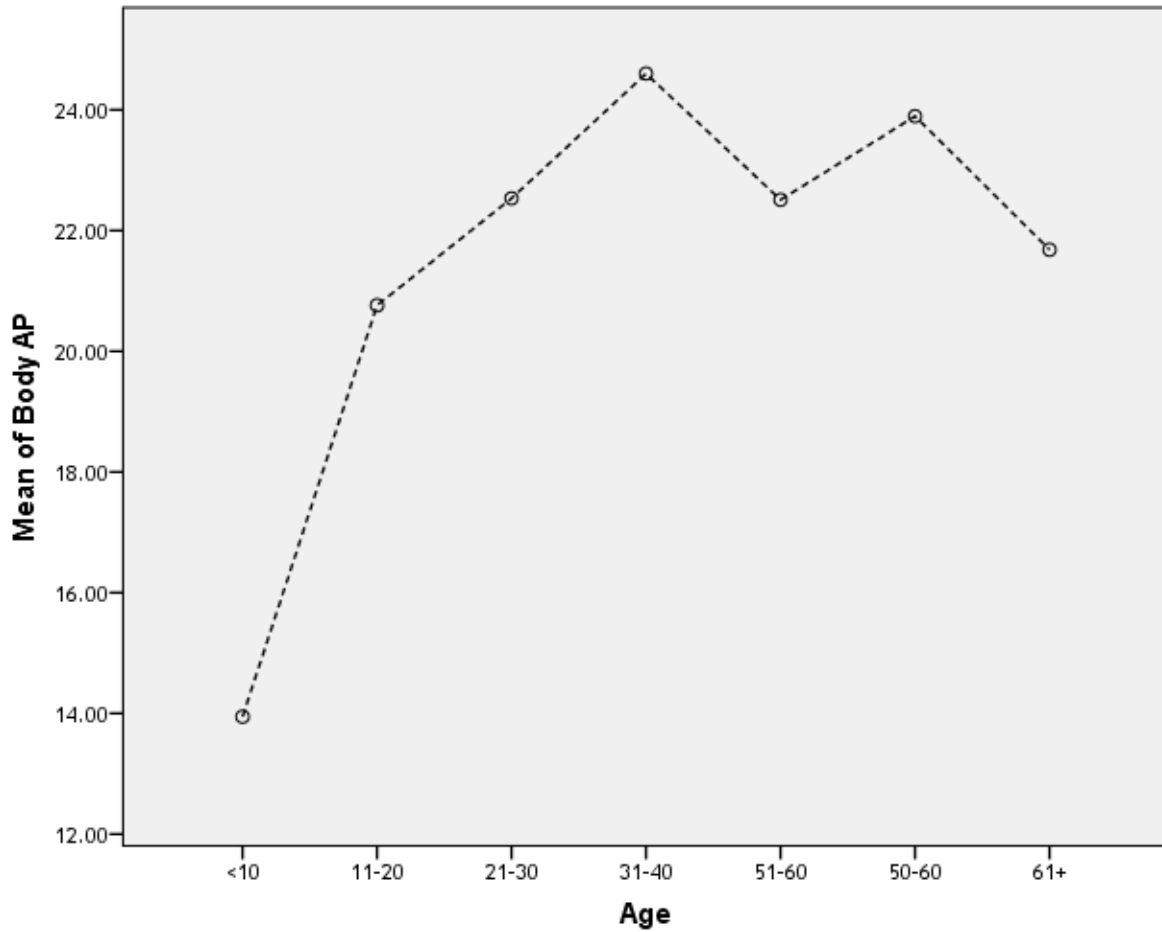


Figure 4.9 show the relation between the subjects ages classified in to age classes and pancreas body AP diameter for non-diabetic

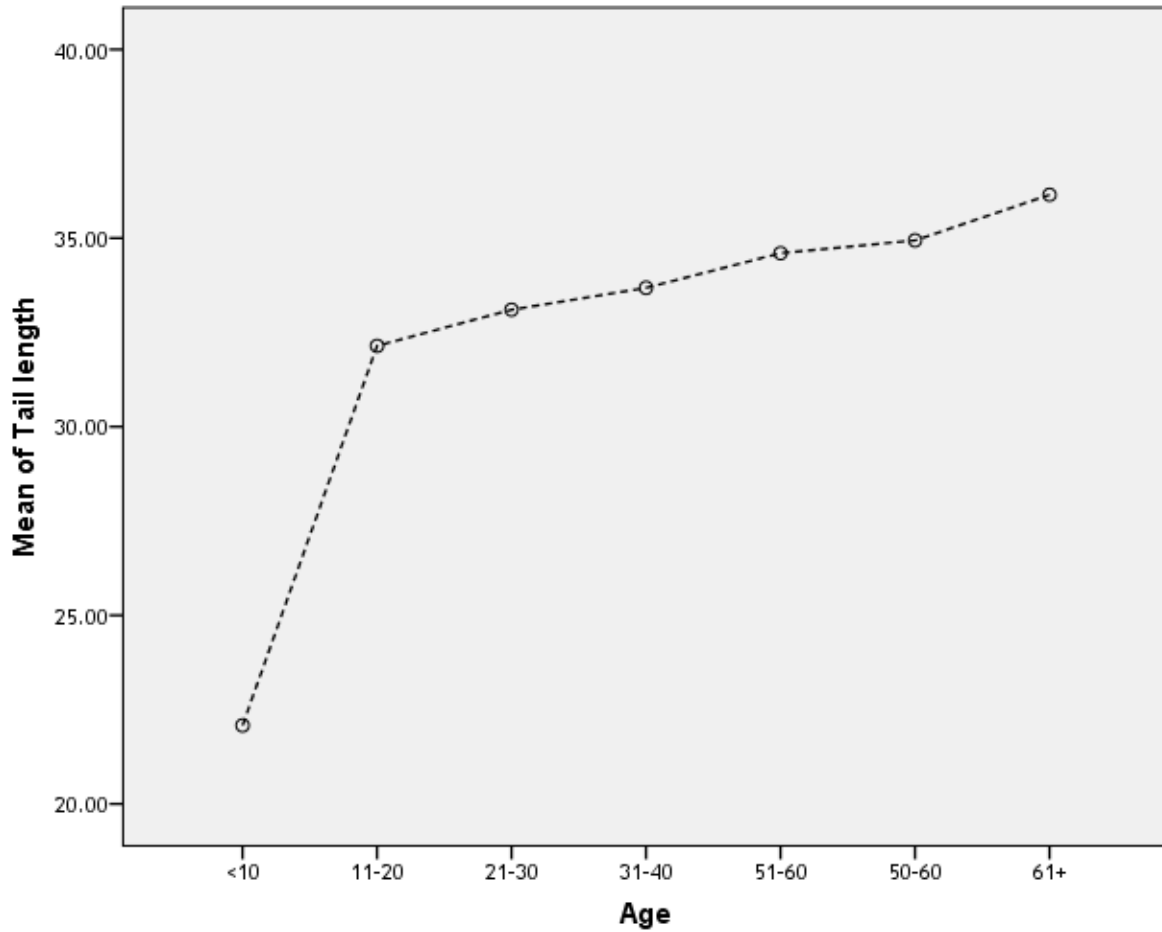


Figure 4.10 show the relation between the subjects ages classified in to age classes and pancreas tail length for non-diabetic

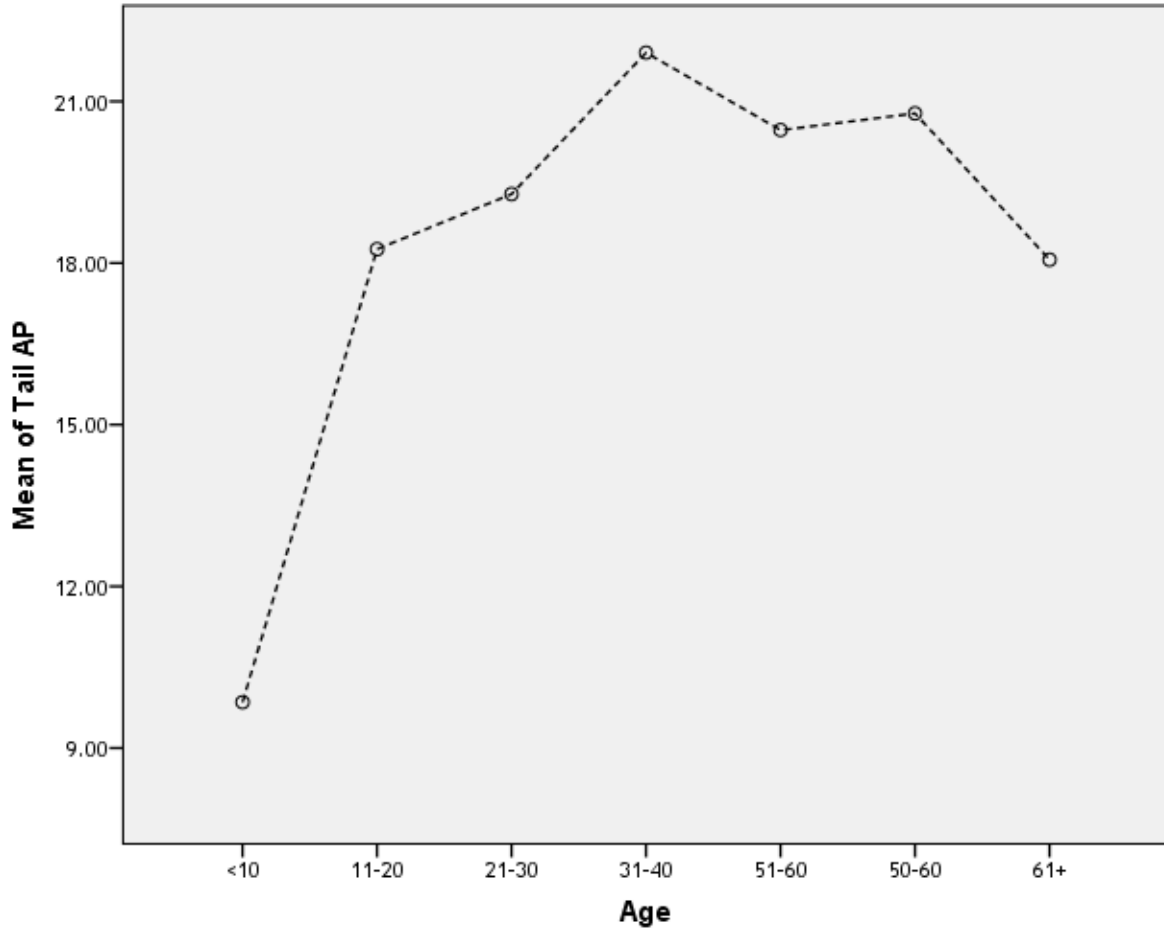


Figure 4.11 show the relation between the subjects ages classified in to age classes and pancreas tail AP diameter for non-diabetic

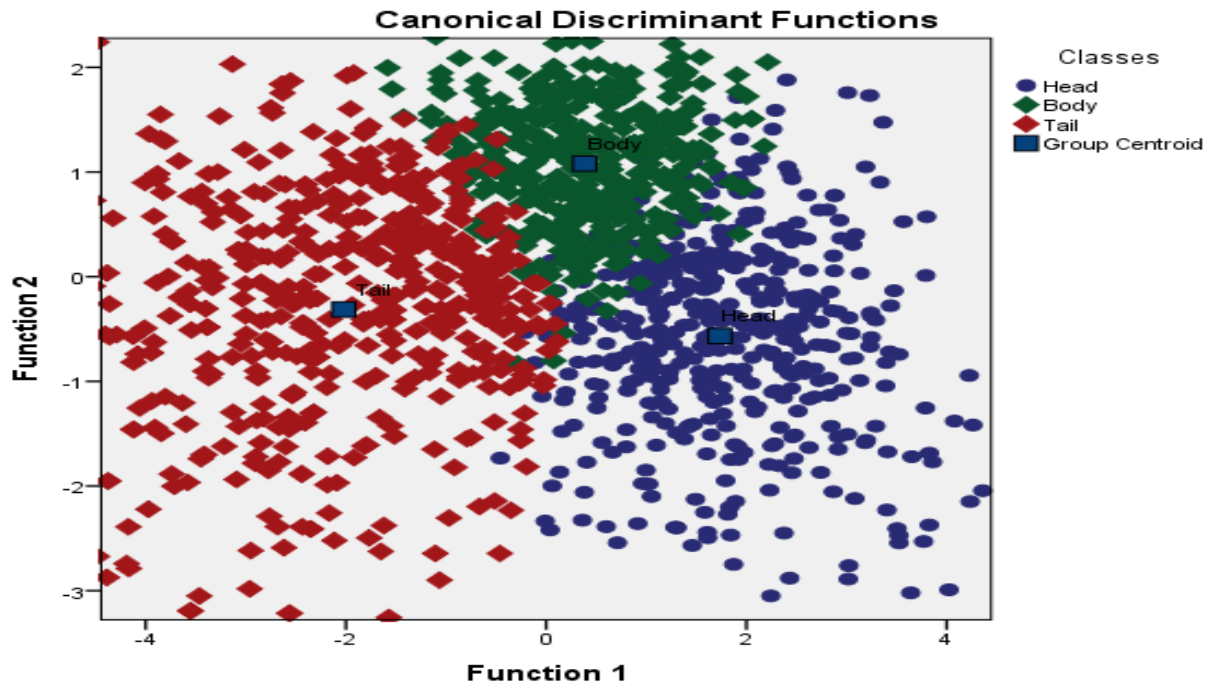


Fig4 .12 Scatter plot generated using discriminate analysis function for three classes represents: pancreas head, body and tail for diabetic patient

Table 4.6: *Showed the classification accuracy of the pancreas regions using linear discriminant analysis for diabetic patient*

Classes		Predicted Group Membership			Total
		Head	Body	Tail	
Original	Head	<u>89.2</u>	9.9	1.0	100.0
	Body	4.2	<u>93.6</u>	2.1	100.0
	Tail	1.1	5.3	<u>93.5</u>	100.0

92.0% of original grouped cases correctly classified

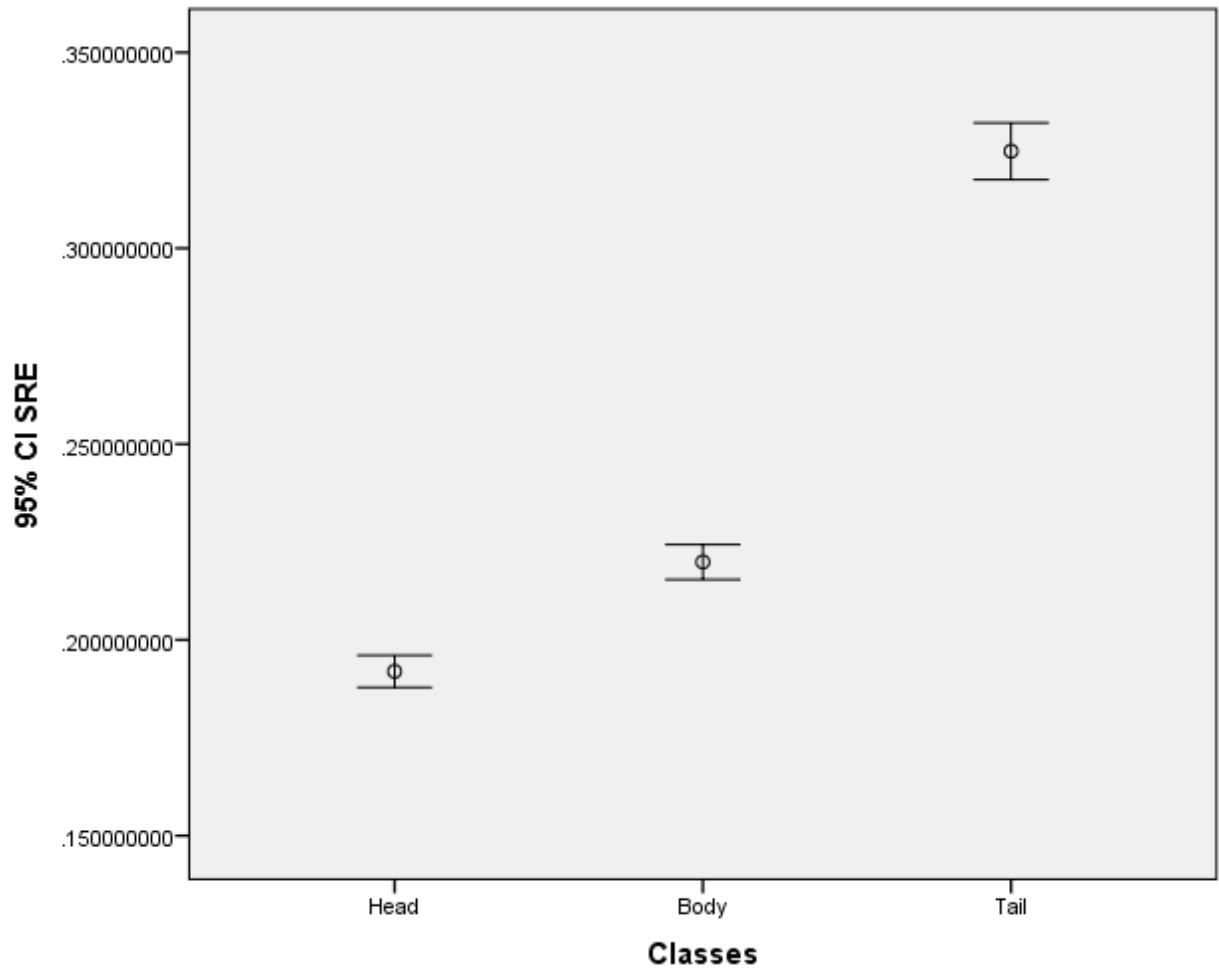


Figure 4.13 show error bar plot for the CI SRE textural features that selected by the linear stepwise discriminate function as a discriminate feature where it discriminates between all features. From the discriminate power point of view in respect to the applied features the SRE can differentiate between all the classes successfully for diabetic patient

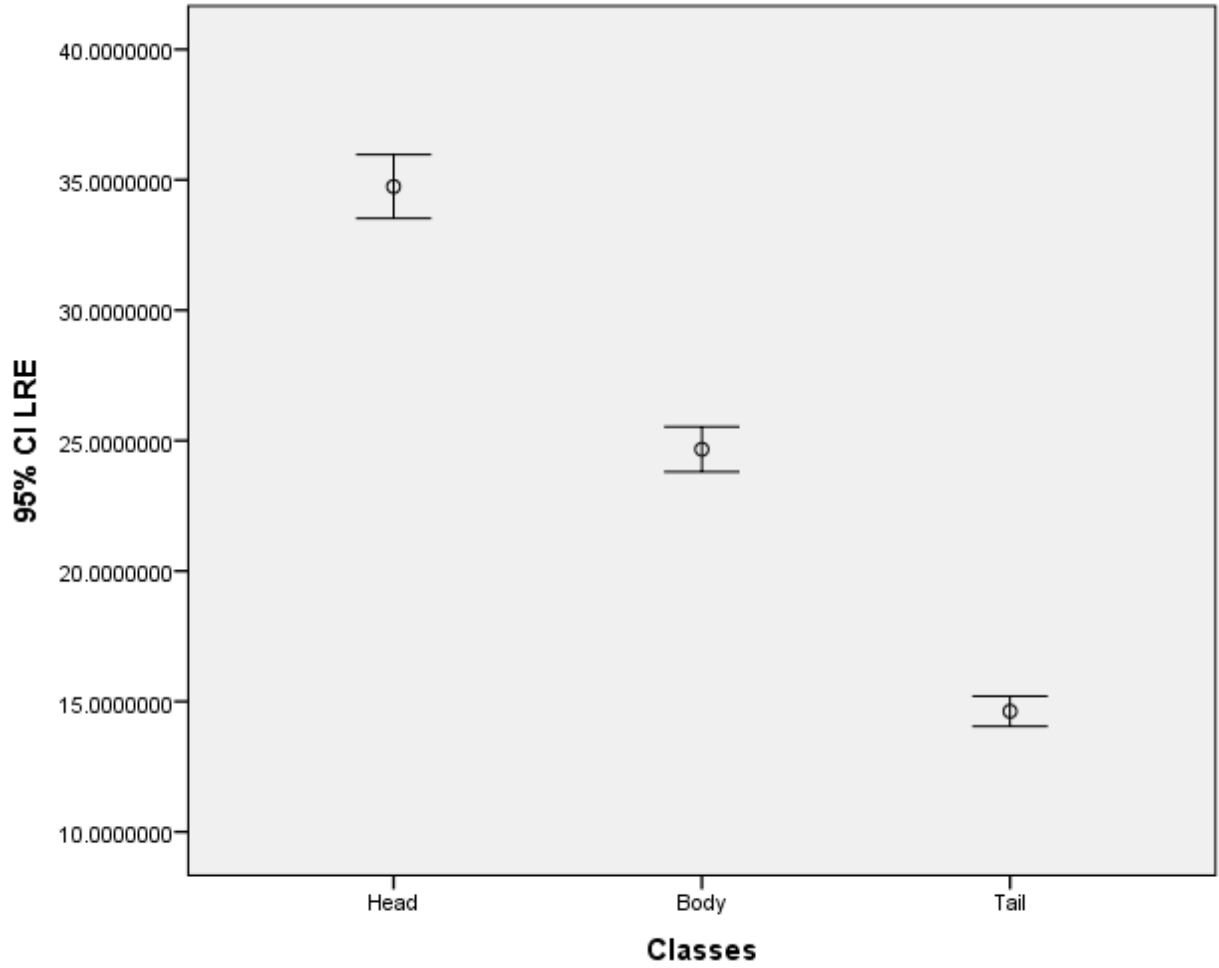


Figure 4.14 show error bar plot for the CI LRE textural features that selected by the linear stepwise discriminate function as a discriminate feature where it discriminates between all features for diabetic patient

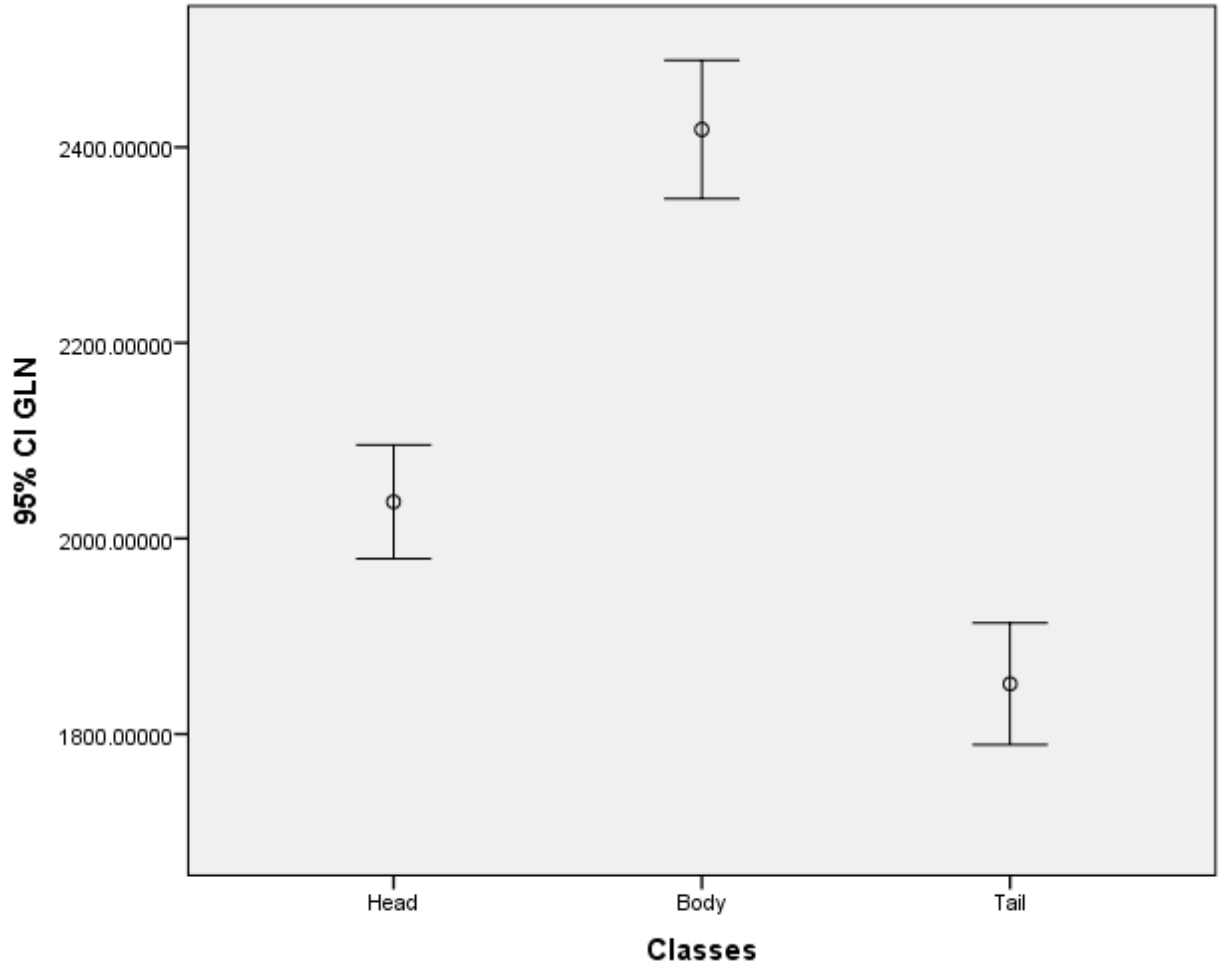


Figure 4.15 show error bar plot for the CI GLN textural features that selected by the linear stepwise discriminate function where it discriminate between all features for diabetic patient

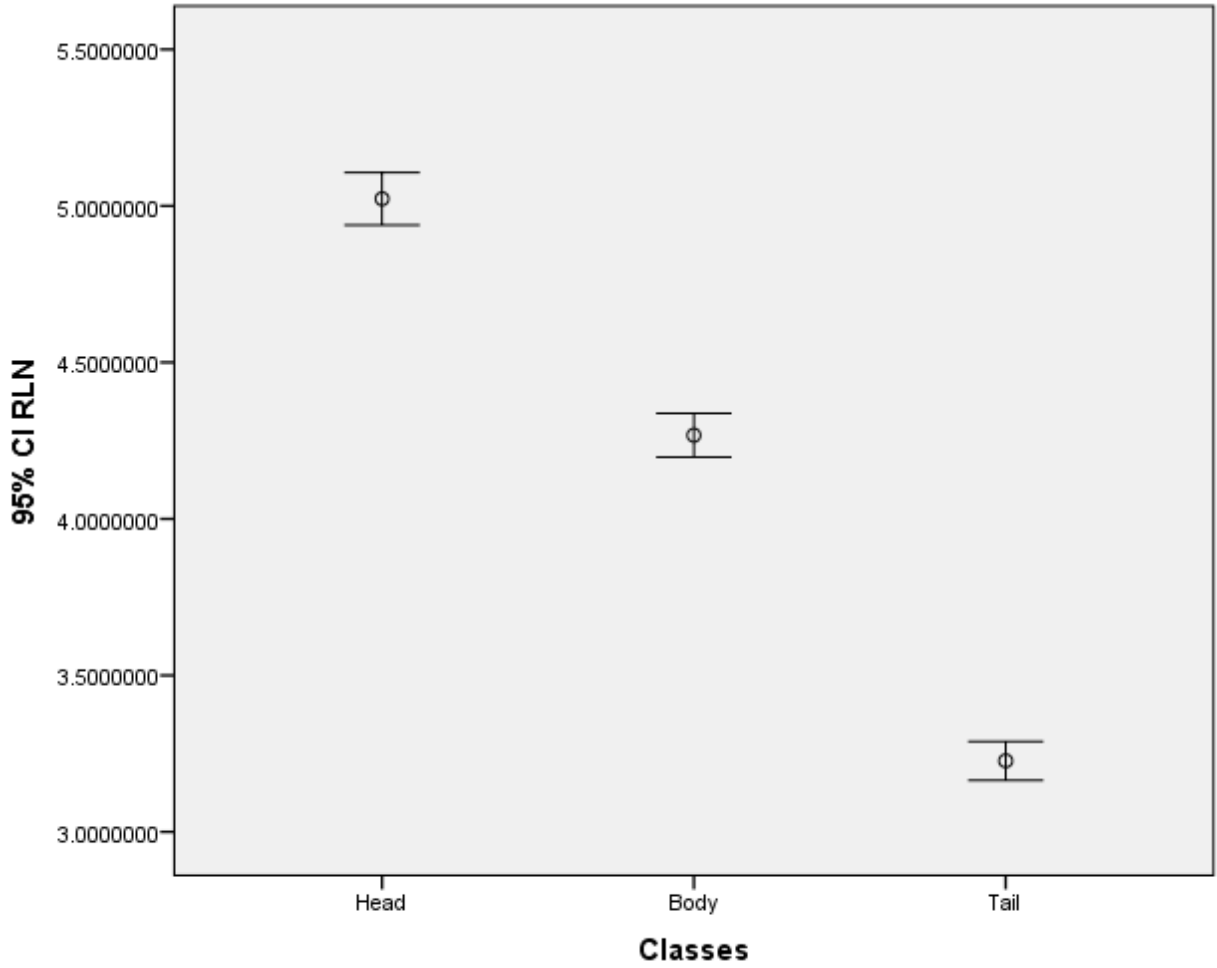


Figure 4.16 show error bar plot for the CI RLN textural features that selected by the linear stepwise discriminate function as a discriminate feature where it discriminate between all features for diabetic patient

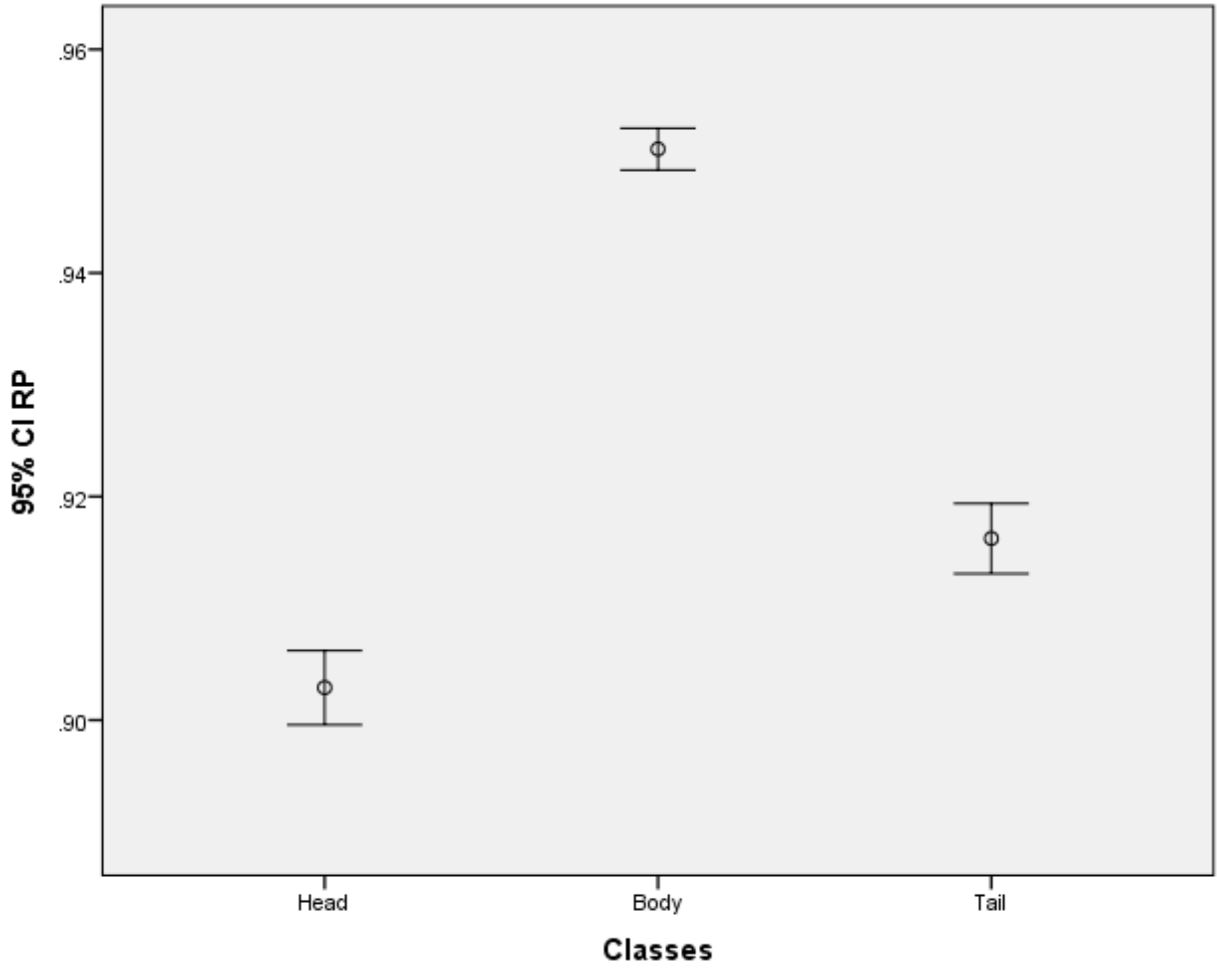


Figure 4.17 show error bar plot for the CI RP textural features that selected by the linear stepwise discriminate function as a discriminate feature where it discriminates between all features for diabetic patient

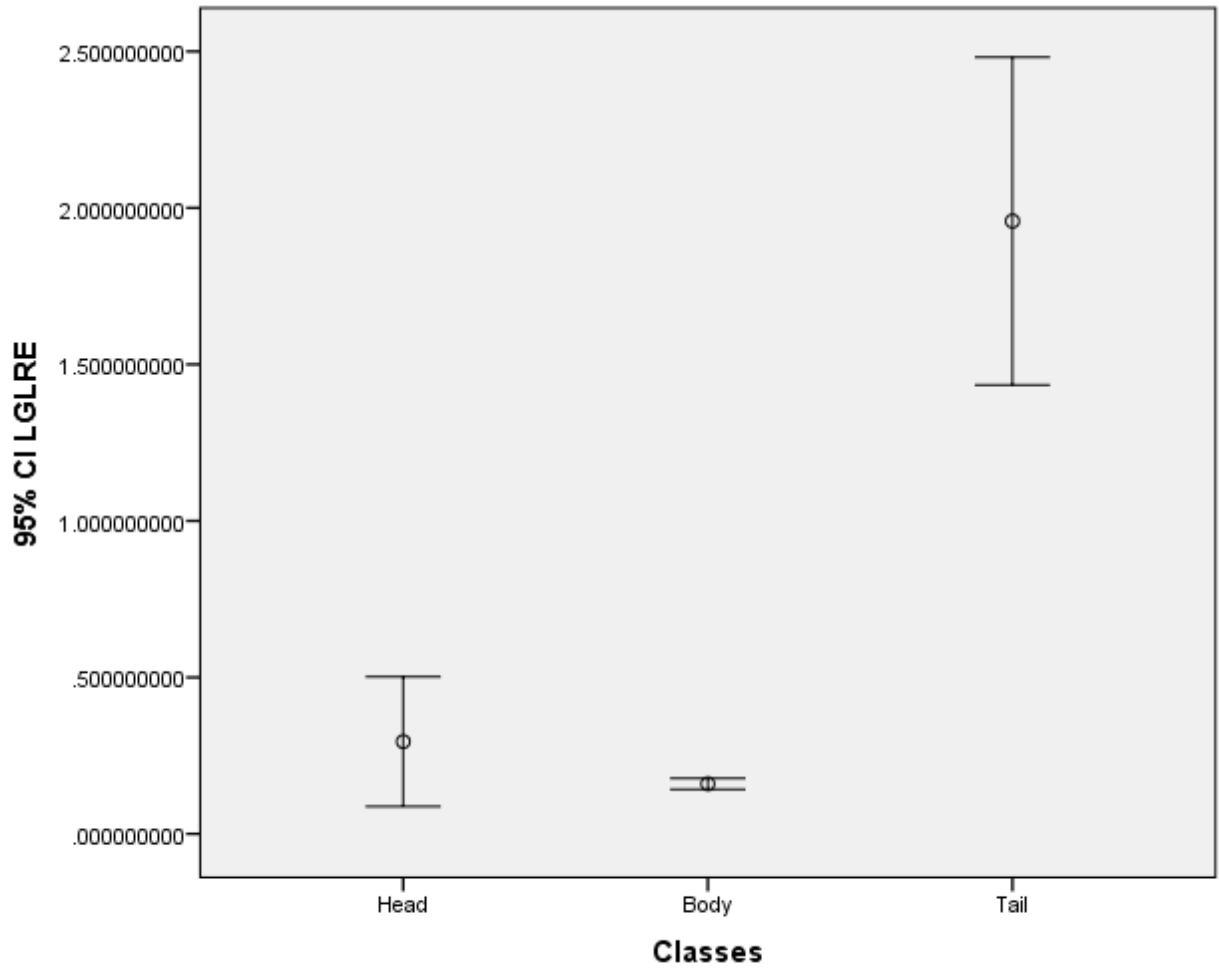


Figure 4.18 show error bar plot for the CI LGLRE textural features that selected by the linear stepwise discriminate function as a discriminate feature where it discriminates between all features for diabetic patient

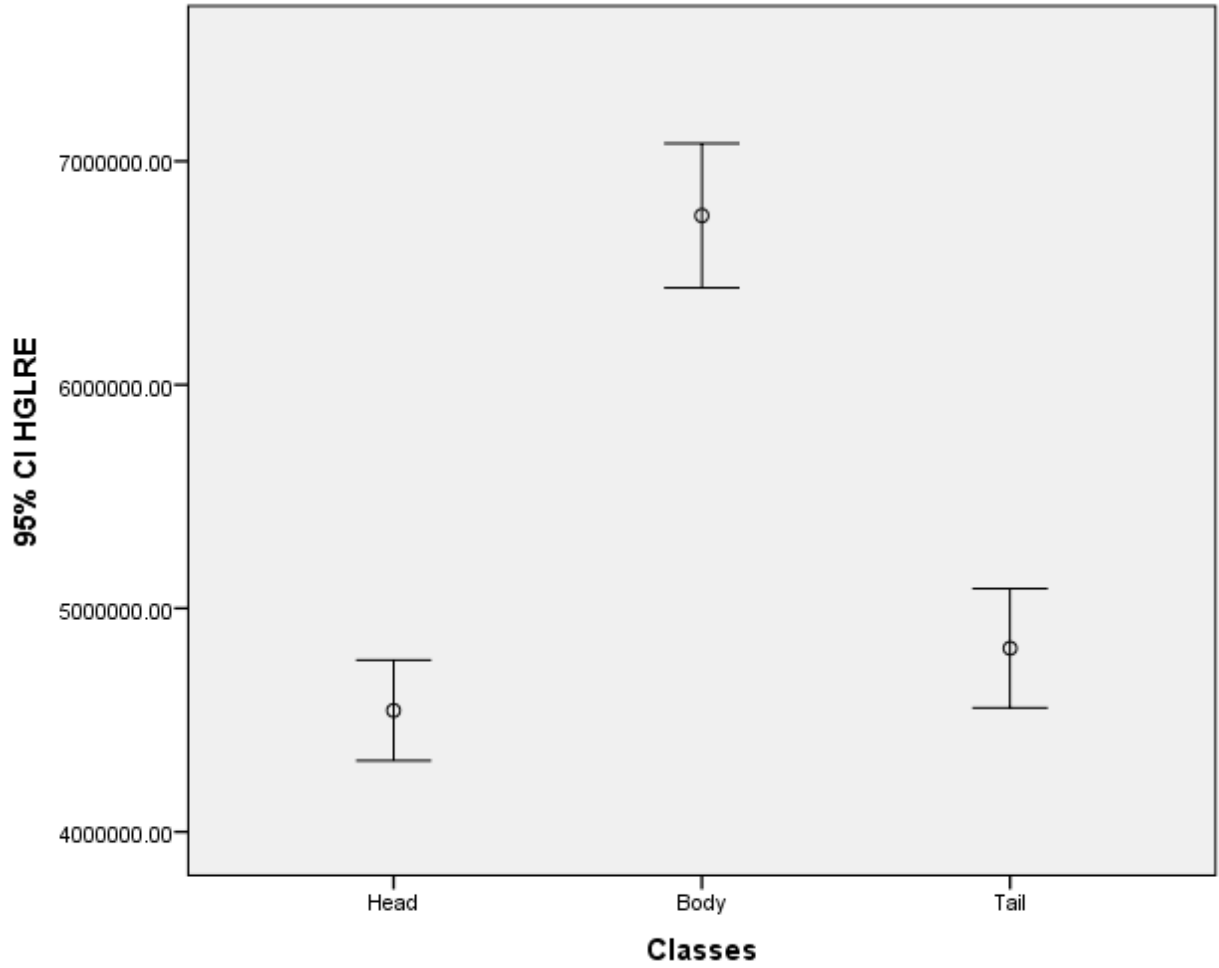


Figure 4.19 show error bar plot for the CI HGLRE textural features that selected by the linear stepwise discriminate function as a discriminate feature where it discriminates between all features for diabetic patient

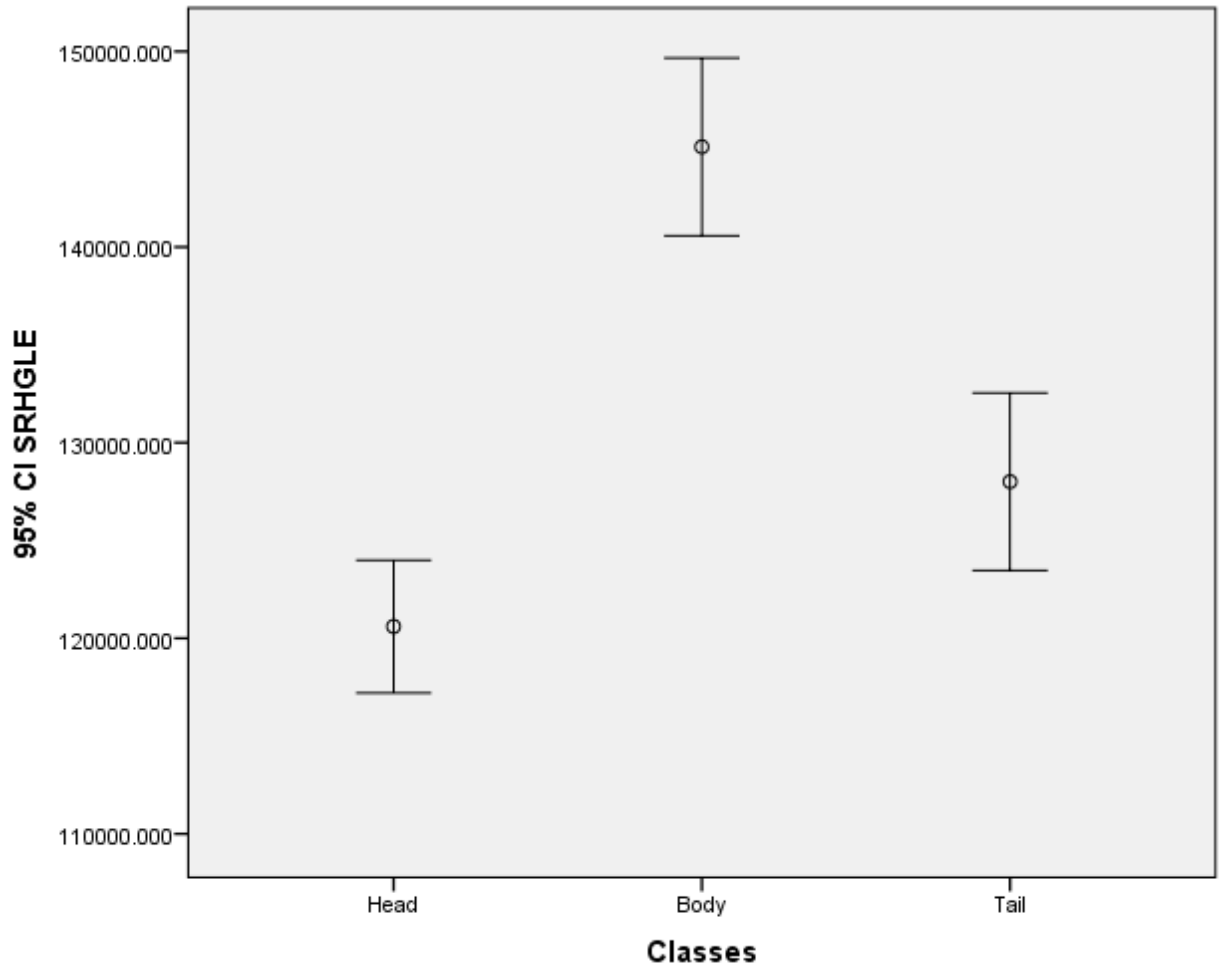


Figure 4.20 show error bar plot for the CI SRHGLE textural features that selected by the linear stepwise discriminate function as a discriminate feature where it discriminates between all features for diabetic patient

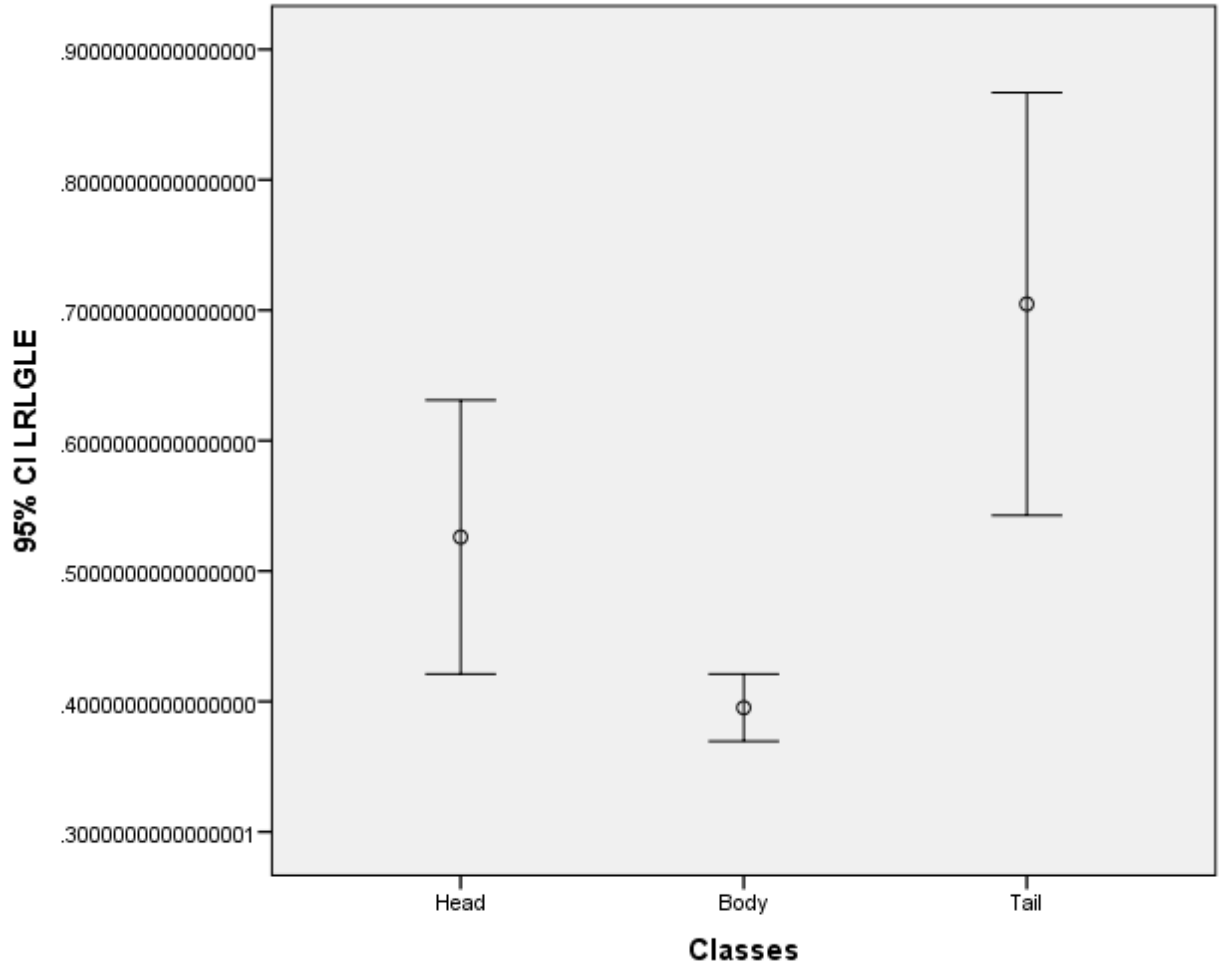


Figure 4.21 show error bar plot for the CI LRLGLE textural features that selected by the linear stepwise discriminate function as a discriminate feature where it discriminates between all features for diabetic patient

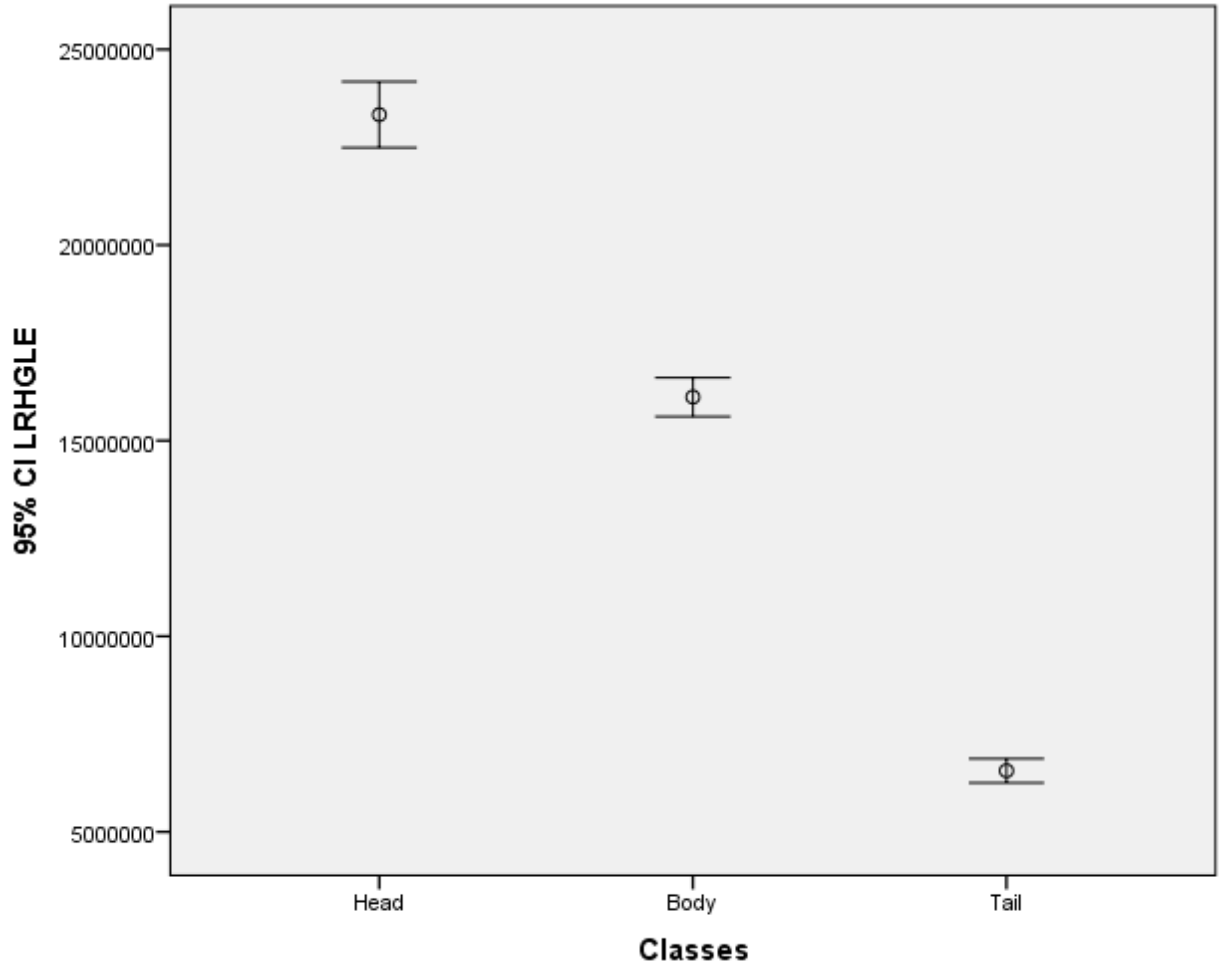


Figure 4.22 show error bar plot for the CI LRHGLE textural features that selected by the linear stepwise discriminate function as a discriminate feature where it discriminates between all features for diabetic patient

Table 4.7 Showed the classification accuracy of the pancreas in Diabetic and Non diabetic using linear discriminant analysis

Type		Predicted Group Membership		Total
		Normal	Diabetic	
	Non diabetic	100.0	.0	100.0
	Diabetic	.0	100.0	100.0

100.0% of original grouped cases correctly classified.

Table 4.8 Showed statistical analysis for GLCM features to diabetic patient & Non diabetic using t-test:

Type		Mean	Std. Deviation	Std. Error Mean
SRE	Non diabetic	7.1430	1.8509	0.1380
	Diabetic	0.2714	0.4568	0.0119
LRE	Non diabetic	533.4965	2148.4318	155.8636
	Diabetic	24.6240	13.4871	0.3523
GLN	Non diabetic	6.0173	1.0907	0.0791
	Diabetic	2080.9220	748.2793	19.5432
RLN	Non diabetic	4.4397	2.1215	0.1539
	Diabetic	4.1611	1.1194	0.0292
RP	Non diabetic	0.3832	0.0573	0.0042
	Diabetic	0.9216	0.0387	0.0010
LGLRE	Non diabetic	0.1077	0.0128	0.0009
	Diabetic	0.8514	4.0069	0.1046
HGLRE	Non diabetic	42020.8325	10322.6680	748.8850

	Diabetic	5282888.8802	3174292.5786	82904.8559
SRHGLE	Non diabetic	416606.9767	33010.8735	2460.4852
	Diabetic	130344.9783	47930.9724	1251.8412
LRLGLE	Non diabetic	44764.3927	18974.9132	1376.5849
	Diabetic	0.5522	1.3545	0.0354

Table 4.9 Showed differences in means for Diabetic patient & Non diabetic using t-test:

Independent Samples Test		
	t-test for Equality of Means	
	t	p.value
SRE	116.378	0.000
LRE	9.086	.000
GLN	-38.212	.000
RLN	2.835	.005
RP	-169.355	0.000
LGLRE	-2.558	.011
HGLRE	-22.752	.000
SRHGLE	77.881	0.000
LRLGLE	90.510	0.000

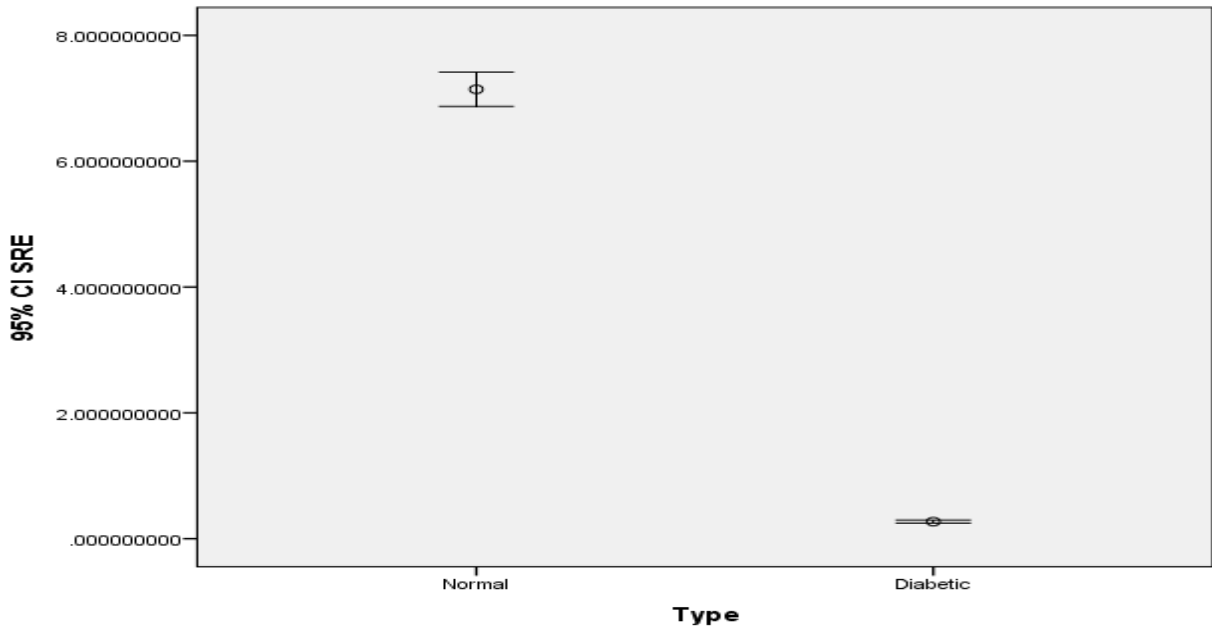


Fig 4.23 Show error bar plot for CI SRE textural feature that selected by the linear stepwise discriminate function as a discriminate feature where it discriminates between all features. From the discriminate power point of view in respect to the applied features the SRE can differentiate between all the classes successfully.

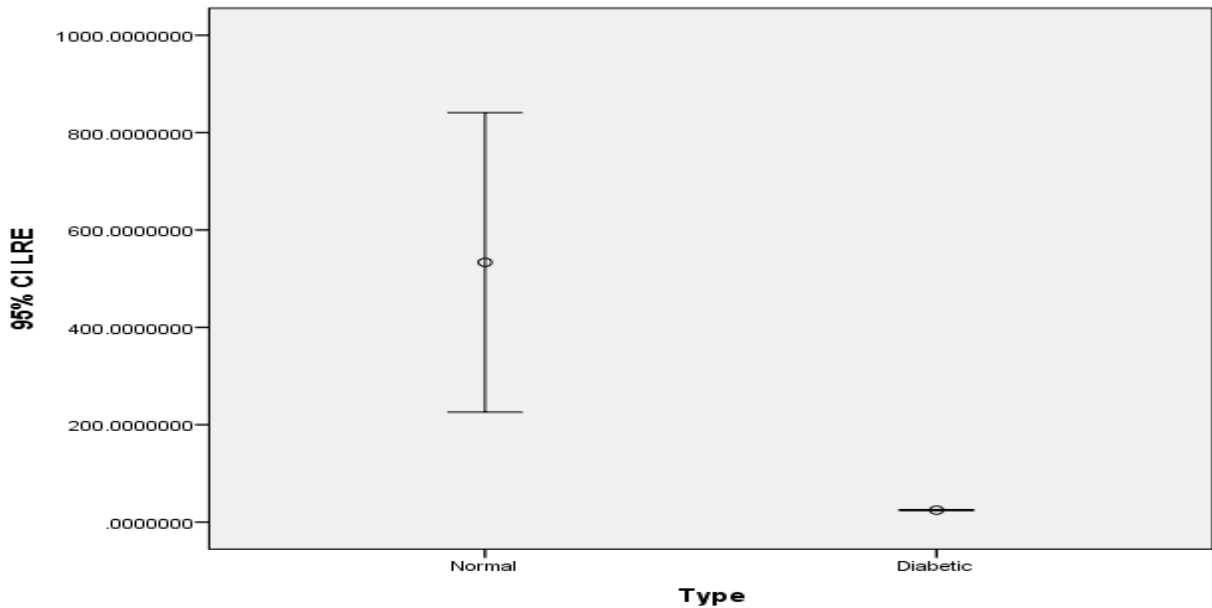


Fig 4.24 show error bar plot for the CI LRE textural features that selected by the linear stepwise discriminate function as a discriminate feature where it discriminates between all features.

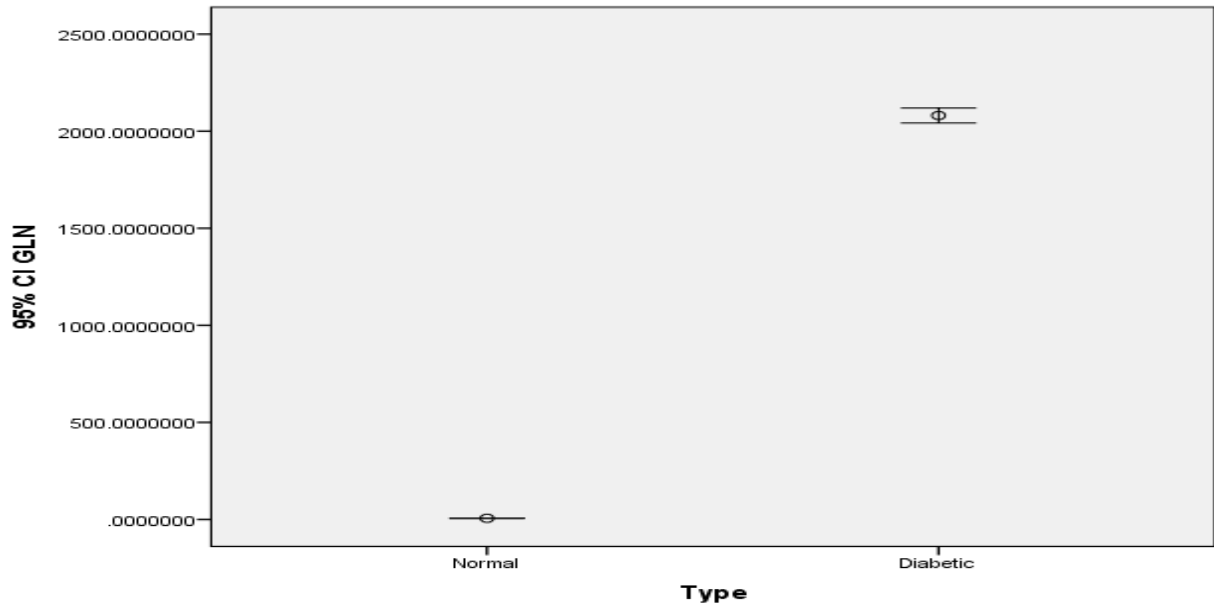


Figure 4.25 show error bar plot for the CI GLN textural features that selected by the linear stepwise discriminate function where it discriminate between all features.

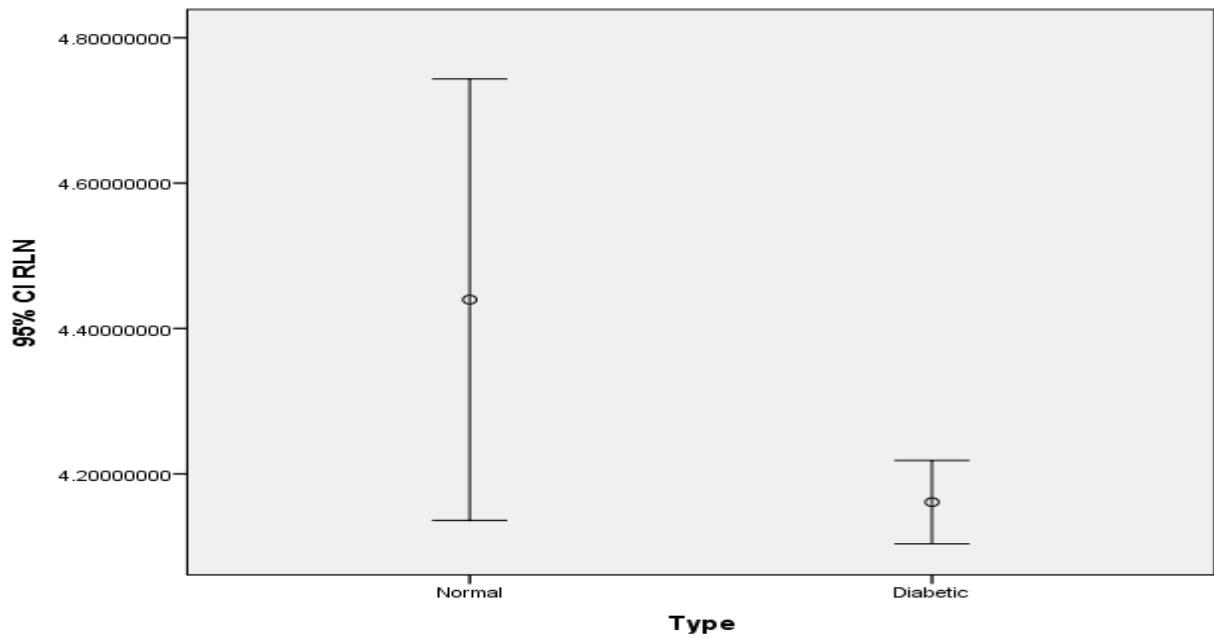


Figure 4.26 show error bar plot for the CI RLN textural features that selected by the linear stepwise discriminate function as a discriminate feature where it discriminate between all features.

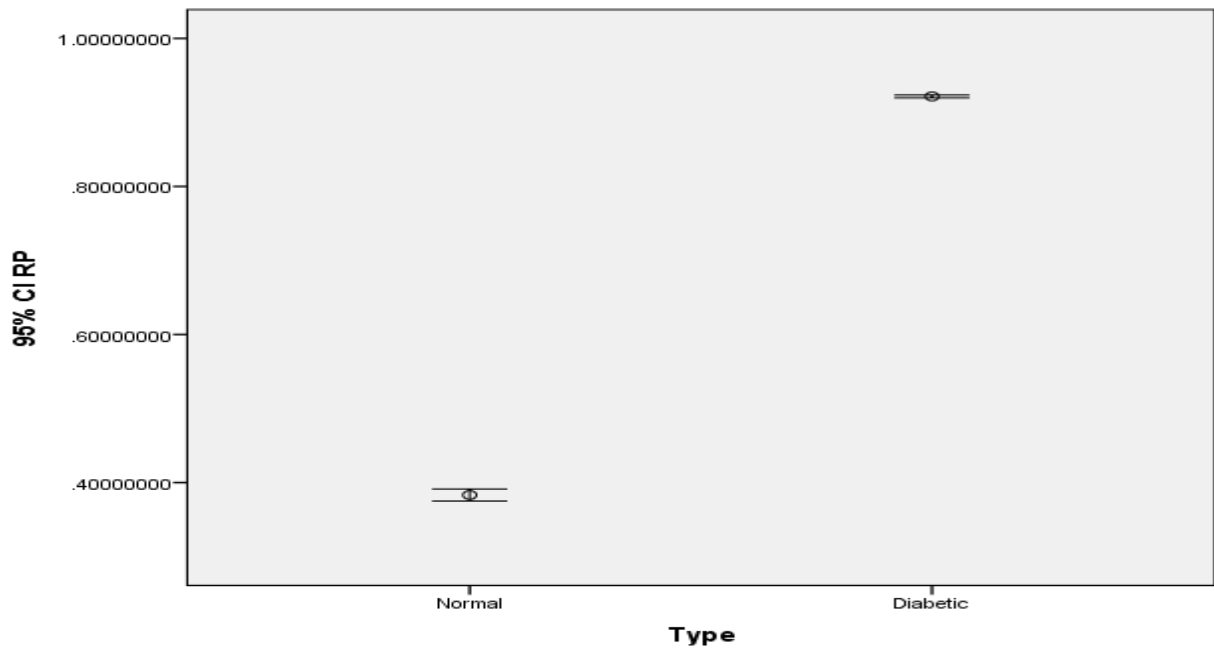


Figure 4.27 show error bar plot for the CI RP textural features that selected by the linear stepwise discriminate function as a discriminate feature where it discriminates between all features.

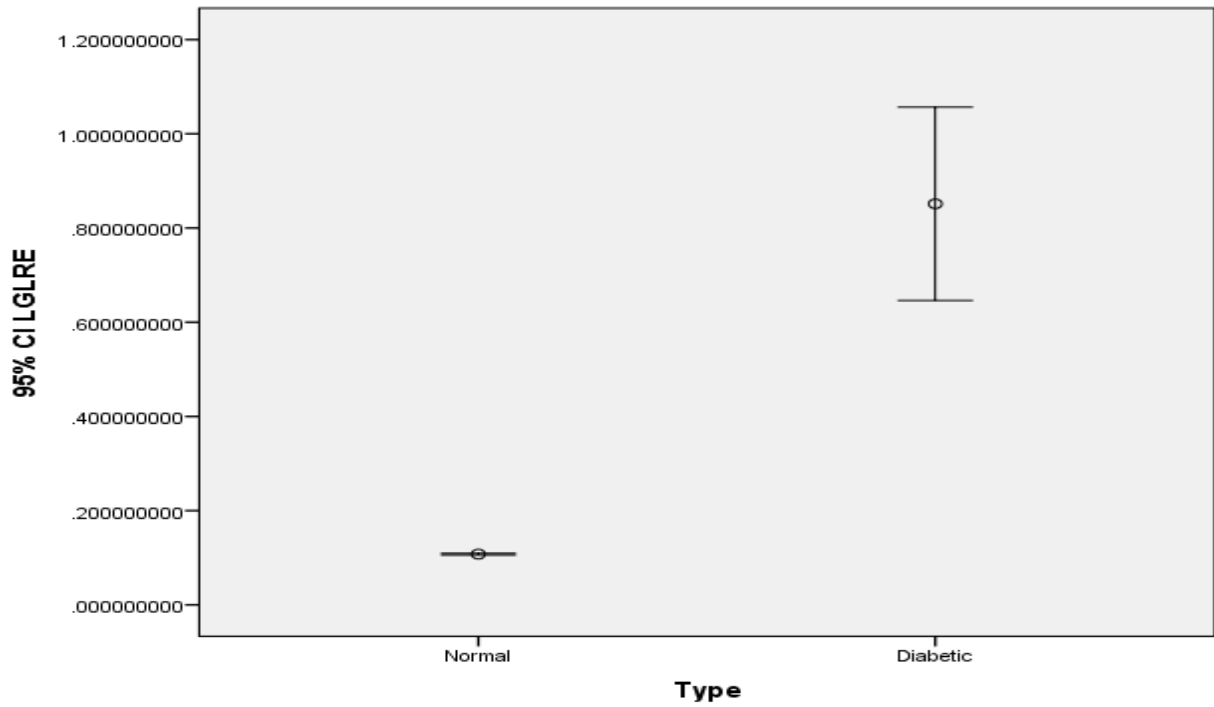


Figure 4.28 show error bar plot for the CI LGLRE textural features that selected by the linear stepwise discriminate function as a discriminate feature where it discriminates between all features.

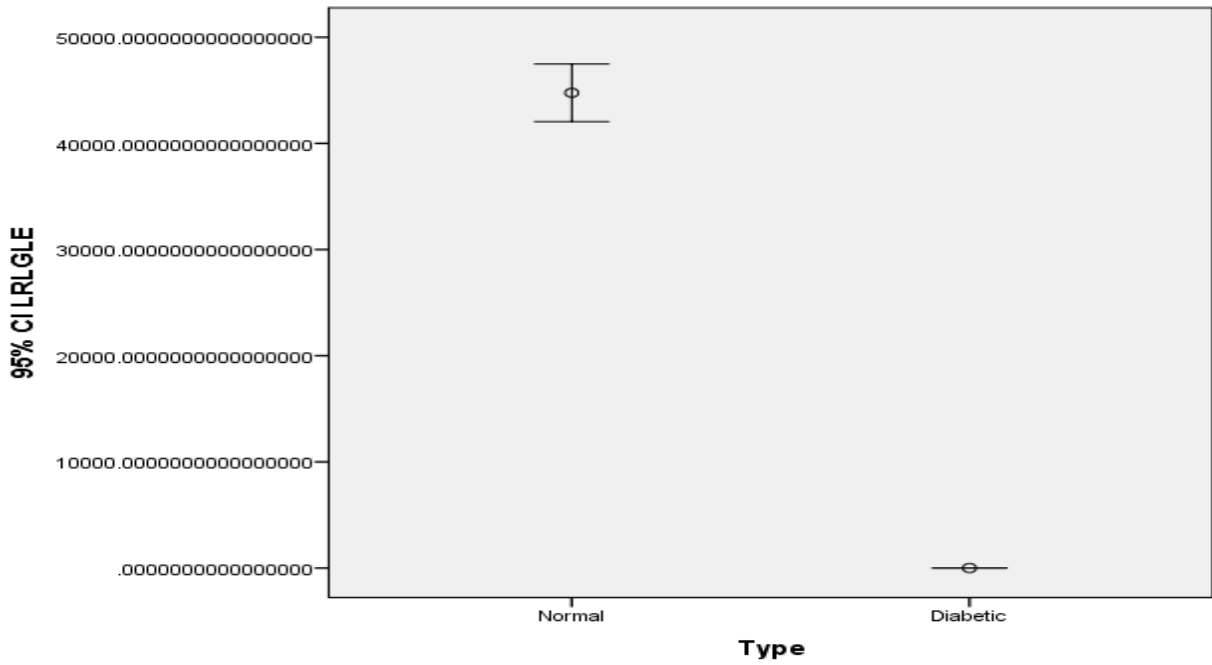


Figure 4.29 show error bar plot for the CI LRLGLE textural features that selected by the linear stepwise discriminate function as a discriminate feature where it discriminates between all features

Chapter Five

Discussion, Conclusion and Recommendation

5.1 Discussion

The main objective of this descriptive study was to analysed the texture of computed tomography images of pancreas in Diabetic patient and to find the values of various parameter of texture prosperities for classification.

The sample of this study consisted of 213 non-diabetic with different genders, 142 were male and 71 were female. were represent 66.7% considered as male, 33.3% considered as female, as seen in table 4.1 ,distribution of sample size according to gender showed that the males were more than females (table 4.1). The sample was classified according age starting from ages <10 and >61 , this was presented in table 4.2. A wide range of the pancreatic measurements for head, body and tail AP diameter and length values were observed. Descriptive Statistics mean and SD of the variables which includes age, pancreas CT No, spleen CT No, vertebra diameter, head length, head AP, body length, body AP, tail length, tail AP represented in table 4.3. The classifications of measurements and CT number according to age for male & female was presented in table 4.4.

The classifications of measurements and CT number according to age for normal subject was found to be significant for all variables this was presented in table 4.5.

Geraghty et al. (2004) reported results concerned with pancreas measurements in normal subjects .Moderately less mean pancreatic measurements in the Japanese series than in the series of Geraghty et al. was found. This might be explained by different anthropometric characteristics of the Japanese population, in comparison to Europeans.

Anterior–posterior (AP) diameters of the tail, body, and head of the pancreas are the most widely used measuring diameters for the determination of pancreatic size by the cross-sectional imaging methods: ultrasonography (US), computed tomography (CT), and magnetic resonance imaging (MRI). Cranial–caudal (CC) dimensions are also measurable, but rarely used in regular clinical practice. (Stefanovic et al . 2012)

The length of the pancreas measured by CT was reported in two available studies, but the methodology of measurement was different in each study (Stefanovic et al. 2012). AP diameters of the pancreas in our series: 19.8 ± 6.4 mm, 22.7 ± 6.0 mm, and 25.0 ± 5.6 mm for the tail, body, and head, respectively, were compatible with the values reported in the (Stefanovic et al. 2012) and Mean of the head length was 29.9 ,body length was 61.43 and tail length was 33.94 mm.

There are differences in the measurements when compared with the available reported data (Von Schulz et al. 1986), (Wegener.1993). Mean length of the pancreatic body and tail in present study 95.37 ± 24.48 mm, and in the study that reported by (Acar et al. 2010) was 105 ± 18 mm whom measurements differ from the measurements done by (Stefanovic et al. 2012) which was found to be 90.5 ± 12.2 mm, whilst this measurements are less than the Sudanese results (body and tail length was 144.90mm).Our justification may be due to authors measurement methods at the transversal projection of the length of body and tail, which normally lie in oblique direction. This was also reasonably mentioned by study done previously (Stefanovic et al. 2012) Strong correlation between the measurement of the pancreas, CT number of pancreas, and vertebra with age was found, this was noticed in Table(4.3). We established a new equation for measuring the CT number of pancreas for a subject with known age ;in the formula:(pancreas CT Number = $-0.1698 \times \text{Age} + 56.516$). The use of the proposed formula, which includes commonly measured diameters of the pancreas by cross-sectional imaging, will provide fast calculation of the approximate pancreatic CT number in the regular clinical practice. This could be

particularly useful if automatic counteracting software for CT measurements is unavailable.

The current study used the CT numbers for the pancreas as well as the CT number of vertebra as references which is similar to the method done by (Afraa, et al 2014) in order to evaluate the changes that may happen due to increasing age. The justification to have relation with age, could be due to decline in the glandular tissue as well as the fatty connective tissue within the substance of the gland in elderly people and thinning atrophy of the gland . (Afraa, et al 2014) One study has mentioned that there is no statistically significant correlation found between the measurement of the pancreas and the age of individuals, although tendency of pancreas measures decrease with the increasing age. (Saisho et al. 2007)found that the measurement of the pancreas was not age dependent within the years 20–60, yet in older individuals the pancreatic measures was gradually decreased as age increased. Study of(Heuck et al.1987) reported that dimensions of pancreas were age related: pancreas decreased in size as age increased. This was also confirmed in our series (Figures (4.6),(4.7),(4.8),(4.9),(4.10),(4.11)). The impact of age on pancreas measurements was studied previously (Afraa et al 2014), (Stefanovic et al. 2012) Our study findings were not consigned with most of these results. Other results had mentioned that parenchymal pancreatic measurements have reached a maximum in the third decade of age, remaining constant until 60 years of age thereafter and it gradually decreases (Afraa et al 2014), (Stefanovic et al. 2012). However the study in Sudanese pancreas size was best described by the established age related formula. One study had also reported that in adults beyond 60 years of age, both total and parenchymal pancreas measurements gradually decline and fat infiltration of the pancreas have been reported with aging in humans (Haertel et al 1977), (Salgadoinho et al. 1981) this is why the CT number of pancreas and spleen in our study is decreased by increasing

age (Figures (4.3)&(4.4)). Previous anatomical studies reported that pancreas measurements decreased after age 60 (Afraa et al 2014). The vertebra diameter was found to be increased with age; our justification is due to calcium deposition on bones due to increasing age. Unfortunately, the important anthropometric data, height and weight of the subjects, were not available because these values were not recorded in their medical records, which is a serious drawback of our study. Thus, we were not able to analyze the correlation between the measurements of the pancreas and height, weight, body mass index (BMI), and body surface area (BSA) of subjects, as it was done in the other published studies.(Geraghty et al. 2004)

In this study were features extracted from CT images using higher order statistic (CLRLM) contain eleven's features and All these features were calculated for all images and then the data were ready for discrimination which was performed using step-wise technique in order to select the most significant feature that can be used to classify the abdomen CT imaging for pancreas regions and the results show that in Fig4 .12. the classification showed that the pancreas areas were classified well from the rest of the tissues although it has characteristics mostly similar to surrounding tissue.

Table (4.6) show classification score matrix generated by linear discriminate analysis and the overall classification accuracy of pancreas parts 92%, were the classification accuracy of head 89.2 %, body accuracy 93.6 %, While the tail showed a classification accuracy of 93.5%.

Figures 4.13, 4.14, 4.15, 4.16, 4.17, 4.18, 4.19, 4.20, 4.21 and 4.22 show Error bar plot for SRE, LRE, GLN, RP, GLRE, HGLRE, SRHGIE, LRLGLL, LRHGLE, that selected by the linear stepwise discriminate function as a discriminate feature where it discriminate between all features between head, body and tail of the pancreas.

Table 4.7 show classification score matrix generated by linear discriminate analysis and the overall classification accuracy of pancreas in normal and diabetic patient 100%, were the classification accuracy of normal , While the diabetic patient showed a classification accuracy of 100%.

Table 4.8, 4.9 Showed statistical analysis for GLCM features to normal & diabetic patient using t-test and Showed differences in means for Normal & Diabetic patient using t-test respectively.

In figures 4.23, 4.24, 4.25, 4.26, 4.27, 4.28 and 4.29 showed classification in features SRE, LRE, GLN, RLN, RP, LGLRE and LRLGLE that selected by the linear stepwise discriminate function as a discriminate feature where it discriminate between all features between normal and diabetic patient.

5.2 Conclusion

Considerable individuals variations in the measurements of normal pancreas, measured by CT in the adult Sudanese population were observed in the presented study; It has been confirmed that pancreatic measurements is related to the individual's age. We found that, by means of presented formula the pancreas measurement could be estimated using a simple linear measurements and enables fast calculation of an approximate pancreas. In our opinion, it could be useful in regular practice if automated software for the CT is not available for the initial and follow-up assessment of the pancreas in many pathological conditions.

The classification processes of CT Abdomen were defining the pancreas to head, body and tail and carried out using Interactive Data Language (IDL) program as platform for the generated codes. The result of the classification showed that the pancreas areas were classified well from the rest of the tissues although it has characteristics mostly similar to surrounding tissue. Several texture features are introduced from GLRLM and the classification score matrix generated by linear discriminate analysis and the overall classification accuracy of pancreas regions 92%,

and the classification accuracy of pancreas head 89.2 %, body 93.6 %, While the tail showed a classification accuracy 93.5%. Using Linear discrimination analysis generated a classification function which can be used to classify other image into the mention classes as using the following multi regression equation;

$$\text{Head} = (\text{SRE} * 1240.457) + (\text{LRE} * - 8.996) + (\text{GLN} * 0.236) + (\text{RLN} * 221.674) + (\text{RP} * 1228.690) + (\text{LRLGLE} * -0.182) - 1117.167$$

$$\text{Body} = (\text{SRE} * 1227.026) + (\text{LRE} * -9.080) + (\text{GLN} * 0.227) + (\text{RLN} * 220.826) + (\text{RP} * 1288.936) + (\text{LRLGLE} * -0.145) - 1158.080$$

$$\text{Tail} = (\text{SRE} * 1121.857) + (\text{LRE} * - 8.944) + (\text{GLN} * 0.215) + (\text{RLN} * 213.636) + (\text{RP} * 1289.326) + (\text{LRLGLE} * -0.445) - 1123.302$$

In compare between the normal and diabetic patient using GLCM show a huge variation in the means, that would be helpful in improving the confidence in diabetes mellitus diagnosis as well as facilitating more accurate diagnosis.

In conclusion, the applied algorithm showed a potential success to adopt such procedure in medical image processing.

5.3Recommendation

- Farther research for measuring the pancreas should increase the sample size
- Farther research for measuring the pancreas of diabetic Sudanese population regarding the type drug used and compared with the normal measurement.
- Measure the volume of the pancreas and area to be stander reading for both normal and diabetic.
- Existing technique can be applied to classify and differentiate other pathology of pancreas especially Ca head of pancreas.
- More texture features and technique can be used to improve the performance.

- Study can also be done in depth for other types of medical images like US and MRI.
- Initiation of image processing unit in radiology department can help a lot in activation of image processing projects.

Reference

- A. Djuric-Stefanovic, D. Masulovic, J. Kostic, K. Randjic & D. Saranovic (2012) CT volumetry of normal pancreas: correlation with the pancreatic diameters measurable by the cross-sectional imaging, and relationship with the gender, age, and body constitution *Surgical and Radiologic Anatomy* Volume 34, Number 9 *Surg Radiol Anat* 34:811-817
- A. Djuric-Stefanovic, D. Masulovic, J. Kostic, K. Randjic & D. Saranovic (2012). CT volumetry of normal pancreas: correlation with the pancreatic diameters measurable by the cross-sectional imaging, and relationship with the gender, age, and body constitution *Surg Radiol Anat* 34:811-817
- Acar M, Degirmenci B, Tatli S. (2010) Short pancreas: evaluation with multi-detector row CT. *Surg Radiol Anat*;32: 853-8.
- Afraa Siddig Hassan, Caroline Edward Ayad, Elsafi Ahmed Abdalla, TagEldeen Mohammed Ebrahim . (2014) Characterization Of pancreas In Sudanese Population Using Computerized Tomography *International Journal Of Medical Imaging* *International Journal of Medical Imaging*; 2(5): 119-124
- Alzaid A, Aideyan O, Nawaz S. The size of the pancreas in diabetes mellitus. *Diabet Med* 2006; 10(8):759-763.
- April, Ernest W. 1997, clinical anatomy, 3rd edition, Williams & Wilkins, Philadelphia.
- Balthazar EJ, Megibow AJ, Pozzi Mucelli R (2009) Imaging of the pancreas. Acute and chronic pancreatitis. Springer, Berlin
- Carla J Green Baum 2011, 378(9789:412-413).
- Colledge, Nicki, Walker, Brian. Ralston, H. Stuart 2010, Davidson's principles & practice of medicine, edition 21, Elsevier, Philadelphia.

- Conners, R. & Harlow, C. (1980). Theoretical comparison of texture algorithms. IEEE Transactions on Pattern Analysis and Machine Intelligence, Vol. 2, No. 3, pp. 204-222.
- Da Ponte, J.S.; Gelber, J.; Fox, M.D.; “Effect of co-occurrence displacement vector on quantization of ultrasonic image texture” Bioengineering Conference, Proceedings of the 1988 Fourteenth Annual Northeast, 1988, Page(s): 298 - 300
- Daniel Longnecker, MD Anatomy and Histology of the Pancreas.[DOI: 10.3998/panc.2014].
- David A.; Can. J.; “An analysis of co-occurrence texture statistics as a function of grey level quantization”, Remote Sensing, Vol. No. 28, Issue 1, 2002.
- DiabetesJournals.org American Diabetes Association National Office 1701 N. Beauregard St. Alexandria VA 22311 diabetescare@diabetes.org CrossRefMedline Print ISSN: 0149-5992 Online ISSN: 1935-5548
- Duncan J.S.,Ayache N., “ Medical Image Analysis- Progress Over two decade and challenges ahead”, IEEE Trans on PAMI , Vol 22,pp. 85 – 106,2000.
- Geraghty EM, Boone JM, McGahan JP, Jain K. (2004). Normal organ volume assessment from abdominal CT. Abdom Imaging 29:482–490.
- Goda K, Sasaki E, Nagata K, Fukai M, Ohsawa N, Hahafusa T (2001) Pancreatic volume in type 1 and type 2 diabetes mellitus. Acta Diabetol 38:145–149
- Galloway M. M., “Texture analysis using grey level run lengths”, Computer Graphics Image Processing, vol. 4, p. 172-179, July, 1975.
- Haralick, Robert M.; Shanmugam, K.; Dinstein ; “Textural Features for Image Classification”, IEEE Transactions on Systems, Man and Cybernetics, Vol. No. 3, Issue 6, 1973, Page(s): 610 – 621

- Haralick; “Statistical and Structural Approaches to Texture”, Proceedings IEEE 67, 1979, Page(s): 786 – 804
- Innes JT, Carey LC. Normal pancreatic dimensions in the adult human *Amer J Surg* 1994; 167: 261-3
- Ji, Q.; Engel, J.; Craine, E.; “Texture analysis for classification of cervix lesions”, Medical Imaging, IEEE Transactions on Vol. No. 19, Issue 11, 2000, Page(s): 1144 - 1149
- JP Gilbeau, Vponcelet, Elbibon, GDeru, and FR Heller The density, contour and thickness of the pancreas in diabetics finding ,American Journal of Rontgenology september 1992 , copy right 2012 by American Rontgen Ray Society.212.305.946z Williams1993 (From Goldfine ID, Williams JA: Receptors for insulin and CCK in the acinar pancreas: Relationship to hormone action. Int Rev Cytol 85:1, 1983.)
- K Jayaprakash, R Anandan Development of pancreatic CT Scan image dataset and retrieval process for diagnosis, 2012 Journal of Scientific & Industrial Research Vol 71, pp 601-605.
- Koo HJ, Sung YS, Shim WH, Xu H, Choi CM, Kim HR, et al. Quantitative Computed Tomography Features for Predicting Tumor Recurrence in Patients with Surgically Resected Adenocarcinoma of the Lung. Rubin DL, editor. PLoS One. Public Library of Science; 2017;12(1):e0167955
- Kachouie, N. & Fieguth, P. (2007). A medical texture local binary pattern for TRUS prostate segmentation, *Proceedings of the 29th International Conference of the IEEE Engineering and Biology Society*, Lyon, France, August 23rd – 26th
- Karahaliou, A.; Boniatis, I; Skiadopoulos, S. & Sakellaropoulos, F. (2008). Breast cancer diagnosis: analyzing texture of tissue surrounding microcalcifications. *IEEE Transactions on Information Technology in Biomedicine*, Vol. 12, No. 6, pp. 731-738.

- Kovalev, V.; Kruggel, F.; Gertz, H. & von Cramon D. (2001). Three-dimensional texture analysis of MRI brain datasets. *IEEE Transactions on Medical Imaging*, Vol. 20, No. 5, pp. 424-433
- Kreel L, Haertel M, Katz D (1977) .Computed tomography of the normal pancreas. *J Comput Assist Tomogr.* Jul;1(3):290-9.
- Kreel L, Haertel M, Katz D (1977) .Computed tomography of the normal pancreas. *J Comput Assist Tomogr.*Jul;1(3):290-9.
- Kumar Vinay, Cotran, Ramzi S. Robbins Stanley L,2002, Robbins Basic phathology, 7th edition, sunder, Philadelphia.
- Lois E. Romans *Computed Tomography for Technologist A Comprehensive Text*, Wolters Kluwer Health|Lippincott Williams & Wilkins. 2011
- Moore ,Dalley et al *Clinical Oriented Anatomy seven edition* Lippincott Williams & Wilkins, a Wolters Kluwer business. 2014 P265,266,267
- McMinn RMH, Rose PG, Hutchings RT, Logan BM.(1995).Pancreas. *McMinn's Functional and Clinical Anatomy* Mosby; 277-9.
- Nailon, W.H. (1997). *Tissue characterisation of intravascular ultrasound using texture analysis*. Ph.D. dissertation, The University of Edinburgh, School of Engineering
- Nailon, W.H.; Everington, D. & Ironside, J.W. (2000). *Prion protein characterisation by image analysis*. Internal communication, National CJD Surveillance Unit, Edinburgh, UK.
- Noronha M, Salgado A, Ferreira De Almeida MJ, Dreiling DA, Bordalo O. (1981). Alcohol and the pancreas. I. Clinical associations and histopathology of minimal pancreatic inflammation. *Am J Gastroenterol* 76:114–119.
- Podda, B.; Zanetti, G. & Giachetti, A. (2005). Texture analysis for vascular segmentation from CT images, *Proceedings of Computer Assisted Radiology and Surgery (CARS)*, pp. 206-211, Berlin, Germany, 22nd-25th June, 2005.

-Ravi Rajput, Mani Ram, Sanjeev Maheshwari, RK Goyal, GL Verma Pancreatic imaging by ultrasonography in type 1 diabetes mellitus, *Int J Diabetes & Metabolism* (2001) 9: 75-8075

-Reza Basiratnia*, Ali Hekmatnia**, Mohammad Reza Kolahriz***. Ultrasonographic alterations of pancreas in diabetic patients *JRMS* 2007; 12(1): 21-23 *Journal of Research in Medical Sciences* Jan & Feb 2007; Vol 12, No 1.

-Richard S. Snell, *Clinical Anatomy By Regions*. Nine Edition, Lippincott Williams & Wilkins, a Wolters Kluwer business 2012 p204

Saisho Y, Butler AE, Meier JJ et al (2007) Pancreas volumes in humans from birth to age one hundred taking into account sex, obesity, and presence of type-2 diabetes. *Clin Anat* 20:933–942

-Sharma, M.; Singh, S.; “Evaluation of texture methods for image analysis”, *Intelligent Information Systems Conference, The Seventh Australian and New Zealand*, 2001, Page(s): 117 - 121

-Sheppard, M.A.; Liwen Shih; “P6C-2 Image Texture Clustering for Prostate Ultrasound Diagnosis”, *Ultrasonics Symposium, 2007. IEEE* 28-31, 2007, Page(s): 2473 – 2476

-Slack J. M. W. (1995) *Developmental biology of the pancreas* *Development* 121, 1569-1580 Printed in Great Britain © The Company of Biologists Limited 1995

-Tourassi,, “ Journey towards computer aided Diagnosis – Role of Image Texture Analysis”, *Radiology*, Vol 2, pp.317 – 320,1999.

-Uppaluri, R.; Mitsa, T.; Sonka, M.; Hoffman, E. & McLennan G. (1997). Quantification of pulmonary emphysema from lung computed tomography images. *American Journal of Respiratory Care in Medicine*, Vol. 156, No. 1, pp. 248-254.

-Vinay Kumar, Abul K. Abbas et al *Robbins Basic Pathology* Ninth edition Saunders, an imprint of Elsevier Inc 2013 P 645-657.

- Von Schulz HG, Christou A, Gursky S, Rother P (1986) Computer-tomographic studies on the normal morphology and volumetry of parenchymatous epigastric organs of man. *Anat Anz* 162:1–12.
- Vesterhus M, Haldorsen IS, Ræder H, Molven A, Njølstad PR. (2008) Reduced Pancreatic Volume in Hepatocyte Nuclear Factor 1A-Maturity-Onset Diabetes of the Young. *J Clin Endocrinol Metabol*; 93: 3505-9.
- Weber, A.G. (2004). The USC texture mosaics. *University of Southern California Viterbi School of Engineering*, <http://sipi.usc.edu/>
- Wegener OH (1993) Whole body tomography. Blackwell Scientific Publications, Boston, pp 291–293
- Williams PL, Warwick R, Dyson M, Bannister HL. The Pancreas. *Gray's Anatomy*. 37th Ed. Edinburg Churchill Livingstone. 1989; 1140-53.
- Widmaier EP, Raff H, Strang KT: *Vander's Human physiology: Mechanism of body function* 11th ed McGraw-Hill, 2008
- Winzenrieth, R. & Claude, I. (2006). Is there functional vascular information in anatomical MR sequences? A preliminary in vivo study. *IEEE Transactions on Biomedical Engineering*, Vol. 53, No. 6, June 2006, pp.1190-1194.
- Xu, Y.; Sonka, G.; McLennan, G.; Junfeng, G. & Hoffman, E. (2006). MDCT-based 3D texture classification of emphysema and early smoking related pathologies. *IEEE Transactions on Medical Imaging*, Vol. 25, No. 4, pp. 464-475
- Xu D., Kurani A., Furst J., Raicu D., “RunLengthEncoding For Volumetric Texture”, International Conference on Visualization, Imaging and Image Processing (VIIP), p. 452-458, 2004.

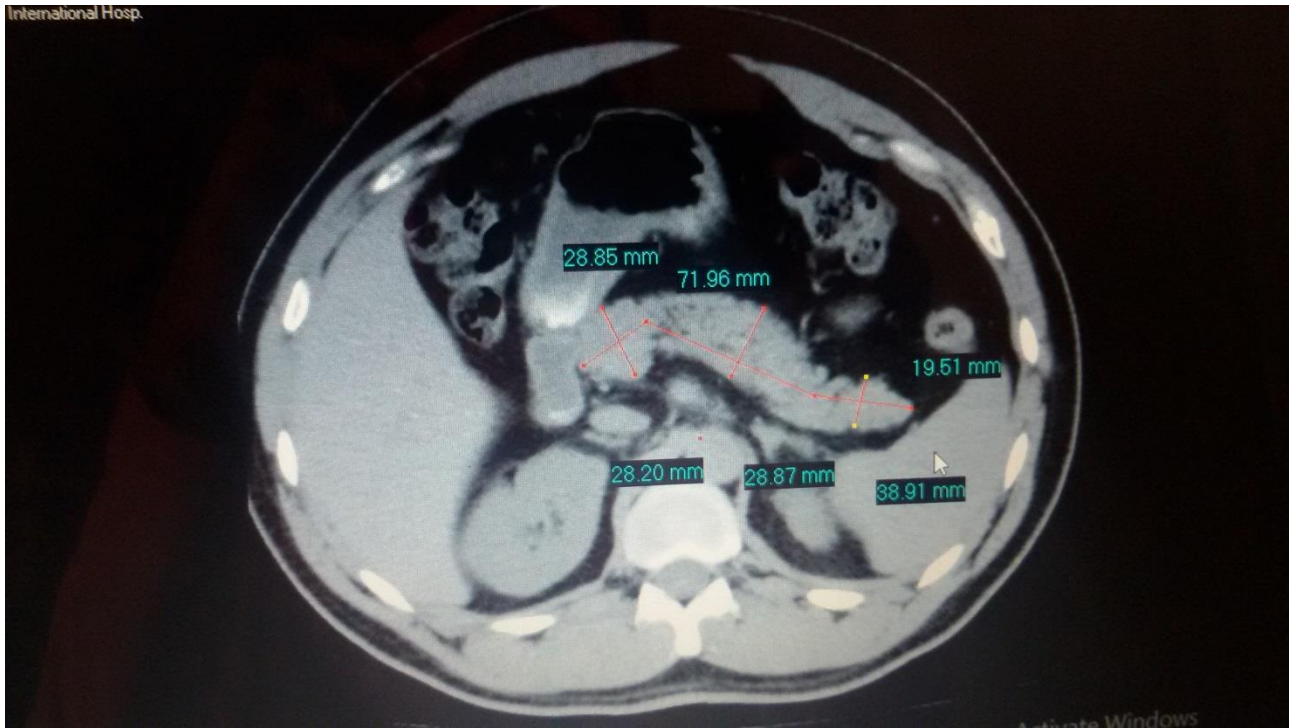


Figure showed the measurement for normal pancreas AP diameter & length of head, body and tail of pancreas using spiral CT 64 slice

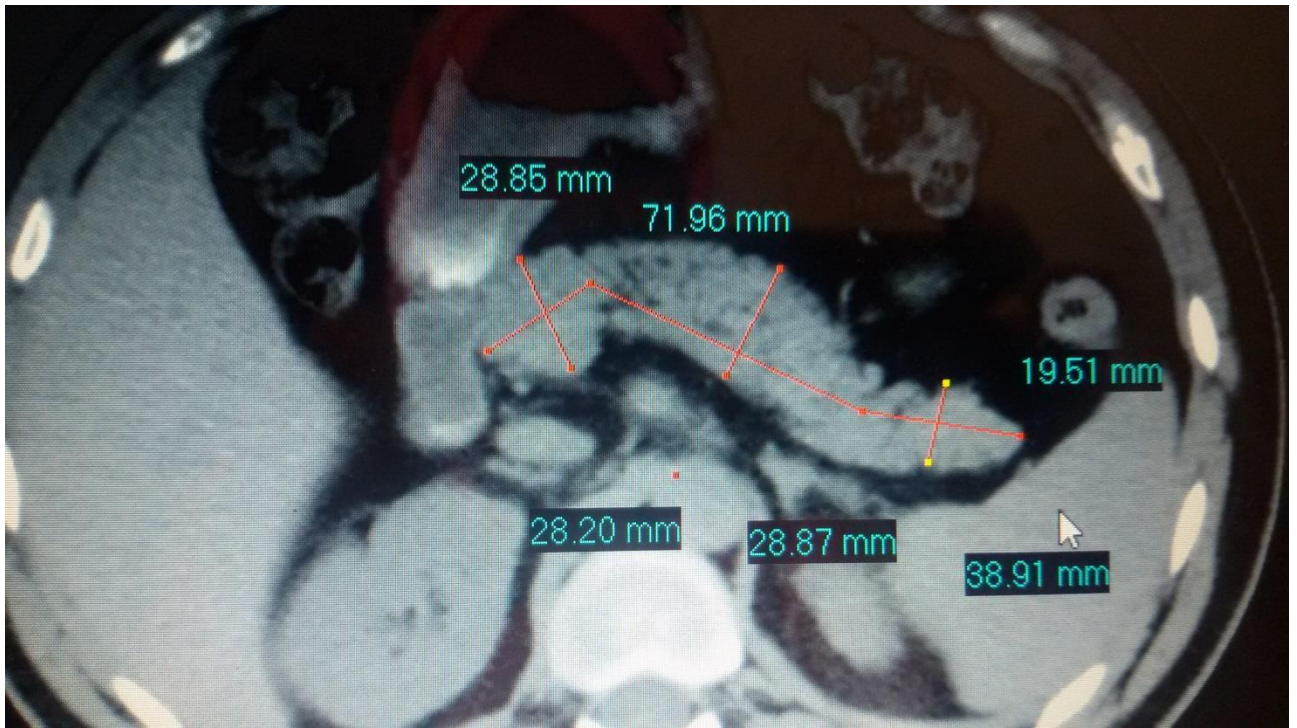


Figure showed the measurement for normal pancreas AP diameter & length of head, body and tail of pancreas using spiral CT 64 slice

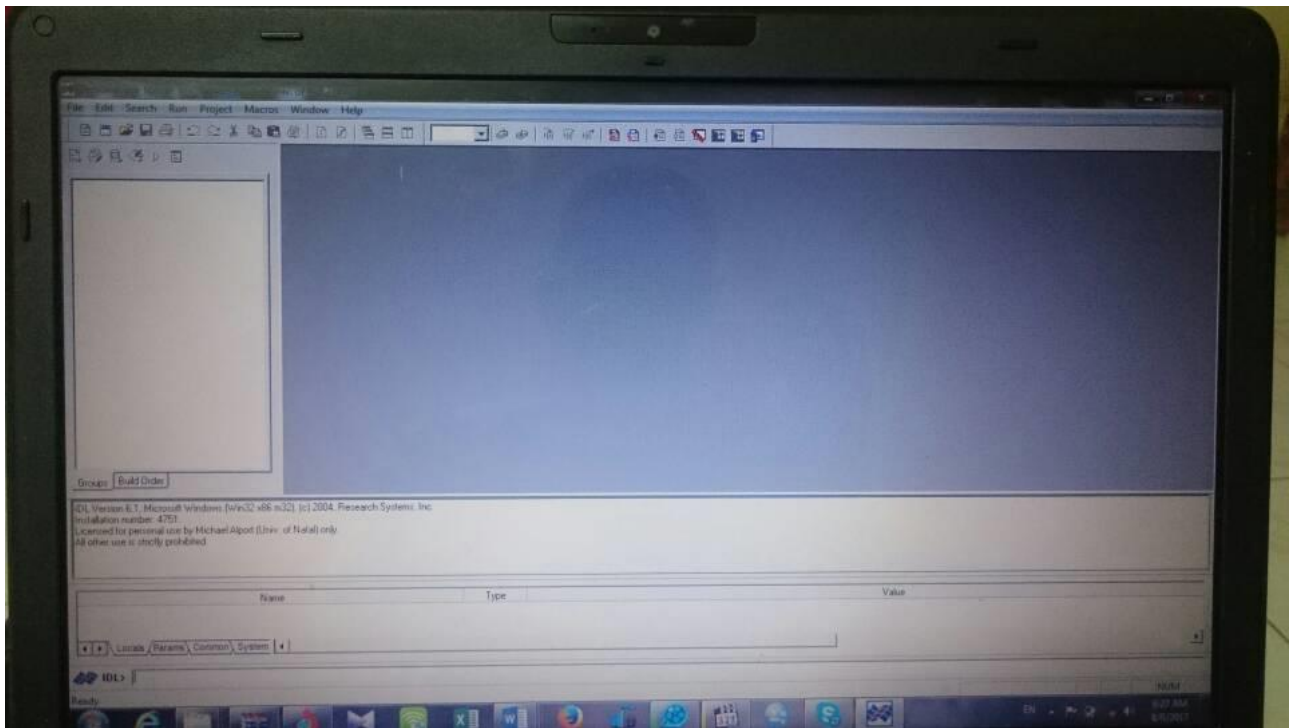


Figure showed IDL program using for data analysis

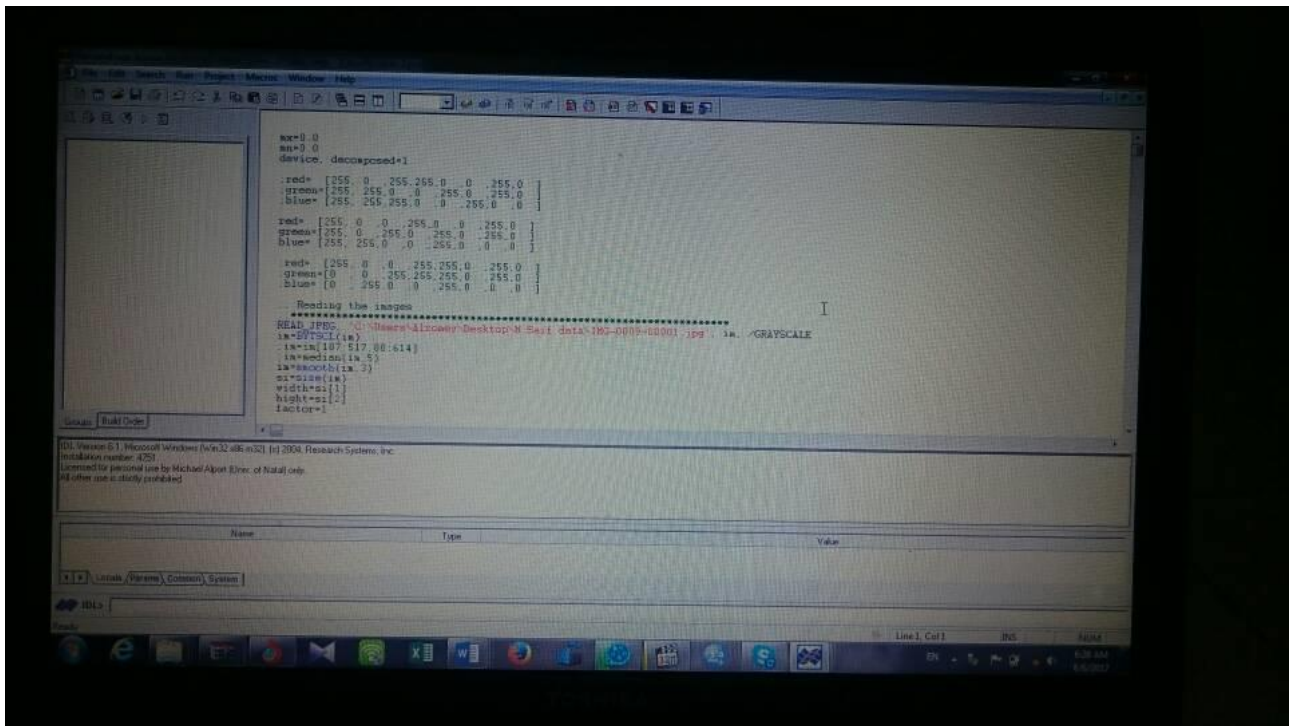


Figure showed IDL program using for data analysis